THREE LAYER MATHEMATICAL MODELLING OF AN ELASTIC ARTERY WITHOUT AND WITH ANEURYSM TO PREDICT THE BEHAVIOR

A THESIS SUBMITTED TO
THE GRADUATE SCHOOL OF NATURAL AND APPLIED SCIENCES
OF
MIDDLE EAST TECHNICAL UNIVERSITY

BY

HOSSEIN JODATI

IN PARTIAL FULFILLMENT OF THE REQUIREMENTS
FOR
THE DEGREE OF MASTER OF SCIENCE
IN
BIOMEDICAL ENGINEERING

APRIL 2015

Approval of thesis:

THREE LAYER MATHEMATICAL MODELLING OF AN ELASTIC ARTERY WITHOUT AND WITH ANEURYSM TO PREDICT THE BEHAVIOUR

Submitted by **HOSSEIN JODATI** in partial fulfilment of requirements for degree of **Master of Science in Biomedical Engineering Department, Middle East Technical University** by,

Prof. Dr. Gülbin Dural Ünver
Dean, Graduate School of **Natural and Applied Sciences** _____

Prof. Dr. Hakan I. Tarman
Head of Department, **Biomedical Engineering** _____

Prof. Dr. Mehmet Zülfü Aşık
Supervisor, **Engineering Sciences Dept., METU** _____

Prof. Dr. Serdar Geyik
Co-Supervisor, **Memorial Healthcare Group** _____

Examining Commitee Members:

Prof. Dr. Hakan I. Tarman
Engineering Sciences Dept., METU _____

Prof. Dr. Mehmet Zülfü Aşık
Engineering Sciences Dept., METU _____

Assoc. Prof. Dr. Hakan Emmez
Neurosurgery Dept., Gazi University _____

Prof. Dr. Caner Durucan
Metallurgical and Materials Engineering Dept., METU _____

Assoc. Prof. Dr Utku Kanoğlu
Engineering Sciences Dept., METU _____

Date: **03.04.2015**

I hereby declare that all information in this document has been obtained and presented in accordance with academic rules and ethical conduct. I also declare that, as required with these rules and conduct, I have fully cited and referenced all materials and results that are not original to this work.

Name, Last name: Hossein Jodati

Signature:

ABSTRACT

THREE LAYER MATHEMATICAL MODELLING OF AN ELASTIC ARTERY WITHOUT AND WITH ANEURYSM TO PREDICT THE BEHAVIOR

Jodati, Hossein

M.S., Department of Biomedical Engineering

Supervisor: Prof. Dr. Mehmet Zülfü Aşık

Co-Supervisor: Prof. Dr. Serdar Geyik

April 2015, 135 pages

Cerebral or intracranial aneurysm is a cerebrovascular disorder, in which weakening and/or thinning of artery's wall leads to a focal and permanent ballooning on the artery's wall. In natural history or evolution of saccular intracranial aneurysm the rupture is the final phase and it is generally lethal. Although the natural history of aneurysm is complicated combination of mechanical and physiological processes that change the composition and strength of arterial wall, it is obvious that aneurismal rupture is stemmed from failure of the wall's structure to endure the wall's stresses resulting from the pressure applied by pulsatile blood flow. In the present study the two dimensional (2D) arterial wall (plane-strain), including three layers with linear elastic, isotropic, homogeneous, and non-viscous material properties, under constant pressure in lumen was modelled and analyzed numerically by using finite element analysis (FEA) principles in both healthy (linear and geometrical nonlinear) and sac-like aneurismal conditions. The sac-like aneurysm was introduced as bulge in healthy wall through decreasing mechanical properties of wall in its small segment and applying pressure to that weak part. Results demonstrate that in linear healthy artery the circumferential stress is

maximum principal (due to absence of shear stress) and most significant stress; and the media layer is supporting the higher values of stress than other layers. Geometrical nonlinearity causes about 20% stress increase in media and adventitia layers and more than 60% increase in intima's circumferential stress. However, radial stress changes with respect to nonlinearity are negligible. It is being observed that the deformation (shape), wall thickness and stress distribution of aneurysm vary with respect to the fact that which layer or layers have been considered to be diseased. The media layer is most fundamental layer that dominates value of stresses, wall thickness and even size of sac and thus shape of aneurysm. However, the adventitia is also very effective in stress distribution pattern and it incurs to more severe thickness changes than media and intima, especially when it is diseased. Finally diagrams with two vertical axes, correspond to wall thickness and circumferential stress changes, contributed to better interpretation of data and consequently better understanding of natural history of aneurysm. These diagrams demonstrated that tendency of aneurismal lesions to rupture can be evaluated due to biaxial stresses instead of overall size.

Keywords: Aneurysm, Stress, Wall Thickness, Intima, Media, Adventitia, Diseased Layer

ÖZ

BİR BEYİN DAMARININ 3 TABAKLI MATEMATİKSEL MODELLEMESİ VE NORMAL VE ANEVRİZMA OLUŞMUŞ GERİLME ÇÖZÜMLEMESİ

Jodati, Hossein
Yüksek Lisans, Biomedikal Mühendisliği Bölümü
Tez Yöneticisi: Prof. Dr. Mehmet Zülfü Aşık
Ortak Tez Yöneticisi: Prof. Dr. Serdar Geyik

Nisan 2015, 135 sayfa

Beyinsel veya kafatası içi anevrizması atardamar duvarının zayıflaması ve/veya incelmesi sonucunda oluşan odaksal ve kalıcı şişmeyle ortaya çıkan serebrovasküler bir hastalıktır. Torbasal kafatası içi anevrizması gelişiminde yırtılma son aşama olup genellikle ölümcüldür. Anevrizmanın doğal süreci karmaşık mekanik ve fizyolojik olaylar sonucunda oluşmaktadır. Ancak bu durum atardamarın duvarının bileşimini ve gücünü yitirmesine sebep olmasına rağmen, anevrizmaya bağlı yırtılma atardamar içerisinde vuruşsal akışın oluşturduğu gerilmeye dayanımın azalmasından kaynaklanmaktadır. Bu çalışmada, iki boyutlu atardamar duvarı sayısal sonlu elemanlar çözümleme yöntemiyle modellenmiştir. Modelleme sonlu elemanlar çözümlemesi, doğrusal elastik, izotropik, homojen ve viskoz olmayan malzeme özelliklerinin sabit basınç altında sağlıklı ve kesemsi anevrizma durumlarına uygulanmasıyla yapılmıştır. Kesemsi anevrizma duvarın küçük bir kısmının mekanik özelliklerinin zayıflatılması sonucunda oluşan şişkinliğe basınç uygulanarak oluşturulmuştur. Sonuçlar göstermektedir ki sağlıklı doğrusal damarda, dairesel gerilme en büyük ve en önemli gerilmedir. “Media” katmanı diğer

kısımlardan daha yüksek gerilme dayanımına sahiptir. Geometrik doğrusal olmayış "media" ve "adventitia" katmanlarında 20% ve "intima" katmanında 60%'dan fazla dairesel gerilmenin artmasına sebep olmaktadır. Yarıçap yönündeki gerilme değişimi ise yok sayılacak kadar azdır. Damar katmanlarından bir veya birden fazlasının hastalıklı oluşu anevrizmanın şekil bozulmasını, duvar kalınlığını ve gerilme dağılımını değiştirebilir. Gerilme miktarını, anevrizmanın duvar kalınlığını, büyüklüğünü ve şeklini tayin edişinden dolayı, "media" katmanı en temel katmandır. Özellikle hastalık durumunda, "adventitia" katmanı gerilme dağılımını etkilemektedir. Ayrıca duvar kalınlığının değişimini "media" ve "intima" katmanlarından daha çok olmaktadır. Duvar kalınlığı ve dairesel gerilme değişimi içeren iki dik eksenli diyagramlar anevrizmanın doğal gelişim sürecini anlamaya daha çok katkıda bulunmaktadır. Bu diyagramlar anevrizmaya bağlı lezyonların yırtılma yatkınlığının genel büyüklükten ziyade iki eksenli streslere bağlı olduğunu göstermektedir.

Keywords: Anevrizma, Gerilme, Duvar kalınlığı, "Intima", "Media", "Adventitia", hasta katman

To My Precious Parents

AKNOWLEDGEMENTS

I wish to express my deepest gratitude to my supervisor Prof. Dr. Mehmet Zülfü Aşık for his guidance, advice, criticism, encouragement and insight throughout the research.

I am also endlessly grateful to my father and mother for their magnificent love and support.

TABLE OF CONTENTS

LIST OF TABLES

TABLES

LIST OF FIGURES

FIGURES

LIST OF ABBREVIATIONS

ABBREVIATIONS

1D: One Dimensional

2D: Two Dimensional

3D: Three Dimensional

AAA: Abdominal Aortic Aneurysm

CCA: Common Carotid Artery

CTA: Computed Tomography Angiography

DOF: Degree of Freedom

ECM: Extracellular Matrix

FEA: Finite Element Analysis

FEM: Finite Element Method

IA: Intracranial Aneurysm

ICA: Internal Carotid Artery

ISA: Intracranial Saccular Aneurysm

MRI: Magnetic Resonance Imaging

PDE: Partial Differential Equation

SAH: Spontaneous Subarachnoid Hemorrhage

VSMC: Vascular Smooth Muscle Cell

MOTIVATION AND AIM

Although no one can precisely predict the rupture of sac-like aneurysm, nowadays estimation of the potential of lesion to rupture or relative prediction of lesion's rupture rely on maximum diameter or size of aneurysm. There is possibility of overestimation of probability of rupture of large aneurysms as well as underestimation of the risk of rupture of small when this simple geometrical criterion is being used. Indeed, this scale has failed to reply some significant clinical questions, such as "why do some lesions stay dormant for long periods while some others rupture short time after formation?" , "why do some small lesions rupture while the bigger ones stay stable?" or "why does rupture tend to happen at a fundus even when the neck is thinner?

Thus, definition of new criteria for calculation of rupture risk, instead of the nowadays reliable method of aneurysm size, seems essential to identify the patients, who would actually profit from intervention treatments. Regarding the fact that wall mechanics and mechanical factors play substantial role in natural history and possible rupture of saccular intracranial aneurysms, offering biomechanical criteria for failure is desirable. To accomplish that goal, analyzing the effect of each layer of arterial wall on mechanics of wall can contribute to better understanding of natural history of aneurysm, including its failure.

CHAPTER 1

PRELIMINARIES

1.1. Introduction to Cardiovascular System

Cardiovascular system (cardio=heart; vascular=blood vessels), also referred as circulatory system [2], is made up of three components: blood, heart and blood vessels [1]. The heart gives service as pump and generates force to push the fluid (blood) forward and circulate it inside of conducting pipes (blood vessels) that disperse throughout the body. Circulatory system is the first system that fully operates in the embryonic life stage [3]. The system provides a network for rapid-transport of nutrients, dissolved gases (such as oxygen and carbon dioxide), hormones and metabolic wastes of tissues and cells. Without any doubt, the cardiovascular system plays pivotal role in survival of tissues and living organs; because without circulation of blood inside vessel, on one hand, the tissues lack the supply of oxygen and nutrients, and on the other hand, wasted materials and carbon dioxide gas build up inside cells. Such circumstance allows cells to undergo irreversible changes, which quickly leads to apoptosis [4].

Adults, in general, have 4 to 6 litres blood. Approximately, 5 litres of blood is being pumped each minute (about 70ml at each cardiac cycle) by the heart into large network of blood vessels, which are extended over entire body and could access to all tissues and cells [2]. Blood carries the oxygen gas to the tissues and cells from lungs, and carbon dioxide gas, released from those tissues and cells back to the lungs. It, further, supplies the cells with nutrients, absorbed at the digestive tract and/or secreted from liver or adipose tissues. Endocrine glands produce hormones,

which are carried by blood into their target cells. Moreover, blood borne wastes, generated by cells, are carried to the kidney for excretion [4]. Briefly, living cells, tissues and organs cannot function or even live without cardiovascular system.

1.1.1. Blood Vessels

Blood vessels as component of cardiovascular system are divided into five classes: arteries, arterioles, capillaries, venules, and finally veins. The blood is carried away from the heart to the other organs of body by arteries. Elastic, large arteries initiate directly from heart and divide into muscular, mid-size arteries as recede from heart. These muscular arteries scatter into the different organs in the body. As approach to other organs more far away from heart the muscular arteries divide into smaller ones, which branch out into smaller arteries referred as arterioles. After entrance of arterioles to tissues they split up into very tiny, thin vessels named capillaries. The thin wall of capillaries lets the material and gases to exchange between blood and tissue [1]. This action is called diffusion between interstitial fluid around cells and blood inside capillaries [3]. After exchange happened, a group of capillaries rejoin together within tissue in order to build up venules. The small venules amalgamate and construct larger veins, which convey blood from organs into heart. Moreover, blood vessel themselves, as living tissue which requires nutrients and oxygen, are feed by class of blood vessels inside their wall referred as *vasa vasorum* [1].

Blood vessels, on one hand, should be resilient enough to bear pressure changes and enough flexible to move with underlying tissue and organ, and on the other hand, tough enough to remain open and functional under all physiological conditions. The imposed pressure on vessels wall alters as function of distance from heart, and structure of vessel's wall is reflecting this fact. In addition, veins, arteries, and capillaries vary in function, and it is obvious that all the specific structural adaptations have been occurred due to these functional differences. Thus, each class of blood vessels shows distinctive anatomical features, with adjustments based on specific local requirements [3].

1.1.2. Wall Structure of Artery

Artery is composed of two words (ar-=air; ter-=to carry) that means carrier of air; indeed, in the ancient ages, it was thought that arteries contain air because they were found empty in dead corpses. The artery's wall is made up of three layers: tunica interna, tunica media, and tunica externa. The materials, which constitute these layers, the arrangement of constituents, and size of these layers themselves separate arteries from veins and one class of arteries from other ones. Figure 1.1 demonstrates overview of different blood vessels structure with views of walls.

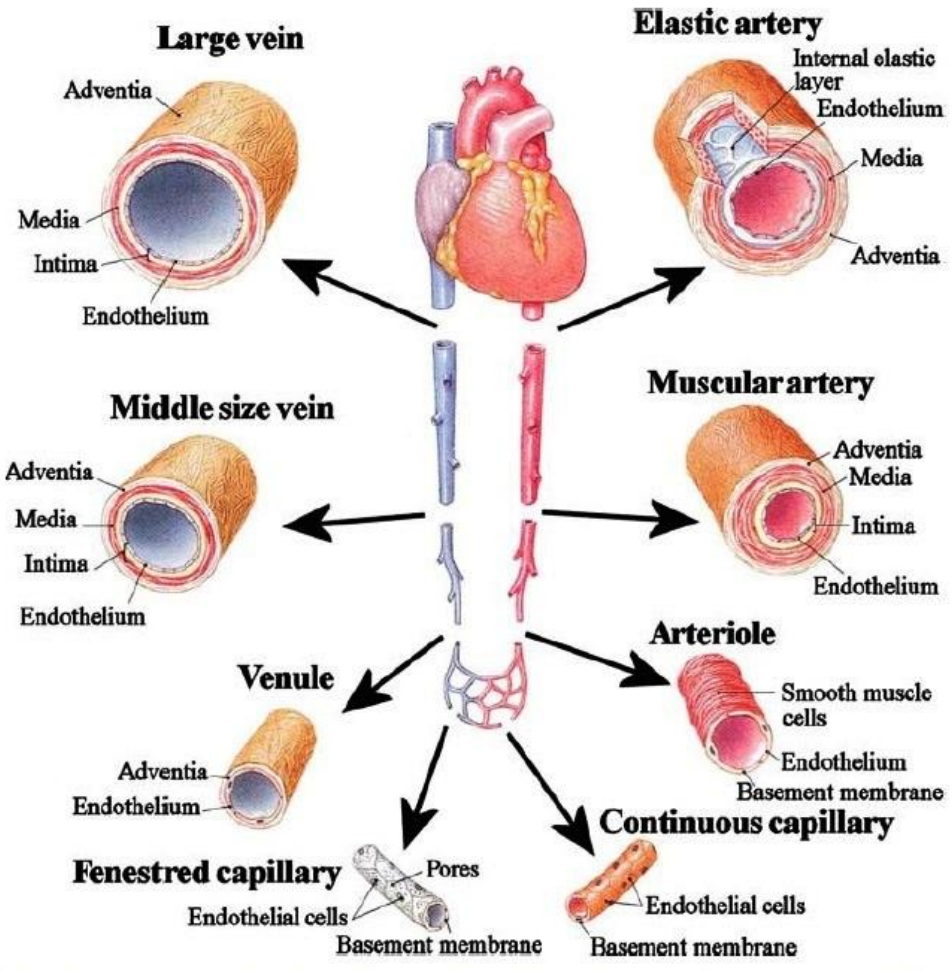

Figure 1.1 Blood vessels structure with views of the walls of arteries, veins and capillaries (adapted from Martini 1989)

The tunica interna or tunica intima is the most inner, and the most close layer to lumen, which is composed of a simple squamous epithelium called endothelium, a basement membrane consists of type IV collagen and laminin, and a layer of elastic tissue referred as internal elastic lamina. Indeed, the endothelium is a continuous, monolayer of endothelial cells, which covers the inner surface of the heart and all blood vessels, lines up in longitudinal direction along artery, and is considered as only tissue that contacts with blood directly; Moreover, it attaches to a basement membrane on the other side [5]. Endothelial cells (ECs) plays important role in regulation of effect of hemodynamic forces on functionality of the artery's wall. Beside barrier to blood flow, they help to the mechanical response of artery.

The tunica media is middle and usually thickest layer and contains vascular smooth muscle cells (VSMCs) embedded in extracellular matrix (ECM), which contains elastin, multiple types of collagen such as type III, and proteoglycans. In fact, it is fibrous helix, with almost circumferential orientation, made up three dimensional (3D) networks of VSMCs, elastin and collagen fibres [6]. Also an external elastic lamina that contains elastic tissue separates media form adventitia. Plentiful elastin fibers, due to extendibility of this specific protein, give arteries high compliance. It means that artery's wall can stretch or extend with no tearing in response to a small increase in pressure (Figure 1.2).

Arterial diameter is regulated by VSMCs activity through vasodilation and vasoconstriction [7]. Smooth muscles of media are connected to sympathetic neurons of the autonomic nervous system. Smooth muscle is being contracted in response to increase of stimulation from these neurons, thus the lumen of artery is narrowing (vasoconstriction). In contrast, when sympathetic simulation reduces or when even specific chemicals, like lactic acid and/or nitric oxide emerge the smooth muscles relax and cause enlargement in lumen diameter (vasodilation).

The adventitia is the most outer layer and composed of fibroblasts, which are embedded in and extensive lattice of collagen, especially type I [8], with some elastin. In healthy artery this layer serves as stiff protective sheath that precludes

over extension of arterial wall. Moreover, this layer acts as primary load bearing layer when media layer is destroyed by some diseases such as aneurysm [9].

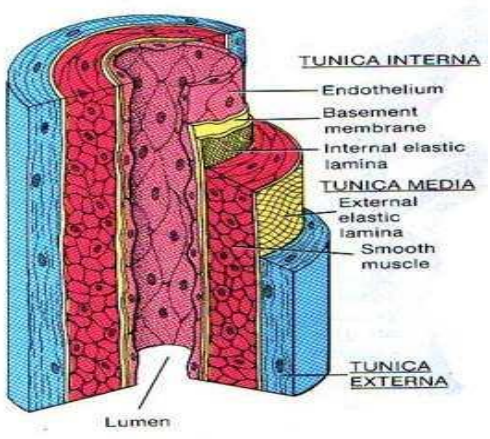

Figure 1.2 General structure of artery

1.1.3. Elastic and Muscular Arteries

In general, elastic and muscular arteries are two different types of arteries. In arteries with diameter greater than 1 cm media layer has a high proportion of elastic fibres, since they are called elastic arteries. Wall thickness diameter ratio is relatively small in these types of vessels. Also, internal elastic lamina is incomplete and external elastic lamina is thin. These arteries contribute to propel blood forward when the ventricles are in relaxing state. When the heart pumps the blood into elastic arteries, their wall is stretching and accommodating the surge of blood. The stretched wall stores mechanical energy as potential energy in itself, and then, as elastic fibres recoil this potential energy is converted to kinetic energy and forces the blood move forward in artery. Therefore, the blood is propelled onward even while the ventricles are resting. The aorta, subclavian vertebral pulmonary, and common iliac arteries are examples of elastic arteries.

Muscular arteries include medium-size vessels, in which diameter ranges from 0.1 to 10 mm. They have media layer with more SMCs and lesser elastic fibres in comparison to elastic arteries. Due to greater capability of vasodilation and

vasoconstriction, these arteries are able to adjust the blood flow rate. Also, their thickness diameter ratio is higher than elastic ones. Internal and external carotid arteries are example of muscular arteries.

1.1.4. Mechanobiology of Artery

Composition and structure of arterial wall are two principle features that determine mechanical properties (e.g. stiffness) of artery. Vascular cells are responsible to maintain structure of artery continuously. Local mechanical environment of these cells guide their functionality. Cellular response to blood flow forces is moderated by extracellular matrix. In fact, the substantial role of ECM in signalling cascade, by which cellular proliferation, migration and apoptosis being regulated, is investable [10]. Cellular mechanosensors are transducing forces into signalling cascade, leading to inter- and intra-cellular responses. For instance, endothelial cells are replying to increased flow (increase of wall shear stress) by increasing the production of vasodilators. Successively, vasodilators cause relaxation of VSMCs and this leads to expansion of lumen, and by that means wall shear stress returns to baseline levels. Regularly repeated stretching of the ECM, resulting from pulsatile blood flow, is changing the degradation and secretion rate of ECM substances and materials by fibroblasts. For example, if there was increase in strain, collagen production would increase and matrix-degrading enzymes would reduce.

This feedback control system, by which stiffness (elasticity) of arterial wall is persistently adjusted via the regulatory activity of the ECs, is very stable, and enables the circulatory system to accommodate the large changes in cardiac output in a very short time. These changes are dictated by increasing request of tissues and organs to oxygen and nutrients in case of doing exercise or any other similar events. Indeed, the rapid response of arterial wall to altered mechanical condition arises from dynamic nature of it. Adaptation to long-term physiological circumstances could also happen in arteries by thickening or thinning of muscular layer, and changing the organization of different assemblies or relative composition of structural proteins; this process is referred as *remodelling* in general. During whole

lifetime of a healthy person, the living constituents of artery's wall should continuously regenerate and remodel in order to tolerate cyclic wall stresses and let the system retains its function and integrity. However, some diseases or other complicated processes occasionally destabilize the stable and dynamic regulatory and remodelling processes and cause extreme disorders like aneurysms.

1.2. Aneurysm

The phrase "aneurysm", from the Greek $\alpha\nu\varepsilon\upsilon\rho\upsilon\sigma\mu\alpha$ (aneurysma), means dilation, and is defined as a localized dilatation of blood vessel; while this blood-filled balloon-like bulge in the wall of a blood vessel is not temporary and reversible [8]. These pathological, permanent dilatations form predominantly in arteries; however, in some cases they also appear in veins and even in the heart [11]. Aneurysms might be classified according to their etiology, location or shape. For instance, with respect to origin or cause of aneurysm, it can be called mycotic, traumatic, atherosclerotic, or developmental [12]. However, aneurysms classification according to their location is more common. Aneurysms have been seen in various sites of the whole vasculature, but the cerebral arteries and abdominal aorta are majority of them. Intracranial aneurysms (IAs) and abdominal aortic aneurysms (AAAs) take roots from different underlying processes and display different potentials to rupture, but still, many histopathological and biomechanical characteristics are same in both of them [13].

1.2.1. Intracranial Aneurysm

Intracranial aneurysm, also referred as cerebral or intracerebral aneurysm is considered as cerebrovascular disorder, in which weakening and/or thinning of artery's wall leads to a focal and permanent ballooning on the artery's wall. It might cause pressure upon adjacent brain tissue or even nerves [14]. Intracranial aneurysms occur in the basic cerebral arteries, but primary near or along circle of Willis, apex of a bifurcation or in the basilar artery [15]. Concise information about

the circularity system of brain contributes to better understanding of cerebral aneurysms. The internal carotid arteries and vertebral arteries supply blood into brain. The posterior areas of the brain are fed by vertebral arteries, while the internal carotid arteries feed the anterior parts. The left and right vertebral arteries connect together to make a basilar artery. Finally, the internal carotid artery and basilar artery connect to each other at the base of brain and form a ring, which is called circle of Willis (Figure 1.3).

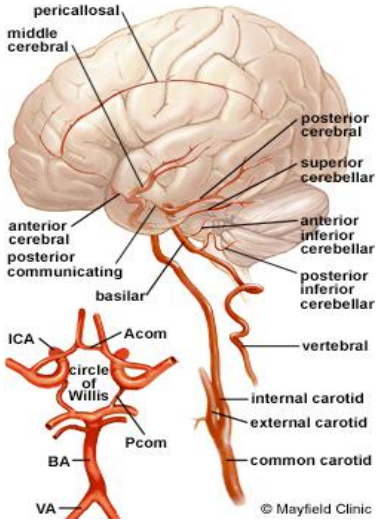

Figure 1.3 Blood supply of brain (side view) and circle of Willis [16]

According to the shape, intracranial aneurysm is divided into two general categories: *fusiform* and *saccular*. The saccular lesions (spherical sac connected to vessel by a neck), unlike fusiform, usually remain dormant up to the time of rupture. Since the saccular cerebral aneurysm incidence reported near 90% of all types [11], the focus of this study will be on saccular lesions (Figure 1.4). About 20% of aneurysms occur in the back (posterior) of the brain, whereas 80% happen in the front (anterior) and middle areas of the intracranial vasculature. In one study [17], the frequency of aneurysms reported as 37% internal carotid artery, 31% anterior cerebral and anterior communicating arteries, 13% middle cerebral arteries, 9% basilar artery, and 5% in the vertebral artery.

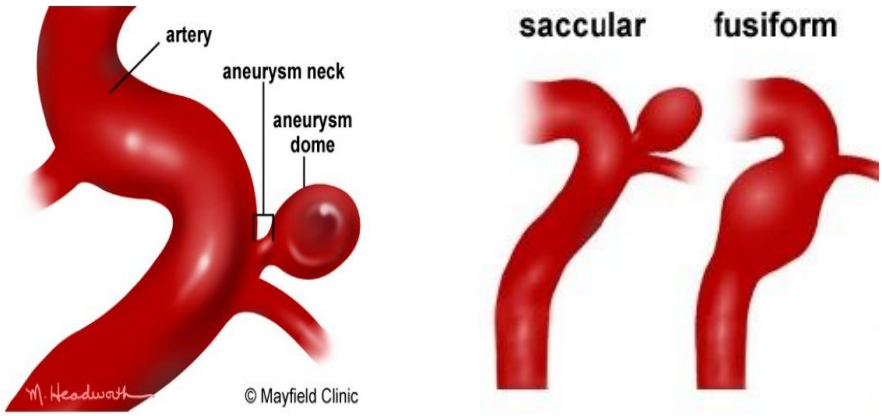

Figure 1.4 Anatomy of aneurysm (left), different types of IAs (right)

Unfortunately, 2% to 5% of the adult population in the industrialized world suffer from saccular aneurysms, ruptured or unruptured [13]. Clinical studies indicate a higher abundance of aneurysms in females (55%-65%) rather than males. In addition, multiple aneurysms have been observed in the 15% to 30 % of patients with aneurysm disease [18, 19, and 20].

1.2.2. Symptoms and Treatment

The physicians are rarely diagnosing SIA at early stages [21, 22]. In most cases, there exist no symptoms until the size of lesion tremendously increases; or they are detected in an incidental test. Interestingly, many unruptured aneurysms have been figured out during examination for some other medical problems. Computed tomography angiography (CTA), angiogram, and magnetic resonance imaging (MRI) are diagnostic exams that contribute physicians to determine the location, size, and type of aneurysms. Double vision, dilated purple, pain above and behind eye, or newly unexplainded headache can be symptoms of unruptured aneurysm, in seldom cases that they shows some symptoms [16].

Sometimes just watching and decreasing the risk of rupture, by control high blood pressure, give up smoking and alcohol assumption are the best cures to aneurysm. For asymptomatic, small, and unruptured aneurysms, imaging techniques might help to follow the lesion’s growth until the size or exposed symptoms dictate other

treatments. For example, observation of patients, who suffer from other health problems, could be the best idea. However, invasive treatments are widely executed when they necessitate. Furthermore, the risk of interventional treatments of unruptured cerebral aneurysms should not be forgotten. Some studies determine <2.5% mortality and <6% morbidity rates for such treatments [23].

Interventional methods, which are used for treatment of intracranial aneurysms, include craniotomy, bypass and coiling. Craniotomy is direct surgical clipping of lesion by placing a metallic clip across its neck; therefore blood would not be able to enter the bulged section (Figure 1.5.a). The titanium made clip remains on artery permanently. This treatment is considered as the most common method, in which general anaesthesia besides small opening of skull is inevitable.

If the artery was extremely damaged and/or the craniotomy was impossible, the complete blocking of the artery, in which aneurysm has been formed, would be option for surgeons. This aim is achieved by inserting of small artery, taken from leg, and detouring blood flow (bypass) around occluded part of vessel (Figure1.5.b).

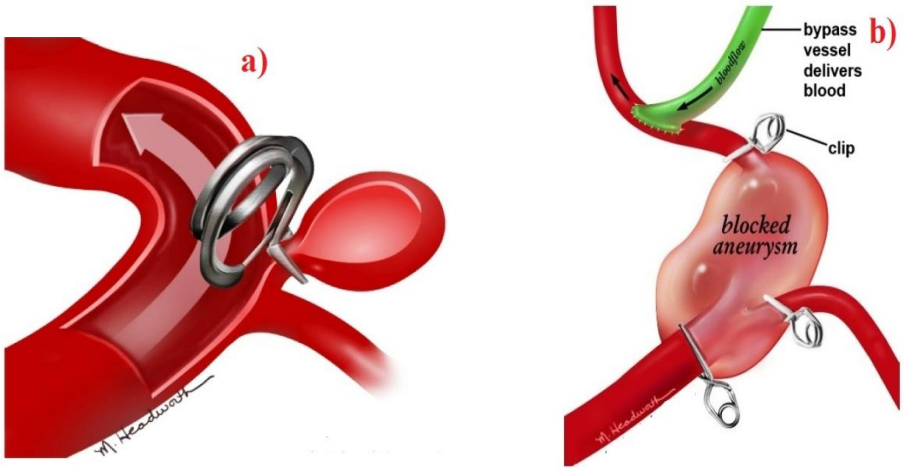

Figure 1.5 a) Clipping technique; notice that arrow indicates blood flow through the artery, but not the aneurysm b) Bypass technique (Taken artery is called vessel graft, connects two ends of blocked artery, and allows blood flows via it)

Two previous mentioned methods need surgery. On contrary, another treatment, which is using minimally invasive technique, is endovascular coiling. For coiling, a catheter reaches aneurysm bulge after inserting into artery in the groin and passing through the blood vessels. Neuro-Interventionalists guide the catheter along the bloodstream via fluoroscope. As the catheter is located inside aneurysm bulge, the lesion is packed with materials, such as platinum (Guglielmi Detachable Coils), hydrocoils, onyx, hardening polymers, or even glue. This procedure stops blood entrance into the aneurysm (Figure 1.6). The bypass technique excludes the sac from the circulation; while other two methods are designed either to reduce the blood flow into sac, or to fully block it [24, 25, and 26]. Notice, all current methods are designed in the ways that just address the mechanical factors. The risk of interventional treatment techniques versus potentially lethal scenario of rupture faces physicians and clinicians with a dilemma, between choosing interventional treatment or to monitor the patient [9].

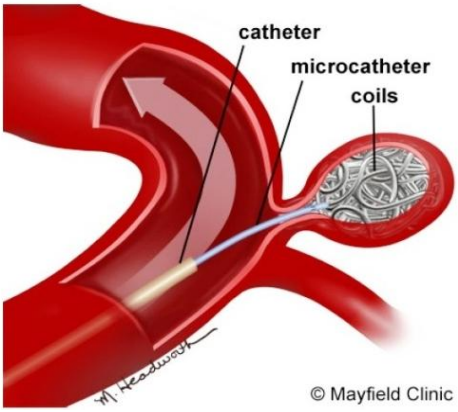

Figure 1.6 Coiling interventional method

1.2.3. Natural History

In healthy bodies, in order to sustain the function and integrity of blood vessel as well as tolerating cyclic wall stresses, remodelling and regenerating of living constituents of arterial wall are inevitable. However, the stability of this system is disrupted by some diseases or any other complicated factors or processes occasionally and causes weakness in a segment of artery's wall. Hence, the wall of

artery bulges and forms aneurysm [11]. The natural history or evolution [9] of saccular intracranial aneurysms is conceptually made up of three different phases: pathogenesis (formation or inception), enlargement (progression), and rupture [15].

Once the aneurysm initiates, weakened portion of artery' wall is gradually inflating due to hemodynamic forces inserted by pulsatile blood flow. During enlargement, the wall's composition, strength and geometry are deteriorated progressively. Recall that the artery's wall is in a repetitive state of remodelling and growth as response to changed mechanobiology [13]. Suddenly, when the expanded arterial wall fails to bear the stresses, it ruptures and causes to internal hemorrhage. In fact, the rupture of aneurysm is considered as leading cause of spontaneous subarachnoid hemorrhage (SAH).

SAH is a life threatening type of stroke, leads to high rate of morbidity and mortality because of its dangerous sequel (cerebral vasospasm).In 35%-50% cases, the patients with SAH pass away [17,20,27]. For example, in one study [28] fatal rate of SAH documented 45% and 30% of survivors suffer from severe morbidity.

1.2.3.1. Pathogenesis

Of course there exist several hypothesises about the genesis of saccular aneurysm, but there is not much consistency. Nevertheless, the substantial role of mechanical factors (e.g. wall mechanics or hemodynamic forces) is unavoidable. Some factors are increasing the susceptibility of cerebral arterial wall to local weakening under repetitive action of hemodynamic loads including lack of external elastic lamina[29], devoid of supporting surrounding tissue, existence of sparse Medial elastin, and structural irregularities at the apex of bifurcations[30,31 and 32].

The last consensus about genesis of aneurysm states that genetic structural or biochemical flaws, infection or diseases, aging, hemodynamic, and some other risk factors unleash complicated and interrelated degenerative biological processes [11], those finally cause to formation of aneurysm. As general concept, saccualr

intracranial aneurysm (SIA) is created when the media and the internal elastic lamina are significantly degrading or fragmenting [33, 34, and 35]. Few decades ago, it was thought that syphilis infects the arterial wall, via accommodation of bacteria (e.g. Clemencia Pneumonia) from bloodletting, or from infected heart valve, and causes aneurysm. But now, these wall degrading primary causes have been markedly reduced and substituted with other factors. Nowadays, Mycotic infection, high blood pressure, genetic disorders, smoking, and aging are examples that predominantly increase probability of aneurysm formation.

In some population, increasing familial morbidity of SIA, up to 12%, convinced scientists that genetics also has role in formation of lesion. Sometimes, the inherited flaw disrupts the normal synthesis of particular types of collagen, which successively leads to weakening of arterial wall [36, 37]. For instance, patients who suffer from SIA are more likely to have less collagen type III [38]. In general, Marfan's and Ehlers-Danlos's Syndromes [39] are two genetic collagen vascular disorders that responsible for formation of aneurysm. As consequences of these rare syndromes, structural proteins (collagen and elastin) cannot be synthesized and/or organized normally, and resulting in pathological weakness of arterial wall.

The anatomic differences of circle of Willis are thought to have inherited origin. Surprisingly, about 60% of the population devoid completely closed circle. Therefore, the asymmetric structure of circle of Willis, might lead to distinct hemodynamic stresses [27, 40], which ultimately may cause different tendency for aneurysm formation.

However, other potentially possible inherited and genetic agents have not been figured out. For instance, various studies have not succeeded to find a connection between mutation in any of basic candidates , such as genes for fibronectin, fibrillin-2, lysyl oxidase, α1-antitrypsin, matrix metalloproteinases (MMP-1, -3, -9, -12), tissue inhibitors of MMPs (TIMP-1,-2, -3), endothelial-derived nitric oxide synthase, or prostacyclin-stimulating factor, and aneurysm [41-46].

Some risk factors render cerebral arteries more vulnerable to formation of aneurysm. Alcohol consumption, cigarette smoking, hypertension, and prolonged oral use of analgesics and/or contraceptives are some of them [47, 48, and 49]. Among the risk factors hypertension is centre of attention in many studies. The occurrence rate of hypertension has been reported twice as often in patients with aneurysm rather than in patients without. There was wrong attribute that Atherosclerosis is one of the main causes of wall degradation in aneurysms. Nevertheless, over past two decades the reliability of this hypothesis has been questioned frequently [50]. Moreover, despite the fact that influential mechanism of smoking is not clear, but it is considered as important risk factor [51].

In the hypothesis, proposed by Nichols and O,Rourke [94], The fatigue failure of the wall components is used as foundation for mechanism of degenerative arterial dilatation with known risk factors such as hypertension. In the presence of this risk factor, which acts as accelerated form of aging, fracture in load-bearing elastic sheets is observed due to the fatigue of cycle stresses. Inert and stable elastic sheets (with 40 years mean lifetime), under the cyclic increased fatigue stresses due to hypertension, are experiencing reorganization in the polymerized structure of elastin fibers and sheets, leading them to fail at less tensional stresses than those they are normally can resist.

The elastic sheets and fibers rip up and some elastic coils disappear, leads to permanent continuing dilation of artery. Then, remodelling process is accompanying permanent stretching of smooth muscles, and as consequence of remodelling the collagen content increasing in muscular media layer. Formation of aneurysm is the ultimate result of such process. Notice that the fatigue-like remodelling hypothesis emphasizes on interplay among pathological changes and mechanical stimuli, resulting from hypertension or other risk factors, and needs more researches.

1.2.3.2. Enlargement

After aneurysm initiated, the small permanent out-pouching appears on artery's wall. That small dilation is often enlarging to 5-10 mm in diameter [13], and might grow up to 30mm [15]. Meanwhile, bulged lesion contains very complicated shape and composition. Previously, some hypothesises suggested that the dilatation's expansion rate is high, and due to structural instabilities, referred as limit point instability or resonance, the lesion expands very quick [52-55]. On those researches, the material properties of arterial wall has been assumed rubber-like or linear; while recent studies, which use nonlinear material properties, reject such instabilities [56, 57].

Some aneurysms enlarge at specific undetermined rate, although some others grow rapid at first then the speed of expansion is decreasing after certain point. Because of variational expansion rates, some lesions remain almost the same size for years; however, some others expand substantially during a few months [58].

Briefly, according to a statistical study [59], SIAs experience a short period of rapid enlargement and potential to rupture soon after formation, whereas those that remain unruptured present lower risk of rupture for a longer time. For optimal clinical management of SIAs knowing expansion rate of aneurysm is probably the most precious information needed, therefore this idea encouraged a large number of multidisciplinary researches. Blood flow pattern of SIA differs from other aneurysm types (e.g. fusiform abdominal aortic aneurysm), due to their location either on the side walls of bent arteries or at the apex of bifurcations. Three-dimensional flow pattern, which is formed by entrance of blood flow into the circumscribed sac, includes one or two 3D vortices (Figure 1.7). This rotational flow pattern continues even through diastolic stage of cardiac cycle [60]. Persevering non-vanishing circulation coupled with constant flushing off of the blood inside sac is preventing the thrombus formation. On contrary, formation of thrombus is a problem that clinicians deal with in AAAs.

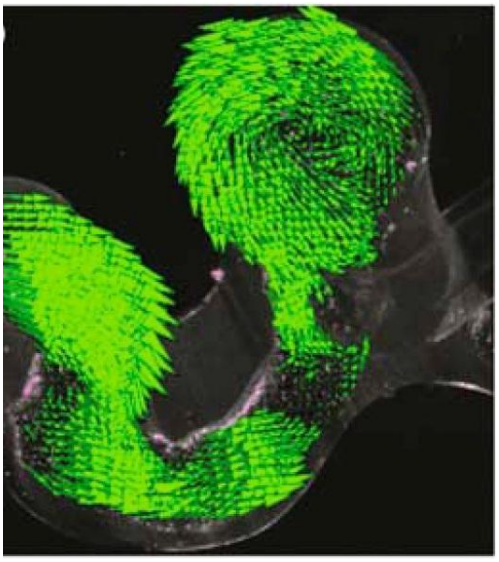

Figure 1.7 Instantaneous velocity field in a longitudinal plane; the measurements were obtained by digital particle image velocimetry (DPIV) and correspond to peak systole. [60]

Several experimental and numerical studies have been executed in order to discover a relationship between temporal and spatial changes of flow-induced shear stresses on the endothelial cells of sac wall and aneurysm expansion rate [60, 61, and 62]. Devoid of comprehensive quantitative models, which explain behaviour of the endothelial cells as function of abnormal changes in flow-induced shear stresses, caused all those studies were not be able to contribute to the clinical management of aneurysms.

Then, according to those studies, hypothesis that enlargement rate is controlled and governed by endothelium mediated mechanism, was more unlikely to be correct. Verification of the fact that muscular layer of media is absent at the later stages of enlargement of SIAs [11] increased the doubt on this mechanism's effect. In other words, flow influenced shear stress appears less determinant factor in expansion rate [11, 95]. However, new studies about intracranial aneurysm, by Watton, emphasize on effect of low wall shear stress on mechanobiology of IA evolution [9].

Indeed, for saccular intracranial aneurysms, it seems that the understanding of dynamics of the ongoing and developing remodelling process of the structure of arterial wall under influence of internal blood pressure must be used as base for the prediction of expansion rate. Therefore, discussion of remodelling of arterial wall due to increasing tensile stresses can seem logical.

After aneurysm formed, the median layer is being subjecting to permanent stretch, and remodelling process occurs at the same time. Throughout remodelling process, the collagenous content in the muscular layer is increasing, makes the wall stiffer [95, 96, and 97]. As the arterial wall distended and stiffened, the indelible stretched smooth muscle cells would be excluded from cyclic stimulation, which is essential for synthesis of connective tissue and their normal proliferation. In turn, this process results in progressive loss of connectivity and the apoptosis of smooth muscle cells. Finally, gradual thinning of wall and ultimate destruction of muscular layer happens. Recall that whole process resembles the fatigue remodelling hypothesis about pathogenesis of aneurysms [98, 99].

To satisfy such goal, analysis of tensional stresses on the wall of lesion, generated by internal pressure, is essential [11]. Moreover, occasionally-noticed high-frequency vibration of the wall, and small peak systolic pressure change inside sac could affect remodelling and expansion rate of aneurysm. Nowadays, determination of expansion rate, due to lack of precise data about lesion's wall thickness and composition, and exact remodelling quantitative model of enlargement process, seems out of reach. In other words, the requirements to predict expansion rate of aneurysm include magnitude of the change in the systolic pressure inside of sac, geometry, composition and material properties (e.g. stiffness) of lesion's wall, dynamics of the arterial remodelling, appropriate initial and boundary conditions, and tensional stress analysis [11].

1.2.3.3. Rupture

The rupture is the final phase in natural history of SIAs, and it is generally lethal. Gratefully, only 0.1% to 1% of diagnosed intracranial aneurysms undergo rupture every year [76]. Many aneurysms might remain unruptured and asymptotic for years; however, the small percentage is more likely to rupture throughout the fifth and seventh decades of life. 52 years old is the mean age at which rupture occurs [77]. According to one study [78], after 10, 20, 30 years, at which the aneurysms have been diagnosed, the maximum chances of rupture are 10%, 25%, and 32% respectively.

The rupture may happens in two ways, either as catastrophic rend in a part of lesion and substantial bleeding, or transient leak and small bleeding, in which a fibrin patch generally seals the wound up. Although the histomechanical mechanisms of failure have been not revealed yet, rupture is being a mostly observing at the fundus (Figure 1.8), despite of the thinner neck region [79, 35]. Interestingly, on contrast to histopathology of other portions of lesion (recall that they are composed of collagen in distinctive layers with different orientations), in the fundus area of spherical ones, orientation of all collagen layers are spanned at same angle. This could explain the isotropic response of fundus and consistent with axisymmetry necessities in mechanical analysis [37].

Furthermore, the larger one would generally rupture first, if there was more than one aneurysm. In the case of existence of several aneurysms with almost same sizes, the rupture occurs usually in the proximal one first [79, 80]. Many studies tried to find out the effect of different physical factors on rupture potential. For instance, due to study done by Asari and Ohmoto [82], it thought that amalgam of lesion shape (such as being multilobular or not), location (like middle or interior cerebral arteries), and excess loading (e.g. presence of hypertension) represent the higher rupture risk.

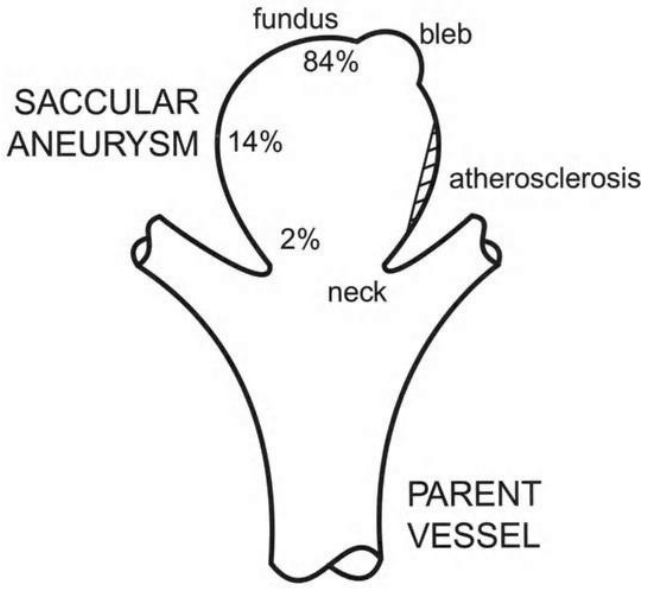

Figure 1.8 Saccular aneurysm illustrating the neck and fundus with possible factors such as presence of bleb and atherosclerosis. The numbers represent the percentage location of rupture based on studies. Note that intima thickening might be the first symptom of atherosclerosis; proliferating SMCs, activated macrophages, and lymphocytes are major signs of advanced atherosclerosis. Also, the disease is considered as result of aneurysm not its pathogenesis. [15]

Considering other studies, it has been documented that there are more rupture chance in multilobular lesions and less-common posterior aneurysms [83]. Increasing asymmetric contact between saccular aneurysm and its peripheral tissue in posterior cerebral arteries might expose those arteries more prone to rupture [84]. Indeed, symmetric contact constraints are thought to have potentially shielding role on sac-like aneurysms [85]. Overall, all aspects of natural history, rupture potential included, are influenced by Lesion location, due to alteration in inlet flow stream, and consequently changes in intra-aneurismal hemodynamic and followed mechanobiology responses [86]. For instance, if heterogeneities appear in shear stress of wall, the collagen will be produced in changed pattern and/or rate, and finally will lead to local wall weakness [87].

Many pathological and clinical studies give a special prominence to aneurysm size, and found the rupture potential on the maximum dimension of lesion, which is estimated that its critical value is varying between 3-10 mm [88, 89]. Although

from mechanical perspective shape and wall thickness are playing more significant role in determination of stresses as the membranes distend [92], surprisingly, few data has been documented about them in literature. Maybe using shape as theoretical predictor of rupture potential for specific type of aneurysm is reason to this devoid of regard. Regarding to one study [88] 59% of aneurysms are outlined round, 24% oval, and 22% bar-like. Also, tendency of lesions to have greater neck/height ratio, and consequently large rupture incidence, in women has been reported [90].

About thickness of aneurismal wall, few reports ranged it among 30 to 500 μm in the unloaded configuration [91]. Aneurismal wall thickness is not essentially uniform. Previous study on 23 unruptured saccular lesions has divided aneurysms into 4 groups with respect to their wall thickness: thin at neck but variable elsewhere 43%, uniformly thin 22%, which are generally are smaller than others (less than 2mm in radius)[82], thick at fundus but having thin neck 17%, and thick at neck but variable at other portions 18%.

Nowadays, the rupture risk is only estimated according to aneurysm size or dimension [11]. Cardiovascular surgeons find this method more reliable in comparison with other ones. For instance, in case of AAA, if the diameter of aneurysm be about 5 cm and expansions rate oversteps 0.5 cm/year interventional surgical treatment will be executed [93].

There is no consensus about the critical size or shape that surgical interventional treatment to be recommended after lesion expanded beyond; however, the size is only criteria that is considered today. Therefore, pivotal need for development of patient-specific standard, which could weigh surgical interfere risk against rupture probability, is avoidable.

1.2.3.4. Histopathology

It is appropriate now to mention a little bit about histopathology of aneurysm. SIAs growth most probably happens through mechano-regulated remodelling processes and resembles other arterial adaptations, such as response to sustained high blood pressure, or altered blood flow [15], [63]. Peter declard that: “aneurismal dilation results in a highly dynamic cellular environment in which extensive wound healing and tissue/extracellular matrix remodelling are taking place” [23].

Since small saccualr aneurysms are composed of an endothelia layer and thin adventitia layer, it thought that collagen type I is basic structural constituent of those lesions. Some documents approve the slight thickening of endothelial cells. Moreover, increased endoplasmic reticulum indicates deposition of collagen type IV and adhesion molecules (e.g. fibronectin and laminin). Increased replication of endothelial cells accompanied with above mentioned raised synthetic activity helps to cover the growing inner surface of the sac. Thinly scattered irregular smooth muscle cells might have role in regulating the intramural collagen, although this goal is achieved predominantly by fibroblasts.

Notice that the dynamic equilibrium between collagen deposition and degradation carries out that regulating task. Some articles demonstrate significant increase in protease activity [64-67], MMPs, and tissue inhibitors (TIPs) in aneurysms rather than in nearby cerebral vascular [66, 68, and 69]. These heightened activities might cause to reduce collagen type III and V in aneurysms. Presence of more immature collagen, which has less stable cross links, as result of heightened turnover of collagen type I, might attenuate lesion’s strength [66, 70]. In fact, fibrillar collagen primarily determines lesion’s strength, while macrophages, fibroblasts, occasional small patches of smooth muscles, and cellular remnants have less effect. As the aneurysm expands, it thought that intramural macrophages accrue some lipids, especially on lateral area of sac.

Mechanical properties of the wall, hence enlargement as result, not only depends extremely on the type and volume fraction of collagen, but also collagen's cross link density and orientation within the lesion' wall are considered as key factors. P.B Canham and his colleagues used two microscopic tenchniques, which are based on birefringent (optical) properties of collagen, to examine the effect of cross link density and orientation of collagen on wall's mechanical properties.

First, by using Senarmont compensator they measured the intensity of the birefringence, which indicates the cross link density and collagen fibers size; second, the installed universal stage attachment on a polarizing microscope made them able to determine the 3D orientation of collagen fibers [72]. Furthermore, other studies suggested that there exist regional variation in collagen orientation, so new collagen is deposited in the inner wall of lesion. This idea was later aliened with Canham reports [72-74]. Collagen on aneurysm wall is less wavy when perfusion-fixed at physiological pressure that leads to circle trajectories that makes lesions less distensible in comparison to parent vessels. The wall contains seven to eight distinctive layers; almost parallel fibers (± 8 degrees) in each layer. Orientation of fibers is changing suddenly from layer to layer, almost in opposite direction (Figure 1.9).

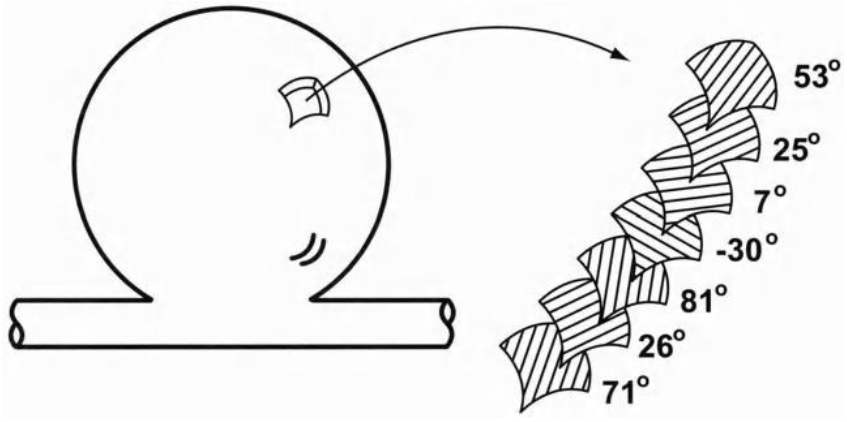

Figure 1.9 Layered structure of collagen in saccular aneurismal wall [15]

Ultimately, according to studies [70] and [75], it has been documented that thin-walled portions of sac is governed by stronger collagen; while abundance of weaker and more immature collagen in thicker- walled regions are apparent. Notice that the deposition of weaker new collagen in the inner regions of wall might partially be impressive factor in this process. Intensity of birefringence along wall thickness in aneurysm is depicted in Figure 1.10. The intensity, which represents wall strength, is decreasing from outer toward inner wall. Note the strength of outer wall still is less than adventitia layer of adjacent parent arteries. Altogether, they declare that "aneurysms are well designed and mechanically stable in general, and their wall might compose of newly polymerized collagens and reorganized fibers from the earlier developing lesions."

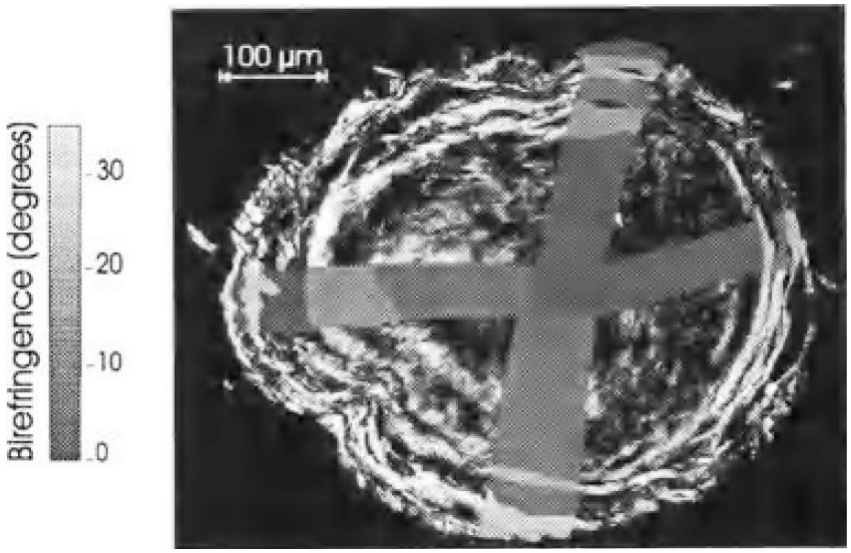

Figure 1.10 Regional variation of intensity of birefringence in the aneurismal wall; greater stiffness (brighter regions) near the outer wall [70]

1.2.4. Stress Analysis

Noticeably, few thorough studies about static response of the aneurismal wall to applied loads have been documented in literature. However, simplified elasticity based analyses such as models of latex balloons [100, 101] or constitutive relations about behaviour of rubber-like [55] or linear materials [52, 102] have been reported.

1.2.4.1. Analytical Results

Laplace equation was primarily being used in the biomechanical studies of saccular cerebral aneurysms. It is valid for whole class of homogenous, isotropic, spherical membranes; and since the equation is evoked from equilibrium equations it can be considered independent form constitutive material models ($\sigma = P\,r/2h$, here p is transmural pressure, h is wall thickness, r is pressurized inner radius, and σ is uniform in plane wall stress). Critical diameter d_c for lesion rupture estimated by Canham and Ferguson [103] was based on Laplace's equation. The volume of aneurismal tissue has been assumed constant ($V_a = 4\pi r^2 h$). With respect to values $V_a = 1mm^3$, $\sigma_c = 10MPa$, and $P = 150mmHg$ the critical diameter value has been reported $d_c = \left(4\sigma_c V_a / P\pi\right)^{1/3} = 8.6mm$.

Moreover, Humphrey and Kyriacou [104] based their study on this equation in order to examine mechanism of aneurysms .Also, Meng [105] stated that rupture potential of daughter aneurysm only relies on two geometric parameters about size of its orifice. In despite of useful insights that have been yield by Laplace's equation, it apparently supports quasi-static inflations of spherical membranes and cannot be used to address complex geometries, elastodynamics, tendency of rupture at the fundus, or evolution of aneurysms.

In-vitro pressure-volume test on seven saccular intracranial aneurysms came by autopsy, has been executed by Scott [106]. The results were fit by 2D (two dimensional) Fung exponential strain energy function ψ [56]:

$$\psi = c(e^{Q} - 1), \quad \text{where} \quad Q = c_1 E_{11}^2 + c_2 E_{22}^2 + 2c_3 E_{11} E_{22} \tag{1.1}$$

c and c_i are material parameters, E_{11} and E_{22} are principal values of Green strain, and ψ is Fung-exponential strain energy function, which is used to obtain stress-strain relations. Scott reported critical stress σ_c ranges from 1 t 2 MPa. These data are still global and one 1D (one-dimensional) thereby has no apply in evaluation of

local properties or anisotropy. Some other researchers tried to investigate mechanical properties of human aneurysms by performing uni-axial tests [107, 108]. Steiger documented critical stress value between 0.5 and 1.2 MPa. Moreover, Hsu [109] developed a video-based tri-plane system that measures local in-plane strains and curvatures at multiple pressures.

A series of nonlinear elasticity studies were started by Humphrey and colleagues in 1994 in order to examine three biomechanical hypotheses: material instability of saccular cerebral aneurysms [54], dynamic instability of them [53], rupture potential prediction by critical size alone [88]. Restrictions of all these studies, besides approach of Shah and Humphrey [110] were homogenous and in-plane isotropic behaviour of tissue (even no constitutive model were applied explicitly), and uniformity of the computed stress and strain fields. For example, the latter proposed that every material point has equal potential to fail, which is against propensity of fundus to rupture.

1.2.4.2. Finite Element Analysis Results

Although studies that based on perfectly spherical geometry enlighten remarkably many aspects of aneurysms, request for materially and geometrically more realistic studies is still inevitable. In order to approach this goal, Humphrey and colleagues offered nonlinear finite element analyses of class of idealized axisymmetric saccular aneurysms [111, 112]. The assumptions include uniformly pressurized lesions, a truncated elliptical or spherical geometry, initially uniform wall thickness, Fung-type material (constitutive) equation, and clamped boundary condition at the neck. Moreover, stress-strain behaviour has been considered from homogeneous and isotropic to heterogeneous and anisotropic. Recall that the solution for class of axi-symmetic membrane inflation could be obtained via solving simultaneous differential equation via for example Runge-Kutta methods [92].

Figure 1.11 demonstrates deformation and Cauchy stresses for three lesions with various initial geometry. However, thickness, initial lesion volume, isotropic

material, boundary conditions, and quasi-static pressure are same for all cases. A/B represents the geometrical shape of lesion via ratio of the values of aneurysm bulge on major axes in cylindrical coordinates. Figures a-c illustrate deformed (solid lines) and undeformed (dashed line) shapes at two different pressures (80 and 160 mmHg) for elliptical and spherical lesions. Figures d-f show principal Cauchy stresses, circumferential (dashed curve) and meridional (solid curve) against arc length (S/L). For instance, circumferential stress is lower than meridional when $A/B\langle 1$(vertical ellipse), while it is higher when $A/B \geq 1$. From Figures 1.11 it is obvious that the highest multi-axial stresses happens at fundus when A/B ratio is highest, but theses stresses happen around L/S=0.7 when A/B is less than 1; and stresses are uniform along large portion of domain when A/B=1.

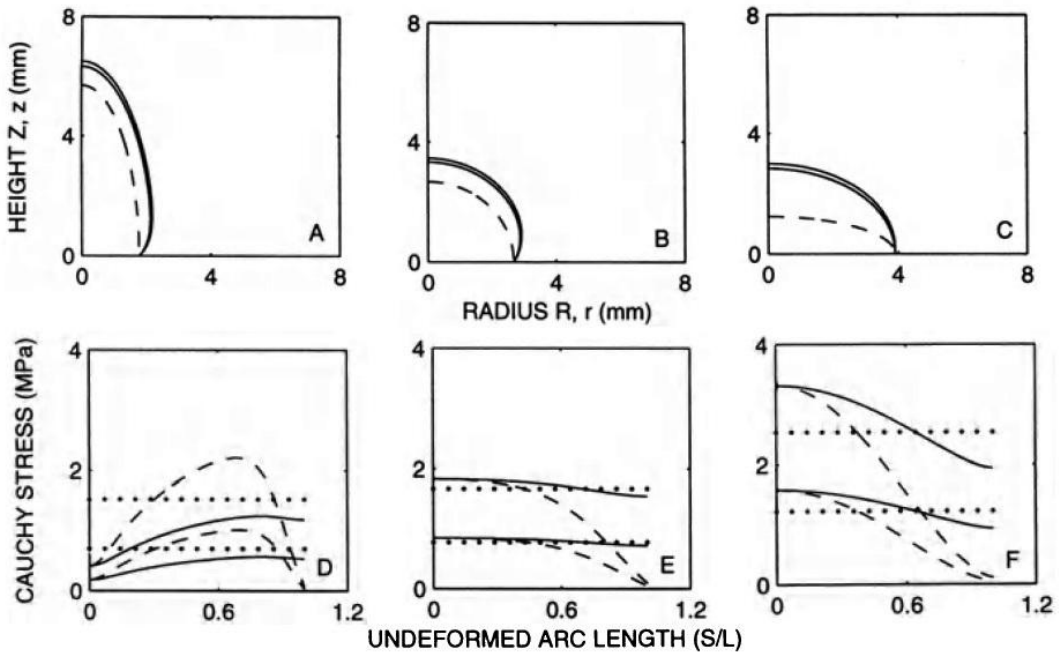

Figure 1.11 Finite element results of stresses in three axi-symmetric aneurysms with isotropic and homogenous material properties. S/L=0 means fundus of lesion and S/L=1 represents neck. In right column figures A/B is greater than 1 (vertical ellipse); in middle column figures the A/B is equal to 1(sphere); and in left column figures the A/B ration is less than 1 (horizontal ellipse). a-c: solid curve represents deformed configuration in 80 and 160 mmHg, and dashed lines show unloaded configuration. d-f: solid lines represent meridional direction while the dashed curves show circumferential one; and dotted lines mean results according to Laplace's equation. [113]

Nonlinear finite element studies revealed that Laplace's equation, solely in case of lesions with small neck and almost spherical shape, leads to rational results in idealized axisymmetric saccualr aneurysms [56, 113]; and it is not suitable for cap-like lesions. Although the rupture generally happens at the fundus, FEA done by Humphrey and colleagues revealed that maximum normal stress could happen either in the fundus, or at the neck, even in the equatorial domain between these two due to variations in the material properties or geometry. But still, in many cases, maximum multiaxial stresses take place in fundus or near it, no matter that if material behaviour is either isotropic or anisotropic, which has been proved experimentally [108]. Note that shear stress estimated almost zero or very small near fundus, so most probability the failure is not happening because of shear stresses. This hypothesis aligns with the studies that claim vessels are more likely to fail in extension [118, 119].

Analytical analyses demonstrated that for this subclass of aneurysms, described by either STZC- or Fung-type stress-strain relations, there is no limit point instability [114]. Dynamic instability might be triggered from static instability; numerical studies [110, 114] (using method of nonlinear dynamics and a Runge-Kutta solution of nonlinear differential equation of the elastodynamics) prove that virtually spherical lesions likely to show dynamic stability. Therefore, for nearly spherical cerebral saccular aneurysms neither dynamic nor static instabilities are unlikely to cause enlargement or rupture.

Moreover, sub-domain inverse finite element analysis, which has combined nonlinear finite elements with a Marquardt-Levenberg regression, was developed in order to deduce best values of material parameters [115]. With respect to that information from four unruptured aneurysms, the best-fit values of material parameters reported as $c = 12.6$ N/m, $c_1 = 10.74$, $c_2 = 13.08$, $c_3 = 11.02$, by which mathematical and physical constraints, like convexity, is being satisfied (recall equation 1.1).

Although aneurysm size is still being considered as one of the most regular clinical meters used to estimate rupture potential, a critical diameter of lesion stays as controversial subject. For axi-symmetric aneurysms principal Cauchy stress resultants, such as circumferential and meridional, are function of transmular pressure and principal curvatures (κ_1 and κ_2), not general size; and are expressed in closed form as [116]:

$$T_1 = \sigma_1 h = \frac{P}{2\kappa_2}, \qquad T_2 = \sigma_2 h = \frac{P}{\kappa_2}\left(1 - \frac{\kappa_1}{2\kappa_2}\right) \tag{1.2}$$

In fact, a reason that there is no consensus on critical size might be ignorance of curvature. Finite element analysis of subclass of axi-symmetric aneurysms has demonstrated the importance of this postulate [56, 85, and 113]. For instance, the large lesion with a small neck-height fraction (A/B less than 1) has lower stresses than small lesion with a large neck-height fraction. Lower stresses in large lesions can be explained as results of interaction between surrounding tissue and lesion, which act as contact constraints and reduce the maximum stresses. Also, FEA results manifest that if material symmetry was altered continuously from fundus to neck, the non-equibiaxial and non-homogenous distributions of stress in axi-symmetric lesions would be brought back to almost equibiaxial and homogenous stress state, but for boundary layers [63].

All those discoveries emphasize on teleological hypothesis that saccular intracranial aneurysms could grow and remodel (through collagen turnover) in order to restore the biaxial state of stress, which cells and tissues in the normal arterial wall experience, if arterial wall underwent local perturbation in mechanical properties (material properties such as loss of smooth muscle cells or elastin), and so geometry.

All in all, computations proposed that in SIAs dynamic and material instabilities don't lead to enlargement, and dimension of lesion (size) cannot primary represent the rupture potential; rather, anisotropic material properties and curvature govern

the distribution of intramural stress . As beginning point, the idealized models are very useful for validation and build general insights into investigated subject. However, finite element models, which are based on more precise geometric and material assumptions, are essential to figure out wall stresses of saccular aneurysms. Recently done study by Ma [117] is very important step toward this goal.

CHAPTER 2

MATHEMATICAL MODELLING

Vascular biology and histology, geometry (e.g. wall thickness), wall composition hence mechanical properties such as stiffness, blood flow dynamics (hemodynamic), wall's mechanics, cell population, genetic, and signaling pathways, as well as their complicated interactions, evolution, and/or change during progression of aneurysm, are multiple factors that play role in aneurismal natural history. Mathematical model may assist physicians to obtain fundamental insight into natural history, including pathogenesis and etiology, expansion, and rupture of saccular intracranial aneurysms.

Developments in vascular biology, biomechanics, computational methods, and medical imaging offer scientists a unique and favourable occasion to develop mathematical models and apply them in order to elicit valuable precise information about natural history of intracranial aneurysms, such as identify the rate at which the aneurysm grows, or determinants of rupture potential. In addition, these models contribute to ameliorate design of medical instruments or artificial organs, and determine clinical strategies. The significance of theory for revealing guides to execute and interpret experimental studies is obvious. Indeed the theoretical frameworks can also offer discriminating ideas to guide effective and sufficient empirical data collection. Although some key questions (e.g. in which rate does aneurysms expand? or when does it rupture?) have not been conclusively answered, efficient advances in the comprehension of related biomechanical processes, and qualitative realization of task of many previously cited factors have been achieved during past few years. Especially, fundamental role of biomechanics and its

application to SIA research has universally accepted and grown extensively in the recent years [8, 120].

In the present chapter, section 1 includes deriving governing equations and boundary conditions of schematic partial annular structure, which resembles blood vessel, by using minimum total potential energy method. In sections 2 and 3 the mechanical properties and geometry of arteries in different studies have been investigated. Section 3 consists of finite element analysis of healthy carotid artery in physiological range of blood pressure. Finally, section 4 is dedicated to finite element modelling of aneurismal artery.

2.1. Governing Equations and Boundary Conditions

The phrase "variational methods" refers to methods that make use of variational principles, such as the principle of virtual displacements, to determine approximate displacement as continuous function of position in the body. Variational principles has to do with the minimization of functional, which includes all the intrinsic features of the problem, such as governing equations, boundary and/or initial conditions, and constraint conditions.

Variational formulations can be useful in different related ways. First, there are problems that can be formulated by other means, such as by vector mechanics (e.g., Newton's laws), but these can also be formulated by means of variational principles. Second, variational formulation forms a powerful basis for obtaining approximate solution to practical problem [49]. If it was possible to write the energy of system as an integral functional, then the minimization of that functional via using variational principles would make us able to obtain governing equations and boundary conditions of that system. As an example, a total potential energy of system can be written in the integral functional form.

A minimum total potential energy is a special case of the principle of virtual work that deals with elastic (linear as well as nonlinear) bodies. If we define the potential

energy of applied loads, V, and the strain energy, U, then the sum $U+V$ is called the total potential energy of elastic body (Eq.2.1). The equation (2.2) is known as the principle of minimum total potential energy.

$$\Pi=U+V \tag{2.1}$$

$$\delta\Pi=\delta(U+V)=0 \tag{2.2}$$

For elastic bodies (in the absence of temperature variation), there exists a strain energy density function (U_0), which is a function of strains at a point and assumed to be positive definitive. Thus:

$$\sigma_{ij}=\frac{dU_0}{d\varepsilon_{ij}} \quad \Rightarrow U_0=\int_0^{\varepsilon_{ij}}\sigma_{ij}d\varepsilon_{ij} \tag{2.3}$$

For linear elastic materials:

$$U_0=\frac{1}{2}\sigma_{ij}\varepsilon_{ij} \tag{2.4}$$

where σ_{ij} and ε_{ij} are stresses and strains in different directions respectively. In order to calculate strain energy it is necessary to compute the strain energy function over volume of domain:

$$U=\iiint_V U_0 dV=\frac{1}{2}\iiint_V \sigma_{ij}\varepsilon_{ij}\ dV \tag{2.5}$$

then strain energy and potential energy of applied loads become as:

$$\mathrm{U}=\frac{1}{2}\iiint_V \sigma_{ij}\varepsilon_{ij}\ dV \tag{2.6}$$

$$V = -\iiint_V f_i u_i dV - \iint_{S_2} \hat{t}_i u_i dS \tag{2.7}$$

where f_i are body forces, u_i are displacements, and $\hat{t}_i$ are surface tractions. The total potential energy of a linear elastic body in three dimensions, where the displacements are considered small, is given by (sum on repeated subscripts is implied):

$$\Pi(u) = \iiint_V \left(\frac{1}{2}\sigma_{ij} e_{ij} - f_i u_i\right) dV - \iint_{S_2} \hat{t}_i u_i dS \tag{2.8}$$

that e_{ij} are linear parts of strains.

As first step, a single-layer partial annular structure, which schematically resembles blood vessel, is proposed (Figure 2.1) in order to model artery and to derive governing equations and boundary conditions using principle of minimum total potential energy. In two-dimensional (2D) space with respect to cylindrical coordinate there are two displacements in radial (u_r) and circumferential (u_θ) directions. For case of simplicity, the material is assumed under plane strain state and linear elastic behaviour. Plane strain problems are simplifications of three-dimensional (3D) elasticity problems into two dimensions. The assumption is that the strains associated with the z-direction are zero (in generalized plane-strain problems, they are assumed to be constant). Hence, in cylindrical coordinate normal strain in z-direction, total shear strain in r-z plane, and total shear strain in θ-z plane are negligible; as consequence shear stress in r-z and θ-z planes are also negligible (Eq.2.9).

$$\varepsilon_z \cong \gamma_{rz} \cong \gamma_{\theta z} \cong 0 \Rightarrow \tau_{rz} \cong \tau_{\theta z} \cong 0 \tag{2.9}$$

To write the total potential energy function, equation (2.8), the relationship between stress and strain is also required. Such relations are referred as *material* or *constitutive* equations (Eq.2.10&13).

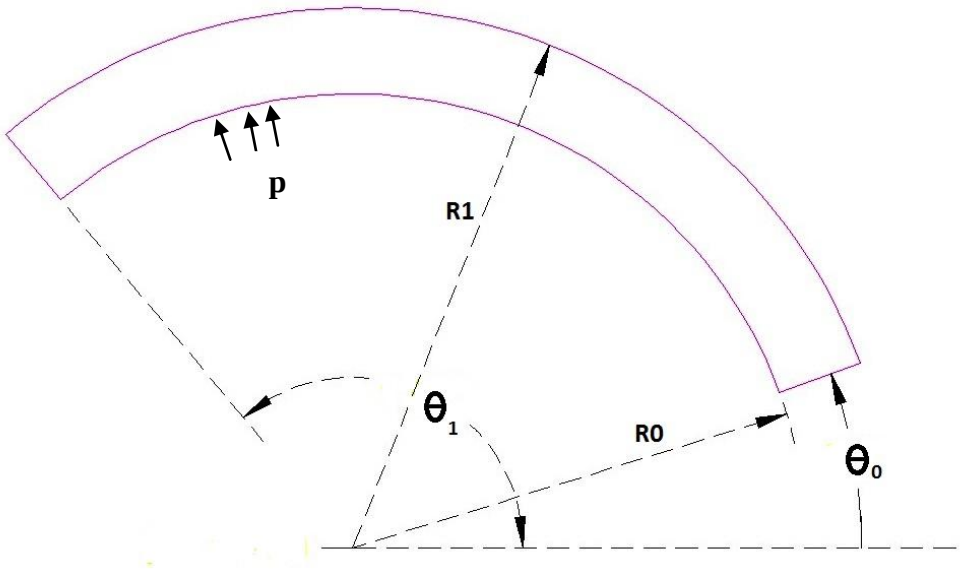

Figure 2.1 Schematic structure of part of single layer artery in cylindrical coordinate subjected to internal pressure

Matrix [D] in equation (2.10) is called material stiffness matrix and its elements are referred as material properties. In fact, the constitutive equation relates the components of stress to the components of strain via material stiffness matrix elements.

$$\{\sigma\} = [D]\{\varepsilon\} \tag{2.10}$$

While for two dimensional problem under plane strain assumption we have:

$$\{\sigma\}^T = \{\sigma_r \quad \sigma_\theta \quad \tau_{r\theta}\} \text{ and } \{\varepsilon\}^T = \{\varepsilon_r \quad \varepsilon_\theta \quad \gamma_{r\theta}\} \tag{2.11}$$

where $\{\sigma\}$ is stress vector and $\{\varepsilon\}$ is strain vector. The stiffness matrix for linear elastic material in plane strain case is:

$$[D]=\frac{E}{(1+\vartheta)(1-2\vartheta)}\begin{bmatrix}1-\vartheta & \vartheta & 0\\ \vartheta & 1-\vartheta & 0\\ 0 & 0 & \frac{1-2\vartheta}{2}\end{bmatrix} \tag{2.12}$$

where E and ϑ are modulus of elasticity and Poisson's ratio respectively. If only the linear strain-displacement relation is considered then strain, $\{\varepsilon\}$, reduces to $\{e\}$ .In fact e_{ij} is infinitesimal strain components. So, by replacing equation (2.12) in (2.10) the constitutive relation can be written as below:

$$\begin{Bmatrix}\sigma_r\\ \sigma_\theta\\ \tau_{r\theta}\end{Bmatrix}=\frac{E}{(1+\vartheta)(1-2\vartheta)}\begin{bmatrix}1-\vartheta & \vartheta & 0\\ \vartheta & 1-\vartheta & 0\\ 0 & 0 & \frac{1-2\vartheta}{2}\end{bmatrix}\begin{Bmatrix}e_r\\ e_\theta\\ \gamma_{r\theta}\end{Bmatrix} \tag{2.13}$$

where $\gamma_{r\theta}=2e_{r\theta}$ is engineering shear strain and $G=\frac{E}{2(1+\vartheta)}$ is shear modulus.

Strain-displacement relation is another item, which is essential to write total potential energy. The linear part of strain-displacement relation in cylindrical coordinate would be as [122]:

$$e_r=\frac{\partial u_r}{\partial r}\ ;\ e_\theta=\frac{u_r}{r}+\frac{1}{r}\frac{\partial u_\theta}{\partial \theta}\ ;\ e_{r\theta}=\frac{1}{2}\left(-\frac{u_\theta}{r}+\frac{\partial u_\theta}{\partial r}+\frac{1}{r}\frac{\partial u_r}{\partial \theta}\right) \tag{2.14}$$

After substitution of strain-displacement relation, equation (2.14), in equation (2.13) and computing stresses:

$$\sigma_r = \frac{E(1-\vartheta)}{(1+\vartheta)(1-2\vartheta)} e_r + \frac{E\vartheta}{(1+\vartheta)(1-2\vartheta)} e_\theta$$
$$\sigma_\theta = \frac{E\vartheta}{(1+\vartheta)(1-2\vartheta)} e_r + \frac{E(1-\vartheta)}{(1+\vartheta)(1-2\vartheta)} e_\theta \qquad (2.15)$$
$$\tau_{r\theta} = \frac{E}{(1+\vartheta)} e_{r\theta} = \frac{E}{2(1+\vartheta)} \gamma_{r\theta}$$

If $\frac{E(1-\vartheta)}{(1+\vartheta)(1-2\vartheta)} = A$, $\frac{E\vartheta}{(1+\vartheta)(1-2\vartheta)} = B$ and $\frac{E}{2(1+\vartheta)} = G$ be constants then equations (2.15) can be rewritten as:

$$\sigma_r = Ae_r + Be_\theta$$
$$\sigma_\theta = Be_r + Ae_\theta \qquad (2.16)$$
$$\tau_{r\theta} = G\gamma_{r\theta}$$

Now there are sufficient data in order to write the total potential energy for structure shown in figure 2.1. Since the body forces are assumed zero then $f_i = 0$; note that surface traction is pressure inside vessel.

$$\Pi(\underset{\sim}{u}) = \iiint_V \frac{1}{2} \sigma_{ij} e_{ij} \, dV - \iint_{S_2} \hat{t}_i u_i dS \qquad (2.17)$$

By restating equation (2.8) in terms of stresses and strains:

$$\Pi(\underset{\sim}{u}) = \frac{1}{2} \int_{R_0}^{R_1} \int_{\theta_0}^{\theta_1} (\sigma_r e_r + \sigma_\theta e_\theta + \tau_{r\theta}\gamma_{r\theta}) r dr d\theta - \int_{\theta_0}^{\theta_1} p u_r R_1 d\theta \qquad (2.18)$$

$$\Pi(\underset{\sim}{u}) = \frac{1}{2} \int_{R_0}^{R_1} \int_{\theta_0}^{\theta_1} \left[(Ae_r + Be_\theta) e_r + (Be_r + Ae_\theta) e_\theta + (G\gamma_{r\theta})\gamma_{r\theta} \right] r dr d\theta - \int_{\theta_0}^{\theta_1} p u_r R_1 d\theta$$

$$\Pi(\underset{\sim}{u}) = \frac{1}{2} \int_{R_0}^{R_1} \int_{\theta_0}^{\theta_1} \left[A(e_r)^2 + 2Be_r e_\theta + A(e_\theta)^2 + G(\gamma_{r\theta})^2 \right] r dr d\theta - \int_{\theta_0}^{\theta_1} p u_r R_1 d\theta \qquad (2.19)$$

By substitution equation (2.14) into (2.19):

$$\Pi(\underline{u})=\frac{1}{2}\int_{\theta_0}^{\theta_1}\int_{R_0}^{R_1}\begin{bmatrix} A\left(\frac{\partial u_r}{\partial r}\right)^2+2B\left(\frac{\partial u_r}{\partial r}\right)\left(\frac{u_r}{r}+\frac{1}{r}\frac{\partial u_\theta}{\partial \theta}\right)+A\left(\frac{u_r}{r}+\frac{1}{r}\frac{\partial u_\theta}{\partial \theta}\right)^2 \\ +G\left(-\frac{u_\theta}{r}+\frac{\partial u_\theta}{\partial r}+\frac{1}{r}\frac{\partial u_r}{\partial \theta}\right)^2 \end{bmatrix} rdrd\theta$$
$$-\int_{\theta_0}^{\theta_1} pu_r R_1 d\theta \qquad (2.20)$$

The equation (2.20) is total potential energy of structure, which is shown in Figure 2.1. In order to derive equilibrium equations and stress boundary conditions, the principle of minimum total potential energy should be applied. Recall that strain energy is sum of different energies, $U=U_m+U_b+U_\theta$, where U_m is membrane strain energy due to membrane deformation; U_b is bending strain energy; and U_θ is part of strain energy that results from heat. In present model, since bending resistant is relatively negligible and the body obtains isothermal condition, the only membrane strain energy is considered ($U=U_m$) [123]. In next step governing equations and boundary conditions will be derived via application of the principle of minimum total potential energy, first due to virtual displacement in radial direction (δu_r) and second due to virtual circumferential displacement (δu_θ).

$$\delta\Pi\big|_{\delta u_r}=0 \quad \Rightarrow$$

$$\int_{\theta_0}^{\theta_1}\int_{R_0}^{R_1}\begin{bmatrix} Ar\left(\frac{\partial u_r}{\partial r}\right)\delta\left(\frac{\partial u_r}{\partial r}\right)+Br\left(\left(\frac{u_r}{r}+\frac{1}{r}\frac{\partial u_\theta}{\partial \theta}\right)\delta\left(\frac{\partial u_r}{\partial r}\right)+\left(\frac{\delta u_r}{r}\right)\left(\frac{\partial u_r}{\partial r}\right)\right)+ \\ Ar\left(\frac{u_r}{r}+\frac{1}{r}\frac{\partial u_\theta}{\partial \theta}\right)\left(\frac{\delta u_r}{r}\right)+Gr\left(-\frac{u_\theta}{r}+\frac{\partial u_\theta}{\partial r}+\frac{1}{r}\frac{\partial u_r}{\partial \theta}\right)\frac{1}{r}\delta\left(\frac{\partial u_r}{\partial \theta}\right) \end{bmatrix} drd\theta$$
$$-\int_{\theta_0}^{\theta_1} P\delta u_r R_1 d\theta=0$$

By arranging same items:

$$\int_{\theta_0}^{\theta_1}\int_{R_0}^{R_1}\left[\begin{array}{l}\left(Ar\left(\frac{\partial u_r}{\partial r}\right)+Br\left(\frac{u_r}{r}+\frac{1}{r}\frac{\partial u_\theta}{\partial\theta}\right)\right)\delta\left(\frac{\partial u_r}{\partial r}\right)+Gr\left(-\frac{u_\theta}{r}+\frac{\partial u_\theta}{\partial r}+\frac{1}{r}\frac{\partial u_r}{\partial\theta}\right)\frac{1}{r}\delta\left(\frac{\partial u_r}{\partial\theta}\right)\\ \left(Ar\left(\frac{u_r}{r}+\frac{1}{r}\frac{\partial u_\theta}{\partial\theta}\right)\frac{1}{r}+B\left(\frac{\partial u_r}{\partial r}\right)\right)\delta u_r\end{array}\right]drd\theta$$

$$-\int_{\theta_0}^{\theta_1}p\delta u_r R_1 d\theta=0$$

Rewrite equation above:

$$\int_{\theta_0}^{\theta_1}\int_{R_0}^{R_1}\left[\left(Ar\left(\frac{\partial u_r}{\partial r}\right)+B\left(u_r+\frac{\partial u_\theta}{\partial\theta}\right)\right)\frac{\partial}{\partial r}(\delta u_r)\right]drd\theta+$$

$$\int_{\theta_0}^{\theta_1}\int_{R_0}^{R_1}\left[G\left(-\frac{u_\theta}{r}+\frac{\partial u_\theta}{\partial r}+\frac{1}{r}\frac{\partial u_r}{\partial\theta}\right)\frac{\partial}{\partial\theta}(\delta u_r)\right]drd\theta+$$

$$\int_{\theta_0}^{\theta_1}\int_{R_0}^{R_1}\left[\left(A\left(\frac{u_r}{r}+\frac{1}{r}\frac{\partial u_\theta}{\partial\theta}\right)+B\left(\frac{\partial u_r}{\partial r}\right)\right)\delta u_r\right]drd\theta-\int_{\theta_0}^{\theta_1}p\delta u_r R_1 d\theta=0$$

By applying integration by parts rule:

$$\int_{\theta_0}^{\theta_1}\int_{R_0}^{R_1}\frac{\partial}{\partial r}\left[\left(Ar\left(\frac{\partial u_r}{\partial r}\right)+B\left(u_r+\frac{\partial u_\theta}{\partial\theta}\right)\right)(\delta u_r)\right]drd\theta-$$

$$\int_{\theta_0}^{\theta_1}\int_{R_0}^{R_1}\left[\frac{\partial}{\partial r}\left(Ar\left(\frac{\partial u_r}{\partial r}\right)+B\left(u_r+\frac{\partial u_\theta}{\partial\theta}\right)\right)\right]\delta u_r drd\theta+$$

$$\int_{\theta_0}^{\theta_1}\int_{R_0}^{R_1}\frac{\partial}{\partial\theta}\left[G\left(-\frac{u_\theta}{r}+\frac{\partial u_\theta}{\partial r}+\frac{1}{r}\frac{\partial u_r}{\partial\theta}\right)(\delta u_r)\right]drd\theta-$$

$$\int_{\theta_0}^{\theta_1}\int_{R_0}^{R_1}\left[\frac{\partial}{\partial\theta}\left(G\left(-\frac{u_\theta}{r}+\frac{\partial u_\theta}{\partial r}+\frac{1}{r}\frac{\partial u_r}{\partial\theta}\right)\right)\right]\delta u_r drd\theta+$$

$$\int_{\theta_0}^{\theta_1}\int_{R_0}^{R_1}\left[A\left(\frac{u_r}{r}+\frac{1}{r}\frac{\partial u_\theta}{\partial\theta}\right)+B\left(\frac{\partial u_r}{\partial r}\right)\right]\delta u_r drd\theta-\int_{\theta_0}^{\theta_1}p\delta u_r R_1 d\theta=0$$

Consider the divergence theorem [124]:

$$\int_{\theta_0}^{\theta_1}\left[Ar\left(\frac{\partial u_r}{\partial r}\right)+B\left(u_r+\frac{\partial u_\theta}{\partial \theta}\right)\right]\delta u_r\, d\theta\Big|_{R_0}^{R_1}-\int_{\theta_0}^{\theta_1}\int_{R_0}^{R_1}\left[\frac{\partial}{\partial r}\left(Ar\left(\frac{\partial u_r}{\partial r}\right)+B\left(u_r+\frac{1}{r}\frac{\partial u_\theta}{\partial \theta}\right)\right)\right]\delta u_r dr d\theta$$

$$\int_{R_0}^{R_1}\left[G\left(-\frac{u_\theta}{r}+\frac{\partial u_\theta}{\partial r}+\frac{1}{r}\frac{\partial u_r}{\partial \theta}\right)\right]\delta u_r\, dr\Big|_{\theta_0}^{\theta_1}-\int_{\theta_0}^{\theta_1}\int_{R_0}^{R_1}\left[\frac{\partial}{\partial \theta}\left(G\left(-\frac{u_\theta}{r}+\frac{\partial u_\theta}{\partial r}+\frac{1}{r}\frac{\partial u_r}{\partial \theta}\right)\right)\right]\delta u_r dr d\theta+$$

$$\int_{\theta_0}^{\theta_1}\int_{R_0}^{R_1}\left[A\left(\frac{u_r}{r}+\frac{1}{r}\frac{\partial u_\theta}{\partial \theta}\right)+B\left(\frac{\partial u_r}{\partial r}\right)\right]\delta u_r dr d\theta-\int_{\theta_0}^{\theta_1} p\delta u_r R_1 d\theta=0$$

Rewriting the equations:

$$\int_{\theta_0}^{\theta_1}\left[Ar\left(\frac{\partial u_r}{\partial r}\right)+B\left(u_r+\frac{\partial u_\theta}{\partial \theta}\right)\right]\delta u_r\, d\theta\Big|_{R_0}^{R_1}+\int_{R_0}^{R_1}\left[G\left(-\frac{u_\theta}{r}+\frac{\partial u_\theta}{\partial r}+\frac{1}{r}\frac{\partial u_r}{\partial \theta}\right)\right]\delta u_r\, dr\Big|_{\theta_0}^{\theta_1}-$$

$$\int_{\theta_0}^{\theta_1}\int_{R_0}^{R_1}\left[\begin{array}{l}\frac{\partial}{\partial r}\left(Ar\left(\frac{\partial u_r}{\partial r}\right)+B\left(u_r+\frac{1}{r}\frac{\partial u_\theta}{\partial \theta}\right)\right)+\frac{\partial}{\partial \theta}\left(G\left(-\frac{u_\theta}{r}+\frac{\partial u_\theta}{\partial r}+\frac{1}{r}\frac{\partial u_r}{\partial \theta}\right)\right)-\\ A\left(\frac{u_r}{r}+\frac{1}{r}\frac{\partial u_\theta}{\partial \theta}\right)-B\left(\frac{\partial u_r}{\partial r}\right)\end{array}\right]\delta u_r dr d\theta$$

$$-\int_{\theta_0}^{\theta_1} p\delta u_r R_1 d\theta=0$$

Since u_r is not prescribed then $\delta u_r \neq 0$; thus, its coefficient should be zero in equation above in order to obtain field and boundary equations:

If $\delta\Pi\big|_{\delta u_r}=0 \;\Rightarrow$

$$Ar\frac{\partial^2 u_r}{\partial r^2}+\frac{G}{r}\frac{\partial^2 u_r}{\partial \theta^2}+A\frac{\partial u_r}{\partial r}-A\frac{u_r}{r}=-(B+G)\frac{\partial^2 u_\theta}{\partial r\partial \theta}+(A+G)\frac{1}{r}\frac{\partial u_\theta}{\partial \theta} \qquad \text{(F.1)}$$

The valid domain of field equation (F.1) is $R_0\langle r\langle R_1$ & $\theta_0\langle\theta\langle\theta_1$

$$\delta u_r \neq 0 \text{ then } \mathrm{A}\frac{\partial u_r}{\partial r} + B(\frac{u}{r} + \frac{1}{r}\frac{\partial u_\theta}{\partial \theta}) = \sigma_r = -p \quad @\ r = R_0\ \&\ \theta_0 \le \theta \le \theta_1$$

$$\delta u_r \neq 0 \text{ then } \mathrm{A}\frac{\partial u_r}{\partial r} + B(\frac{u}{r} + \frac{1}{r}\frac{\partial u_\theta}{\partial \theta}) = \sigma_r = 0 \quad @\ r = R_1\ \&\ \theta_0 \le \theta \le \theta_1$$

$$\delta u_r \neq 0 \text{ then } G(-\frac{u_\theta}{r} + \frac{\partial u_\theta}{\partial r} + \frac{1}{r}\frac{\partial u_r}{\partial \theta}) = \tau_{r\theta} = 0 \quad @\ \theta = \theta_0\ \&\ \mathrm{R}_0 \le r \le R_1 \qquad \text{(B.1)}$$

$$\delta u_r \neq 0 \text{ then } G(-\frac{u_\theta}{r} + \frac{\partial u_\theta}{\partial r} + \frac{1}{r}\frac{\partial u_r}{\partial \theta}) = \tau_{r\theta} = 0 \quad @\ \theta = \theta_1\ \&\ \mathrm{R}_0 \le r \le R_1$$

Equations (B.1) are natural boundary conditions.

Repeat the same procedure for virtual circumferential displacement:

$$\delta\Pi\big|_{\delta u_\theta} = 0 \Rightarrow$$

$$\int_{\theta_0}^{\theta_1}\int_{R_0}^{R_1}\left[\begin{array}{l} B\left(\frac{\partial u_r}{\partial r}\right)\delta\left(\frac{\partial u_\theta}{\partial \theta}\right) + Ar\left(\frac{u_r}{r} + \frac{1}{r}\frac{\partial u_\theta}{\partial \theta}\right)\frac{1}{r}\delta\left(\frac{\partial u_\theta}{\partial \theta}\right) \\ +Gr\left(-\frac{u_\theta}{r} + \frac{\partial u_\theta}{\partial r} + \frac{1}{r}\frac{\partial u_r}{\partial \theta}\right)\left(-\frac{\delta u_\theta}{r} + \delta\left(\frac{\partial u_\theta}{\partial r}\right)\right) \end{array}\right] drd\theta = 0$$

Restate the equations:

$$\int_{\theta_0}^{\theta_1}\int_{R_0}^{R_1}\left[\left(B\left(\frac{\partial u_r}{\partial r}\right) + A\left(\frac{u_r}{r} + \frac{1}{r}\frac{\partial u_\theta}{\partial \theta}\right)\right)\delta\left(\frac{\partial u_\theta}{\partial \theta}\right)\right] drd\theta +$$

$$\int_{\theta_0}^{\theta_1}\int_{R_0}^{R_1}\left[Gr\left(-\frac{u_\theta}{r} + \frac{\partial u_\theta}{\partial r} + \frac{1}{r}\frac{\partial u_r}{\partial \theta}\right)\delta\left(\frac{\partial u_\theta}{\partial r}\right)\right] drd\theta -$$

$$\int_{\theta_0}^{\theta_1}\int_{R_0}^{R_1}\left[Gr\left(-\frac{u_\theta}{r} + \frac{\partial u_\theta}{\partial r} + \frac{1}{r}\frac{\partial u_r}{\partial \theta}\right)\left(\frac{\delta u_\theta}{r}\right)\right] drd\theta = 0$$

Rewrite the equations:

$$\int_{\theta_0}^{\theta_1}\int_{R_0}^{R_1}\left[\left(B\left(\frac{\partial u_r}{\partial r}\right)+A\left(\frac{u_r}{r}+\frac{1}{r}\frac{\partial u_\theta}{\partial \theta}\right)\right)\frac{\partial}{\partial \theta}\left(\delta u_\theta\right)\right]drd\theta+$$
$$\int_{\theta_0}^{\theta_1}\int_{R_0}^{R_1}\left[Gr\left(-\frac{u_\theta}{r}+\frac{\partial u_\theta}{\partial r}+\frac{1}{r}\frac{\partial u_r}{\partial \theta}\right)\frac{\partial}{\partial r}\left(\delta u_\theta\right)\right]drd\theta-$$
$$\int_{\theta_0}^{\theta_1}\int_{R_0}^{R_1}\left[G\left(-\frac{u_\theta}{r}+\frac{\partial u_\theta}{\partial r}+\frac{1}{r}\frac{\partial u_r}{\partial \theta}\right)\left(\delta u_\theta\right)\right]drd\theta=0$$

Apply integration by parts:

$$\int_{\theta_0}^{\theta_1}\int_{R_0}^{R_1}\frac{\partial}{\partial \theta}\left[\left(B\left(\frac{\partial u_r}{\partial r}\right)+A\left(\frac{u_r}{r}+\frac{1}{r}\frac{\partial u_\theta}{\partial \theta}\right)\right)\left(\delta u_\theta\right)\right]drd\theta-$$
$$\int_{\theta_0}^{\theta_1}\int_{R_0}^{R_1}\left[\frac{\partial}{\partial \theta}\left(B\left(\frac{\partial u_r}{\partial r}\right)+A\left(\frac{u_r}{r}+\frac{1}{r}\frac{\partial u_\theta}{\partial \theta}\right)\right)\right]\delta u_\theta drd\theta+$$
$$\int_{\theta_0}^{\theta_1}\int_{R_0}^{R_1}\frac{\partial}{\partial r}\left[Gr\left(-\frac{u_\theta}{r}+\frac{\partial u_\theta}{\partial r}+\frac{1}{r}\frac{\partial u_r}{\partial \theta}\right)\left(\delta u_\theta\right)\right]drd\theta-$$
$$\int_{\theta_0}^{\theta_1}\int_{R_0}^{R_1}\left[\frac{\partial}{\partial r}\left(Gr\left(-\frac{u_\theta}{r}+\frac{\partial u_\theta}{\partial r}+\frac{1}{r}\frac{\partial u_r}{\partial \theta}\right)\right)\right]\delta u_\theta drd\theta-$$
$$\int_{\theta_0}^{\theta_1}\int_{R_0}^{R_1}\left[G\left(-\frac{u_\theta}{r}+\frac{\partial u_\theta}{\partial r}+\frac{1}{r}\frac{\partial u_r}{\partial \theta}\right)\right]\delta u_\theta drd\theta=0$$

According to the divergence theorem:

$$\int_{R_0}^{R_1}\left(B\left(\frac{\partial u_r}{\partial r}\right)+A\left(\frac{u_r}{r}+\frac{1}{r}\frac{\partial u_\theta}{\partial \theta}\right)\right)\delta u_\theta\, dr\Big|_{\theta_0}^{\theta_1}-$$
$$\int_{\theta_0}^{\theta_1}\int_{R_0}^{R_1}\left[\frac{\partial}{\partial \theta}\left(B\left(\frac{\partial u_r}{\partial r}\right)+A\left(\frac{u_r}{r}+\frac{1}{r}\frac{\partial u_\theta}{\partial \theta}\right)\right)\right]\delta u_\theta drd\theta+$$
$$\int_{\theta_0}^{\theta_1}\left(Gr\left(-\frac{u_\theta}{r}+\frac{\partial u_\theta}{\partial r}+\frac{1}{r}\frac{\partial u_r}{\partial \theta}\right)\right)\delta u_\theta\, d\theta\Big|_{R_0}^{R_1}-$$
$$\int_{\theta_0}^{\theta_1}\int_{R_0}^{R_1}\left[\frac{\partial}{\partial r}\left(Gr\left(-\frac{u_\theta}{r}+\frac{\partial u_\theta}{\partial r}+\frac{1}{r}\frac{\partial u_r}{\partial \theta}\right)\right)\right]\delta u_\theta drd\theta-$$
$$\int_{\theta_0}^{\theta_1}\int_{R_0}^{R_1}\left[G\left(-\frac{u_\theta}{r}+\frac{\partial u_\theta}{\partial r}+\frac{1}{r}\frac{\partial u_r}{\partial \theta}\right)\right]\delta u_\theta drd\theta=0$$

Rewrite the equation above:

$$\int_{R_0}^{R_1}\left(B\left(\frac{\partial u_r}{\partial r}\right)+A\left(\frac{u_r}{r}+\frac{1}{r}\frac{\partial u_\theta}{\partial \theta}\right)\right)\delta u_\theta\, dr\Big|_{\theta_0}^{\theta_1}-\int_{\theta_0}^{\theta_1}\left(Gr\left(-\frac{u_\theta}{r}+\frac{\partial u_\theta}{\partial r}+\frac{1}{r}\frac{\partial u_r}{\partial \theta}\right)\right)\delta u_\theta\, d\theta\Big|_{R_0}^{R_1}-$$

$$\int_{\theta_0}^{\theta_1}\int_{R_0}^{R_1}\left[\begin{array}{l}\frac{\partial}{\partial \theta}\left(B\left(\frac{\partial u_r}{\partial r}\right)+A\left(\frac{u_r}{r}+\frac{1}{r}\frac{\partial u_\theta}{\partial \theta}\right)\right)+\frac{\partial}{\partial r}\left(Gr\left(-\frac{u_\theta}{r}+\frac{\partial u_\theta}{\partial r}+\frac{1}{r}\frac{\partial u_r}{\partial \theta}\right)\right)+\\ G\left(-\frac{u_\theta}{r}+\frac{\partial u_\theta}{\partial r}+\frac{1}{r}\frac{\partial u_r}{\partial \theta}\right)\end{array}\right]\delta u_\theta dr d\theta=0$$

Thus:

$$\text{if } \delta\Pi\big|_{\delta u_\theta}=0 \;\Rightarrow$$

$$Gr\frac{\partial^2 u_\theta}{\partial r^2}+\frac{A}{r}\frac{\partial^2 u_\theta}{\partial \theta^2}+G\frac{\partial u_\theta}{\partial r}-G\frac{u_r}{r}=-(B+G)\frac{\partial^2 u_r}{\partial r\partial \theta}-(A+G)\frac{1}{r}\frac{\partial u_r}{\partial \theta} \qquad \text{(F.2)}$$

The valid domain of field equation (F.2) is $R_0\langle r\langle R_1 \;\&\; \theta_0\langle\theta\langle\theta_1$

$$\left.\begin{array}{ll}\delta u_\theta\neq 0 \text{ then } G(-\frac{u_\theta}{r}+\frac{\partial u_\theta}{\partial r}+\frac{1}{r}\frac{\partial u_r}{\partial \theta})=\tau_{r\theta}=0 & @\ r=R_0 \;\&\; \theta_0\le\theta\le\theta_1\\ \delta u_\theta\neq 0 \text{ then } G(-\frac{u_\theta}{r}+\frac{\partial u_\theta}{\partial r}+\frac{1}{r}\frac{\partial u_r}{\partial \theta})=\tau_{r\theta}=0 & @\ r=R_1 \;\&\; \theta_0\le\theta\le\theta_1\end{array}\right\} \quad \text{(B.2)}$$

$$\left.\begin{array}{ll}\delta u_\theta=0 \Rightarrow A(\frac{u}{r}+\frac{1}{r}\frac{\partial u_\theta}{\partial \theta})+\mathrm{B}\frac{\partial u_r}{\partial r}=\sigma_\theta\neq 0 & @\ \theta=\theta_0 \;\&\; \mathrm{R}_0\le r\le R_1\\ \delta u_\theta=0 \Rightarrow A(\frac{u}{r}+\frac{1}{r}\frac{\partial u_\theta}{\partial \theta})+\mathrm{B}\frac{\partial u_r}{\partial r}=\sigma_\theta\neq 0 & @\theta=\theta_1 \;\&\; \mathrm{R}_0\le r\le R_1\end{array}\right\} \quad \text{(B.3)}$$

Equations (B.2) are the natural boundary conditions, in which u_θ is not prescribed, while equations (B.3) represent the essential boundary conditions with fixed zero u_θ.

After deriving the field and boundary equations for single layer structure, the second step will be to evoke equations of three-layered structure, such as the one

depicted in Figure 2.2 by using principle of minimum total potential energy. The layered structure simulates the artery in more realistic way. Note that for elastic material, the virtual work resulting from internal forces is equal to variation of strain energy; and virtual work resulting from external forces is equal to variation of force potential energy. After implementation of the procedure same as single layer, the results can be concluded for each layer separately.

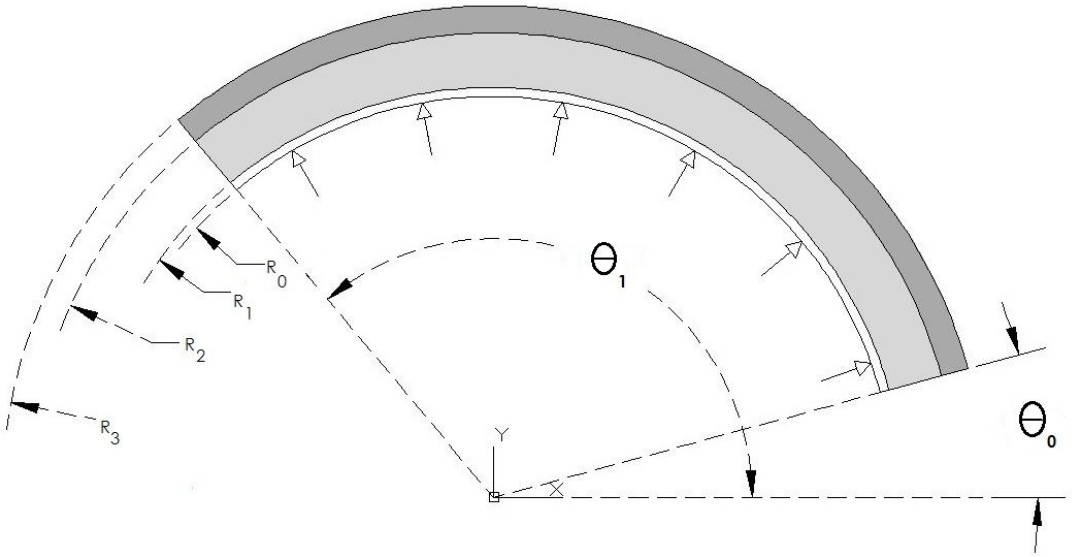

Figure 2.2 Three-layered partial annular structure that schematically resembles artery that is subjected to internal pressure in lumen

Note that $u_r^I = u_r^M$ at $r = R_1$, $u_r^M = u_r^A$ at $r = R_2$; where u_r^I is displacement of intima layer, u_r^M is displacement of media layer, and u_r^A is displacement of adventitia layer, in radial direction. Also, consider the fact that $u_\theta^I = u_\theta^M$ at $r = R_1$ and $u_\theta^M = u_\theta^A$ at $r = R_2$; where u_θ^I, u_θ^M and u_θ^A are circumferential displacements of intima, media and adventitia respectively. Equations (F.3) are field or domain (equilibrium) equations in terms of displacements for intima layer and are valid at $R_0 \langle r \langle R_1$ & $\theta_0 \langle \theta \langle \theta_1$:

$$\delta u_r \neq 0 \Rightarrow$$
$$A^I r\frac{\partial^2 u_r^I}{\partial r^2}+\frac{G^I}{r}\frac{\partial^2 u_r^I}{\partial \theta^2}+A^I\frac{\partial u_r^I}{\partial r}-A^I\frac{u_r^I}{r}=-(B^I+G^I)\frac{\partial^2 u_\theta^I}{\partial r\partial\theta}+(A^I+G^I)\frac{1}{r}\frac{\partial u_\theta^I}{\partial\theta}$$

$$\delta u_\theta \neq 0 \Rightarrow \qquad \text{(F.3)}$$
$$G^I r\frac{\partial^2 u_\theta^I}{\partial r^2}+\frac{A^I}{r}\frac{\partial^2 u_\theta^I}{\partial \theta^2}+G^I\frac{\partial u_\theta^I}{\partial r}-G^I\frac{u_\theta^I}{r}=-(B^I+G^I)\frac{\partial^2 u_r^I}{\partial r\partial\theta}-(A^I+G^I)\frac{1}{r}\frac{\partial u_r^I}{\partial\theta}$$

Also, the domain equations could be written in terms of stress if the principle of virtual work was applied directly. Equations (F.4) are field equation for intima layer in terms of stress and valid at $R_0\langle r\langle R_1$ & $\theta_0\langle\theta\langle\theta_1$:

$$\delta u_r \neq 0 \Rightarrow$$
$$\sigma_r^I+r\frac{\partial\sigma_r^I}{\partial r}+\frac{\partial\tau_{r\theta}^I}{\partial\theta}-\sigma_\theta^I=0 \qquad @\ R_0\langle r\langle R_1 \ \&\ \theta_0\langle\theta\langle\theta_1$$

(F.4)

$$\delta u_\theta \neq 0 \Rightarrow$$
$$\frac{\partial\sigma_\theta^I}{\partial\theta}+r\frac{\partial\tau_{r\theta}^I}{\partial r}+2\tau_{r\theta}^I=0; \qquad @\ R_0\langle r\langle R_1 \ \&\ \theta_0\langle\theta\langle\theta_1$$

The boundary and interface conditions have been stated for intima layer is equations (B.4) and (B.5) as natural and essential conditions respectively.

$$\left.\begin{array}{ll}
\delta u_r \neq 0 \ \text{ then } \ \sigma_r^I=-p & @\ r=R_0 \ \&\ \theta_0\le\theta\le\theta_1 \\
\delta u_r \neq 0 \ \text{ then } \ \sigma_r^I=\sigma_r^M & @\ r=R_1 \ \&\ \theta_0\le\theta\le\theta_1 \\
\delta u_\theta \neq 0 \ \text{ then } \ \tau_{r\theta}^I=0 & @\ r=R_0 \ \&\ \theta_0\le\theta\le\theta_1 \\
\delta u_\theta \neq 0 \ \text{ then } \ \tau_{r\theta}^I=\tau_{r\theta}^M & @\ r=R_1 \ \&\ \theta_0\le\theta\le\theta_1 \\
\delta u_r \neq 0 \ \text{ then } \ \tau_{r\theta}^I=\tau_{r\theta}^M & @\ \theta=\theta_0 \ \&\ \mathrm{R}_0\le r\le R_1 \\
\delta u_r \neq 0 \ \text{ then } \ \tau_{r\theta}^I=\tau_{r\theta}^M & @\ \theta=\theta_1 \ \&\ \mathrm{R}_0\le r\le R_1
\end{array}\right\} N.B.C \qquad \text{(B.4)}$$

$$\left.\begin{array}{ll}
u_\theta^I=0 & @\ \theta=\theta_0 \ \&\ \mathrm{R}_0\le r\le R_1 \\
u_\theta^I=0 & @\ \theta=\theta_1 \ \&\ \mathrm{R}_0\le r\le R_1
\end{array}\right\} E.B.C \qquad \text{(B.5)}$$

Equations (F.5) are field equations for media layer in terms of displacements; and valid at $R_1\langle r\langle R_2$ & $\theta_0\langle\theta\langle\theta_1$:

$$\delta u_r \neq 0 \Rightarrow$$
$$A^M r\frac{\partial^2 u_r^M}{\partial r^2}+\frac{G^M}{r}\frac{\partial^2 u_r^M}{\partial\theta^2}+A^M\frac{\partial u_r^M}{\partial r}-A^M\frac{u_r^M}{r}=-(B^M+G^M)\frac{\partial^2 u_\theta^M}{\partial r\partial\theta}+(A^M+G^M)\frac{1}{r}\frac{\partial u_\theta^M}{\partial\theta}$$

$$\delta u_\theta \neq 0 \Rightarrow \qquad \text{(F.5)}$$
$$G^M r\frac{\partial^2 u_\theta^M}{\partial r^2}+\frac{A^M}{r}\frac{\partial^2 u_\theta^M}{\partial\theta^2}+G^M\frac{\partial u_\theta^M}{\partial r}-G^M\frac{u_\theta^M}{r}=-(B^M+G^M)\frac{\partial^2 u_r^M}{\partial r\partial\theta}-(A^M+G^M)\frac{1}{r}\frac{\partial u_r^M}{\partial\theta};$$

Equations (F.6) are field equations of media layer in terms of stresses:

$$\delta u_r \neq 0 \Rightarrow$$
$$\sigma_r^M+r\frac{\partial\sigma_r^M}{\partial r}+\frac{\partial\tau_{r\theta}^M}{\partial\theta}-\sigma_\theta^M=0;\quad @\ R_1\langle r\langle R_2\ \&\ \theta_0\langle\theta\langle\theta_1$$

(F.6)

$$\delta u_\theta \neq 0 \Rightarrow$$
$$\frac{\partial\sigma_\theta^M}{\partial\theta}+r\frac{\partial\tau_{r\theta}^M}{\partial r}+2\tau_{r\theta}^M=0;\qquad @\ R_1\langle r\langle R_2\ \&\ \theta_0\langle\theta\langle\theta_1$$

The interface conditions have been stated for media layer is equations (B.6) and (B.7) as natural and essential conditions respectively.

$$\left.\begin{array}{ll}
\delta u_r\neq 0 \text{ then } \sigma_r^I=\sigma_r^M & @\ r=R_1\ \&\ \theta_0\le\theta\le\theta_1\\
\delta u_r\neq 0 \text{ then } \sigma_r^M=\sigma_r^A & @\ r=R_2\ \&\ \theta_0\le\theta\le\theta_1\\
\delta u_\theta\neq 0 \text{ then } \tau_{r\theta}^I=\tau_{r\theta}^M & @\ r=R_1\ \&\ \theta_0\le\theta\le\theta_1\\
\delta u_\theta\neq 0 \text{ then } \tau_{r\theta}^M=\tau_{r\theta}^A & @\ r=R_2\ \&\ \theta_0\le\theta\le\theta_1\\
\delta u_r\neq 0 \text{ then } \tau_{r\theta}^I=\tau_{r\theta}^M=\tau_{r\theta}^A=0 & @\ \theta=\theta_0\ \&\ \mathrm{R}_1\le r\le R_2\\
\delta u_r\neq 0 \text{ then } \tau_{r\theta}^I=\tau_{r\theta}^M=\tau_{r\theta}^A=0 & @\ \theta=\theta_1\ \&\ \mathrm{R}_1\le r\le R_2
\end{array}\right\}\ \text{N.B.C}\qquad \text{(B.6)}$$

$$\left.\begin{array}{ll}
u_\theta^M=0 & @\ \theta=\theta_0\ \&\ \mathrm{R}_1\le r\le R_2\\
u_\theta^M=0 & @\ \theta=\theta_1\ \&\ \mathrm{R}_1\le r\le R_2
\end{array}\right\}\ E.B.C\qquad \text{(B.7)}$$

Finally, Equations (F.7) are field equations for adventitia layer in terms of displacements:

$\delta u_r \neq 0 \Rightarrow$

$$A^A r\frac{\partial^2 u_r^A}{\partial r^2}+\frac{G^A}{r}\frac{\partial^2 u_r^A}{\partial \theta^2}+A^A\frac{\partial u_r^A}{\partial r}-A^A\frac{u_r^A}{r}=-(B^A+G^A)\frac{\partial^2 u_\theta^A}{\partial r\partial\theta}+(A^A+G^A)\frac{1}{r}\frac{\partial u_\theta^A}{\partial\theta} \tag{F.7}$$

$\delta u_\theta \neq 0 \Rightarrow$

$$G^A r\frac{\partial^2 u_\theta^A}{\partial r^2}+\frac{A^A}{r}\frac{\partial^2 u_\theta^A}{\partial \theta^2}+G^A\frac{\partial u_\theta^A}{\partial r}-G^A\frac{u_\theta^A}{r}=-(B^A+G^A)\frac{\partial^2 u_r^A}{\partial r\partial\theta}-(A^A+G^A)\frac{1}{r}\frac{\partial u_r^A}{\partial\theta}$$

where @ $R_2\langle r\langle R_3$ & $\theta_0\langle\theta\langle\theta_1$

And equations (F.8) represent field equations for the same layer in terms of stresses:

$\delta u_r \neq 0 \Rightarrow$

$$\sigma_r^A+r\frac{\partial\sigma_r^A}{\partial r}+\frac{\partial\tau_{r\theta}^A}{\partial\theta}-\sigma_\theta^A=0; \quad @\ R_2\langle r\langle R_3\ \&\ \theta_0\langle\theta\langle\theta_1 \tag{F.8}$$

$\delta u_\theta \neq 0 \Rightarrow$

$$\frac{\partial\sigma_\theta^A}{\partial\theta}+r\frac{\partial\tau_{r\theta}^A}{\partial r}+2\tau_{r\theta}^A=0; \quad @\ R_2\langle r\langle R_3\ \&\ \theta_0\langle\theta\langle\theta_1$$

The boundary and interface conditions of adventitia have been cited in equations (B.8) for natural and (B.9) for essential conditions:

$$\left.\begin{aligned} u_\theta^A&=0 \quad @\ \theta=\theta_0\ \&\ \mathrm{R}_2\le r\le R_3\\ u_\theta^A&=0 \quad @\ \theta=\theta_1\ \&\ \mathrm{R}_2\le r\le R_3\end{aligned}\right\} E.B.C \tag{B.8}$$

$$\left.\begin{array}{ll}
\delta u_r \neq 0 \text{ then } \sigma_r^M = \sigma_r^A & @\ r = R_2\ \&\ \theta_0 \le \theta \le \theta_1 \\
\delta u_r \neq 0 \text{ then } \sigma_r^A = 0 & @\ r = R_3\ \&\ \theta_0 \le \theta \le \theta_1 \\
\delta u_\theta \neq 0 \text{ then } \tau_{r\theta}^M = \tau_{r\theta}^A & @\ r = R_2\ \&\ \theta_0 \le \theta \le \theta_1 \\
\delta u_\theta \neq 0 \text{ then } \tau_{r\theta}^A = 0 & @\ r = R_3\ \&\ \theta_0 \le \theta \le \theta_1 \\
\delta u_r \neq 0 \text{ then } \tau_{r\theta}^M = \tau_{r\theta}^A = 0 & @\ \theta = \theta_0\ \&\ \mathrm{R}_2 \le r \le R_3 \\
\delta u_r \neq 0 \text{ then } \tau_{r\theta}^M = \tau_{r\theta}^A = 0 & @\ \theta = \theta_1\ \&\ \mathrm{R}_2 \le r \le R_3
\end{array}\right\} \text{N.B.C} \qquad \text{(B.9)}$$

2.2. Material Properties and Geometric Parameters

The mechanics of arterial wall in healthy and diseased status is governed by the material properties as well as the geometry and applied loads. With no doubt, there is a substantial need for more precise information on thickness, stiffness ,and other mechanical and geometrical features of both healthy and aneurismal artery. In this section the mechanical properties, geometry and applied pressure of arteries, cited in literature, have been investigated.

2.2.1. Stiffness

Elastic properties of arteries have long been recognized as playing a major role in the cardiovascular system [126, 146]. Direct relationship between arterial stiffness and various cardiovascular diseases has been established, making the arterial stiffness an important predictor of cardiovascular diseases [127]. Arterial stiffness has been shown to be an excellent indicator of cardiovascular morbidity and mortality in a large percentage of the population [128], patients with hypertension [129, 130], atherosclerosis [131], abdominal aortic aneurysm [132] and myocardial infarction [133].

Several carotid stiffness indices have been proposed based on the pressure–diameter relationship of arterial distension from the end-diastolic to the end-systolic phase, e.g., arterial distensibility, arterial compliance, Peterson's elastic modulus (Ep) and stiffness index (b) [134-145]. They, however, represent a global stiffness

measurement of the entire arterial wall based on a single measurement site. Among the various indices that have been introduced to quantify arterial stiffness, pulse wave velocity (PWV) is “the most hallowed (and still probably the best)” [146]. In fact, one of the most recognized methods for quantification of vascular stiffening is measurement of the pulse wave velocity (PWV) [147-149].

The European society of hypertension and the European society of cardiology have recently recommended the use of the carotid-femoral pulse wave velocity as a favoured measure of aortic stiffness for the management of arterial hypertension [150]. However, the PWV measured in this way represents the average value between two measurement sites, while the stiffness of the arteries is non-uniform along the vasculature [134]. Therefore, measurements of regional PWV, instead of global PWV, can be of great interest [152].

Pulse Wave Imaging (PWI) is an ultrasound-based method for qualitative visualization of the pulse wave propagation and for quantitative estimation of regional PWV [153-155]. In other words, pulse wave imaging is a novel, non-invasive ultrasound based method to quantify regional arterial stiffness by measuring the velocity of the pulse wave that propagates along arterial walls after each left ventricular contraction.

The PWI method employs 1D cross-correlation speckle tracking to compute axial incremental displacements, then tracks the position of the displacement wave in the anterior wall of the vessel to estimate pulse wave velocity (PWV) [156]. According to paper [152] PWI is feasible in the human carotid artery.

For stiffness identification, the pressure and regional wall displacement of the carotid artery were estimated. The in vivo non-invasive Young’s modulus estimated from the regional stress–strain relationship includes more comprehensive information on the arterial wall properties regarding the effects of the different constituents [157]. Only a few studies have been reported on the in vivo Young’s modulus measurement of the carotid artery based on the pressure–strain relationship

[158-161] or from the slope of the stress–strain relationship [162] at end-diastole and end-systole. Previous studies, however, have not investigated on the complex mechanical interaction of the arterial wall constituents in humans in vivo.

In the studies [152, 163] the in-vivo stress-strain relationship was determined in order to characterize the complex mechanical interaction of constituents and their respective Young's moduli. To establish the stress-strain relationship in vivo, the arterial pressure and wall displacement measurements were respectively acquired and estimated in vivo. Two separate models were employed in this study to estimate the Young's moduli of the carotid arteries.

The first model was two-parallel spring arterial model assumed to be an axi-symmetric, single-walled layer cylindrical tube with isotropic, linearly elastic, homogeneous, incompressible and non-viscous properties. The second model was two-dimensional hyper-elastic arterial model assumed to be an axi-symmetric, double-walled layer cylindrical tube with plane strain, anisotropic, nonlinearly elastic, homogeneous (in each layer), incompressible and non-viscous properties.

The in-vivo regional stress-strain relationship in the left common carotid arterial wall (CCA) of healthy humans was established noninvasively. At the change of the slope, defined as the transition point, it was hypothesized that the collagen fibers start engaging and the Young's modulus of the vessel wall depends on the elastin-collagen fibers modulus instead. In other words, a transition point of the stress-strain relationship was detected representing the change in the contribution of the elastin and collagen fiber during the systolic phase of the cardiac cycle, which means change in material properties of wall throughout systolic phase of cardiac cycle.

The carotid arterial wall constituents were characterized by two separate models. The first model was used for the Young's moduli of the elastic lamellae E1, elastin-collagen fibers E2 and collagen fibers E3; and second one yielded the incremental

Young's moduli of the intact wall, which is composed of the incremental Young's moduli of the tunica adventitia and tunica media.

Figure 2.3 shows the average Young's modulus of E1, E2, and E3. The stress-strain relationship of the intact wall (Figure 2.4), tunica adventitia and tunica media at constant 0% axial stretch before and after the transition point were estimated using a two-dimensional hyper-elastic model with optimized material parameters (Figures 2.5).[163]

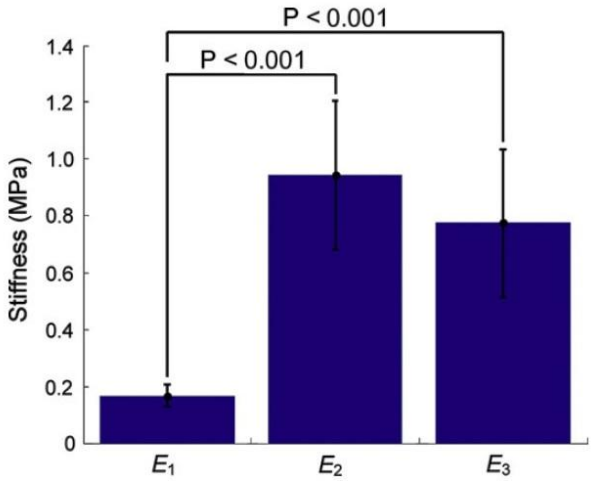

Figure 2.3 Averaged Young's moduli of the elastic lamellae (E1), elastincollagen fibers (E2), and collagen fibers (E3) over 7 subjects [163]

The models, however, do not account for angular dispersion and the geometry of the collagen fibers. This negligence would affect the estimated stress-strain relationship and also the Young's modulus especially in the tunica adventitia, not the tunica media [152].

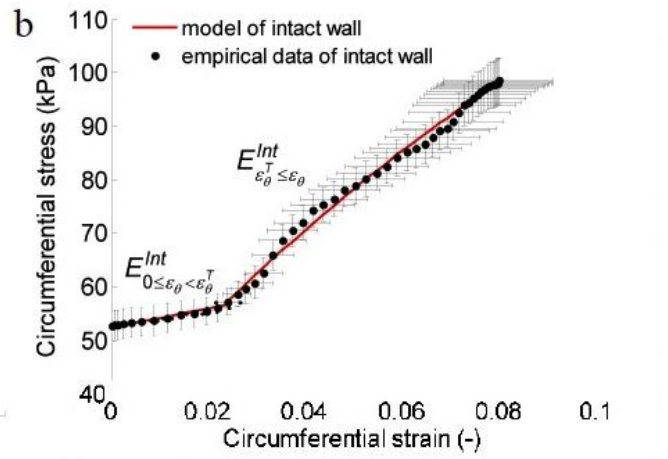

Figure 2.4 Circumferential stress-strain relationship of the human carotid artery averaged along longitudinal locations. The solid red line indicates the model at 0% axial stretch of the intact wall.

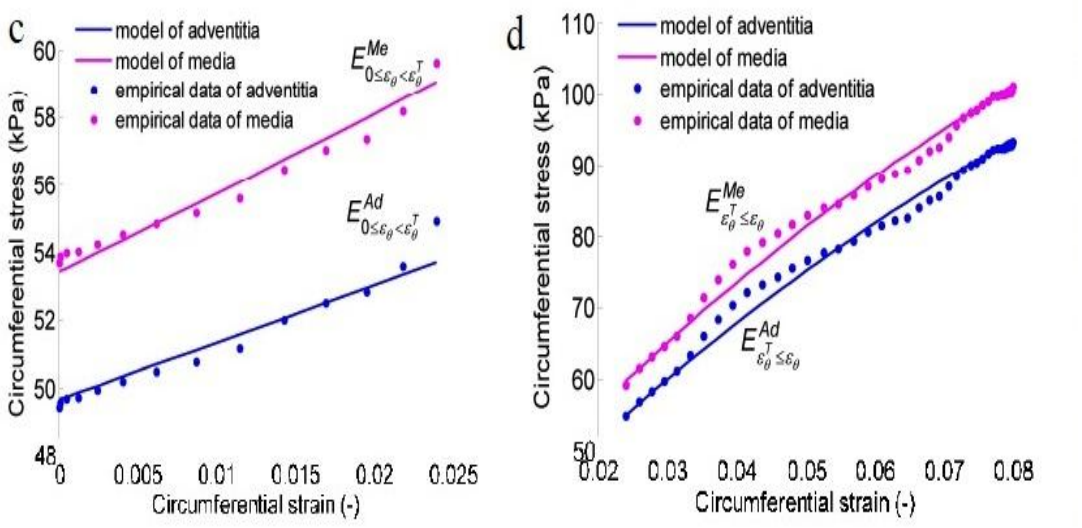

Figure 2.5 Relations of the tunica adventitia and tunica media before and after the transition point were fitted using the two-dimensional hyper-elastic model, respectively. The solid blue and magenta lines indicate the model at 0% axial stretch of the tunica adventitia and tunica media, respectively [163].

Previous studies in the ascending and descending porcine aorta have reported that the Young's moduli, determined from uniaxial testing, of the tunica media were approximately four-fold higher than that of the tunica adventitia. In this study, the Young's modulus of the tunica media was found not to be significantly higher than

those of the tunica adventitia (P > 0.05), since the tunica media deformation underwent small strain with the in-vivo physiologic pressure. Note that the angular dispersion of the collagen fibers was ignored in the model. As a result of the pressure and the angular dispersion, the Young's modulus of the tunica media increased with deformation when subjected to higher pressures, i.e., in the case of pathologic conditions or under in-vitro testing. Moreover the Young's modulus of the tunica adventitia also decreases when the angular dispersion of the collagen fibers was considered [152]. All in all, the values of moduli of elasticity for hyper-elastic and spring models have been summarized as below:

Moduli of elasticity with respect to hyper-elastic model:

$E^{\text{int}}_{0\le\varepsilon_\theta\le\varepsilon^T{}_\theta} = 0.16 \pm 0.04 MPa$; elastic modulus of intact wall before transient point

$E^{\text{int}}_{\varepsilon^T{}_\theta\le\varepsilon_{\theta\theta}} = 0.90 \pm 0.25 MPa$; elastic modulus of intact wall after transient point

$E^{M}_{0\le\varepsilon_\theta\le\varepsilon^T{}_\theta} = 0.19 \pm 0.05 MPa$; elastic modulus of media before transient point

$E^{M}_{\varepsilon^T{}_\theta\le\varepsilon_{\theta\theta}} = 0.90 \pm 0.25 MPa$; elastic modulus of media after transient point

$E^{A}_{0\le\varepsilon_\theta\le\varepsilon^T{}_\theta} = 0.18 \pm 0.05 MPa$; elastic modulus of adventitia before transient point

$E^{A}_{\varepsilon^T{}_\theta\le\varepsilon_{\theta\theta}} = 0.84 \pm 0.22 MPa$; elastic modulus of adventitia after transient point

Moduli of elasticity with respect to two spring model:

$E_1 = 0.15 \pm 0.04$MPa; elastic lamellae modulus

$E_2 = 0.89 \pm 0.27$MPa; elastin-collagen fiber modulus ,

$E_3 = 0.75 \pm 0.29$MPa; collagen fiber modulus

2.2.2. Geometry

In order to find the dimension of arteries, including inner diameter, thickness, thickness/diameter ration and thickness of different layers of artery, various numbers of references have been investigated. Table 2.1 shows the general information about all arteries.

Table 2.1 Dimensions of various types of arteries by permission of Daniel J. Schneck [164]

Vessel	Internal diameter	Wall thickness	Thickness/diameter ratio
Aorta	1–3 cm	2–3 mm	0.125
Main branches	0.5–2.25 cm	2 mm	0.182
Large arteries	4–5 mm	1 mm	0.222
Medium arteries	2.5–4 mm	0.75 mm	0.231
Small arteries	1–2.5 mm	0.5 mm	0.286
Tributaries	0.5–1 mm	0.25 mm	0.333
Small rami	250–500 μm	125 μm	0.333
Terminal arteries	100–250 μm	60 μm	0.342
Arterioles	25–100 μm	20–30 μm	0.400
Metaarterioles	10–25 μm	5–15 μm	0.571

Since, in this thesis the focus is on intracranial arteries, then, the information are restricted to carotid arteries. According to Stroke journal report in 2006 (Table 2.2), which explores relationships among gender, body size, neck size, and the diameters of the common carotid artery (CCA) and internal carotid artery (ICA), Using multivariate regression, the best predictors of sonographic diameters of CCA and ICA were determined based on age, height, weight, body mass index, body surface area, neck circumference, neck length, and blood pressure. Measurements were obtained in 500 consecutive patients (age 52-15 years; 61% women). Mean diameters of ICA (4.66_0.78 mm) and CCA (6.10_0.80 mm) in women were significantly smaller than in men with 5.11_0.87 mm and 6.52_0.98 mm for ICA and CCA respectively. Sex significantly influenced the diameters after controlling for body size, neck size, age, and blood pressure. Carotid arteries are smaller in women even after adjusting for body and neck size, age, and blood pressure.

Table 2.2 Baseline characteristics of studied population [165]

Parameter	Female	Male	Completeness of Data No. of Patients (female, male)
	Mean±SD		
Age, y	51.6±14.6	52.8±16.0	500 (306,194)
SBP, mm Hg	132.3±22.5	135.7±23.1	472 (292,180)
DBP, mm Hg	69.1±13.0	71.9±14.1*	472 (292,180)
MBP, mm Hg	90.2±14.6	93.2±15.1*	472 (292,180)
HR	74.4±13.5	73.4±14.6	459 (285,174)
Height, m	1.63±0.07	1.78±0.08**	495 (305,190)
Weight, kg	73.2±17.8	85.5±15.6**	495 (305,190)
BMI, m^2/kg	27.3±6.6	27.0±4.4	495 (305,190)
BSA, m^2	1.78±0.20	2.03±0.19**	495 (305,190)
Neck circumference, m	0.372±0.035	0.423±0.036**	323 (188,135)
Neck length, m	0.173±0.016	0.188±0.016**	323 (188,135)
ICA diameter, mm	4.66±0.78	5.11±0.87**	437 (266,171)
CCA diameter, mm	6.10±0.80	6.52±0.98**	441 (270,171)
	No. of patients (%)		
History of			
Hypertension	105 (34.3)	73 (37.6)	420 (263,157)
Diabetes	21 (6.7)	23 (11.8)*	408 (255,153)
Hypercholesterolemia	64 (20.9)	47 (24.2)	405 (252,153)
Atrial fibrillation	11 (3.6)	12 (6.2)	407 (257,150)
Heart diseases	51 (16.7)	36 (18.5)	420 (262,158)
Cerebrovascular disease	34 (11.1)	26 (13.4)	415 (260,155)
Smoking (current)	75 (24.5)	40 (21.6)	411 (261,150)
Smoking (former)	47 (15.3)	37 (19.1)	411 (261,150)

SBP, DBP, and MBP indicate systolic, diastolic and mean blood pressure, respectively; HR, heart rate.
*$P<0.05$; **$P<0.001$.

Also, another study [166], which investigated the shear modulus of common carotid arteries as function of pressure for the 25 volunteers via PWI technique, reported CCA dimensions almost as large as values in Table 2.2.

The other important geometrical data, needed to model the artery in three layers, is thickness of arterial wall and thickness value for each layer. An average thickness ratio of intima/media/adventitia of 13/56/31 for arteries was observed in Schulze-Bauer's studies [167]. The thickness ratio of media/adventitia is 2/1 in the computational model for the arterial wall presented by Driessen et al. [168]. In the study [169] in three-layered wall model, the intima/media/adventitia thickness ratio was set to 1/6/3.also, Holzapfel and Gasser used geometric data as Table 2.3 in their study [6].

Table 2.3 Parameters used in Holzapfel model [6]

Parameter	Description	Value
α	Opening angle	0°
R_i	Inner radius (undeformed configuration)	0.71 mm
H_m	Thickness media	0.26 mm
H_a	Thickness adventitia	0.13 mm
G_m	Shear modulus media	3.0 kPa
G_a	Shear modulus adventitia	0.3 kPa
k_{1m}	Fibre parameter media	1.18 kPa
k_{1a}	Fibre parameter adventitia	0.28 kPa
k_{2m}	Fibre parameter media	0.84 (dimensionless)
k_{2a}	Fibre parameter adventitia	0.71 (dimensionless)
p_i	Internal pressure	13.0 kPa
λ_z	Axial stretch	1.6 (dimensionless)
κ	Rate constant	1.0 s^{-1}
$\vec{e}_0$	Initial fibre directions	[0 1 0]
g_r	Degree of alignment of $\vec{e}_\rho$ with r-direction	0.0 (dimensionless)
g_θ	Degree of alignment of $\vec{e}_\rho$ with θ-direction	λ_θ^v (dimensionless)
g_z	Degree of alignment of $\vec{e}_\rho$ with z-direction	λ_z^v (dimensionless)
v	Power of alignment	4.0 (dimensionless)

The carotid arterial wall thickness of 0.48 ± 0.047 and 0.61 ± 0.018 mm (mean ±std) was applied for ages varying between 22–29 and 30–32 years respectively in study [170]. In this study, the wall thickness was evaluated on the B-mode image though manual tracing by a trained expert.

The pressure inside of vessel is also another factor which should be considered for modelling of that vessel. The Table 2.4 shows the common carotid artery parameters in patients with intracranial aneurysm and healthy control subjects [171]. Twenty seven patients with an antecedent of ruptured IA documented by cerebral angiography and who received surgical treatment at the local department of neurosurgery were recruited for the study. Twenty seven control subjects carefully matched for age, sex, body mass index, total, LDL and HDL cholesterol and triglycerides were recruited. None of them had personal or familial history of cerebrovascular disease, aneurysm or heritable connective tissue disorder.

Internal diameter (D_i) and intima-media thickness (IMT) were measured on the far wall of the right and left common carotid arteries. Wall-to-lumen ratio was calculated in diastole as $2\text{IMT}/D_i$. In each group, there was no significant difference for all measured parameters between left and right measurements and thus, the data presented are the combined values of both sites of measurement.

Moreover, the pressure of CCA varies between 9.7kPa (72mmHg) and 16KPa (120mmHg). The mean value is 13KPa (97mmHg) [171].

Table 2.4 Common carotid artery parameters in patients with intracranial aneurysm and control subjects [171]

Carotid artery parameters	Patients with aneurysms ($n = 27$)	Control subjects ($n = 27$)
Systolic blood pressure, mm Hg	122 ± 13	108 ± 9
Diastolic blood pressure, mm Hg	81 ± 7	73 ± 5
Mean blood pressure, mm Hg	98 ± 9	87 ± 6
Pulse pressure, mm Hg	41 ± 8	35 ± 6
Augmentation index, %	21.1 ± 8.5	15.8 ± 10.8
Stroke change in diameter, μm	405 ± 87	471 ± 140
Wall-to-lumen ratio	4.4 ± 0.6	5.3 ± 0.7

Values are mean ± SD.

2.3. Finite Element Modelling of Healthy Artery

In a structural problem, if one of the dimensions is significantly longer than the other dimensions defining a uniform cross-sectional area, and if the structure is subjected to only uniform lateral loads, then plane strain idealization is valid. With regarding to that blood vessels are subjected to lateral pressure from blood stream and their length value is much larger than other dimensions assuming plan strain state seems logical. Similar to plane stress idealization, because the number of nodes and elements in the model is reduced drastically, utilization of plane strain idealization leads to significant savings in computational cost without significant loss of accuracy in the quantities of interest [124].

Mechanical model of healthy artery could be appropriate starting point for a modelling of aneurismal wall. Since the finite element analysis is going to be used for finding of unknown variables, such as displacements and stresses, here some key features of the method are reminded. Finite element method (FEM) is numerical technique in mathematics to find the approximate solutions to partial differential equations (PDEs). Recall that five principal steps of finite element method are:

1- Division of whole into small parts (in order to represent both the geometry and solution of the problem). The domain of the problem is delineated by a collection of smaller simple sub-domains referred as finite elements. Finite element mesh is collection of all finite elements

2- Seeking an approximation to the solution in the form of a linear combination of nodal values and approximation functions over each part. In other words, the physical process is approximated over each finite element via desired type of functions, such as polynomials, and algebraic equations relating physical quantities at selective points, named nodes, of the element (derive element equation for all typical elements in mesh)

3- Assembly of elements (element equation) with respect to continuity and/or balance of physical quantities (internal fluxes) in order to find the solution of whole domain

4- Impose the boundary conditions and constraints

5-To find the solution of assembled equations and post processing of the results

FEM requires enormous amount of computations, so advanced computer technology should support its application. Although the first finite element commercial software published in 1964 [172], nowadays there exist more than hundreds of commercial software packages to select from. However only few of them dominating the market today. The comparison of different software packages barely on finite element basis is very difficult because first the software houses are almost diversified and second the fundamental basis of finite element analysis is often same. In general, the finite element analysis package is being chosen according to requirement of applications. Some of these commercial package have well-developed CAD options, while others are more appropriate for problem solving applications.

ANSYS® as one of the commercial finite element analysis (FEA) software packages [69] offers users two way to interface, command line and Graphic User Interface (GUI). The GUI in featured in a form of step by step menu. The package

has been designed with three principal modules: pre-processor, solution, and post-processor. Finite element model should be created by pre-processor; when the model is generated it will be solved via solution module in straightforward way. Finally, ANSYS provides powerful post process capabilities from plotting stress distribution along user defined path to showing colour strain contour graphs through post-processor module.

It is obvious that first step toward finite element analysis of healthy artery is to create finite element model. Generation finite element model requests information about the domain (geometrical data), material properties, boundary conditions, constraints as well as applied loads. The healthy common carotid artery is modelled under plane strain assumption (2D) as a triple-layered wall, complete annular structure with hollow in centre, which represents blood flow's path. The material has been assumed isotropic, linearly elastic, homogeneous, and non-viscous in each layer. Young's modulus of material in each layer is different from other ones.

The tri-material structure is subjected to uniformly distributed internal pressure *p*, which simulates the pressure inserted by blood flow (Figure 2.6). The radius of the hollow portion is 2.65mm. The other geometric information and material properties of model summarized in Table 2.5, which are assumed according to cited articles in section 2.2. Note that perfect contact without slipping is assumed along interface, implying displacement continuity. In Figure 2.6 each colour represents a layer with different Young's modulus.

After generating geometry of artery (domain) and determination of material properties according to Table 2.5, the next step toward converting geometric model into finite element model will be *discretization* or *meshing* of domain. Recall from FEM principles that domain is divided into set of finite elements, where collection of them is referred as finite element mesh of domain. An element is basic building block of FEA and there exist various types of elements. The type of object that is going to be modelled as well as type of analysis (like structural or thermal) dictates the type of elemen.

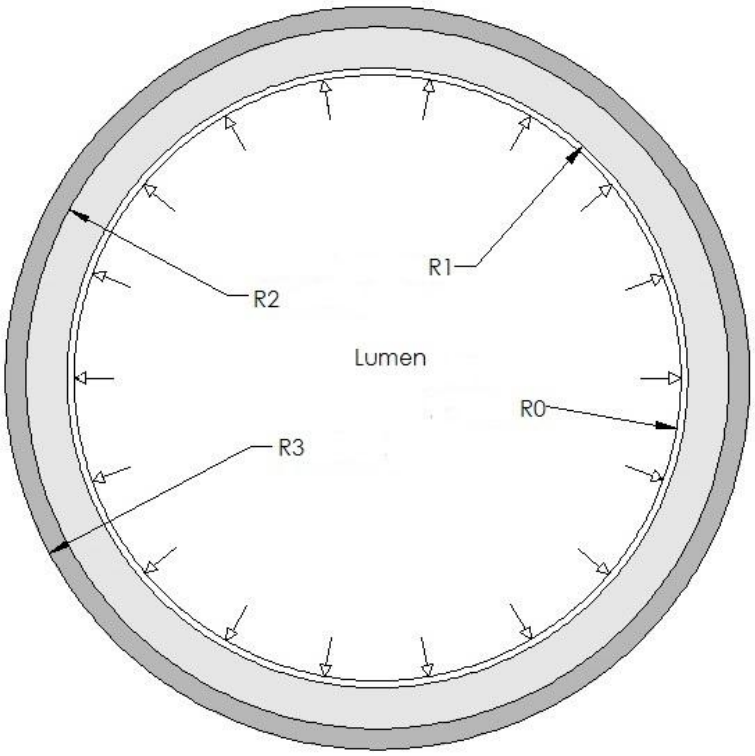

Figure 2.6 Schematic image of artery in 2D; each colour represents different layer

Indeed an element is mathematical relation that defines how the degrees of freedom of nodes relate to next. The elements could be lines (for example to model a beam) areas (2D and 3D) or solids. The element also relates how the deflections create stresses. Elements are connected to each other at common nodes.

Table 2.5 Geometrical parameters and material properties of model

Unit	Young's modulus [MPa]	Thickness [mm]	Poisson ratio	Internal diameter[mm]	Pressure lumen [KPa]
Intact wall	0.90	0.60	0.45	5.30	10-16
Intima	0.15	0.06	0.45	5.30	
Media	0.89	0.36	0.45	5.42	
Adventitia	0.75	0.18	0.45	6.14	

A node is coordinate location in space where the degrees of freedom (DOFs) are defined. DOFs for a point display possible movement of that point due to loadings. In addition, they represent which moments and forces are going to be transferred from one element to next one. The results of FEA (stresses and deflections) are generally demonstrated at the nodes.

The degrees of freedom of node depend on element type and they relate what type of forces and constraints are transferred via nodes to the element. Translation degrees of freedom are equivalent to axial or shear forces, while moments are equivalent to rotational degrees of freedom. For example, in order to transmit a force in specific direction a node should contain translation DOF in that direction. If the node did not have that particular translation DOF, the imposing a force to the node would be ineffective on the analysis. Likewise, putting force constraint in that specific direction will have no effect if the node be unable to transfer that force.

Plane 182 is the element type that has been used to mesh healthy artery domain. This element is quadratic solid element, which is defined by four nodes, having two degree of freedom at each node, translation in x (radial) direction and y (circumferential) direction. Generally it is used to model 2D solid structures. Figure 2.7 demonstrates the meshed model of artery. Note that the number of elements used in model is based on accuracy desired. Each colour represents different layer of arterial wall. It means that despite the fact that element type is same in all layers, the material properties defined for an element in one layer vary from material properties dedicated to elements in other layers. In other words, colours represent different material properties (Young's modulus) of elements.

In order to complete finite element model the constraints and applied loads should be added to meshed model. The artery in-vivo is imposed to cyclic blood pressure by blood stream due to pumping of blood into them via heart. In order to simulate blood pressure the nodes on lumen side of intima layer are subjected to constant pressure. Note that analysis type is limited to static-state in this study.

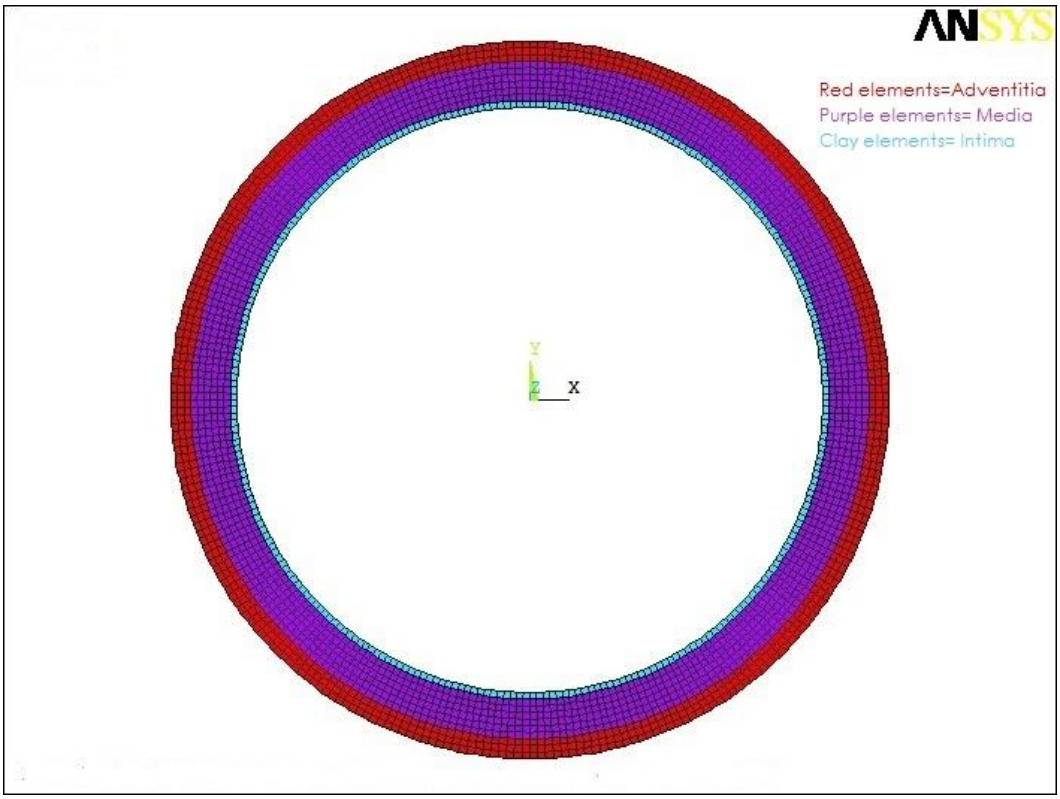

Figure 2.7 Meshed image of healthy artery in three layers: blue-coloured elements represent intima layer, purple and red coloured elements display media and adventitia layers respectively.

The meshed model has to be restrained in some locations to prevent rigid body displacement when the pressure is being applied into lumen's nodes. The constraints positions have been chosen after examination of various patterns. This constraint's pattern resembles the dilation of arteries as it occur in-vivo (Figure 2.8).

Once the finite element model is created, the next step is to solve the model via solution module. The analysis type has been determined as structural static type. The solution control options let users to adjust different parameters, such as small or large displacements. Nonlinearities affect behaviour of structure in different ways and severity, thus it sometimes should be considered in order to make the model more close to reality. The structural nonlinearities are divided into three categories: material, geometric, and constraint or boundary nonlinearities.

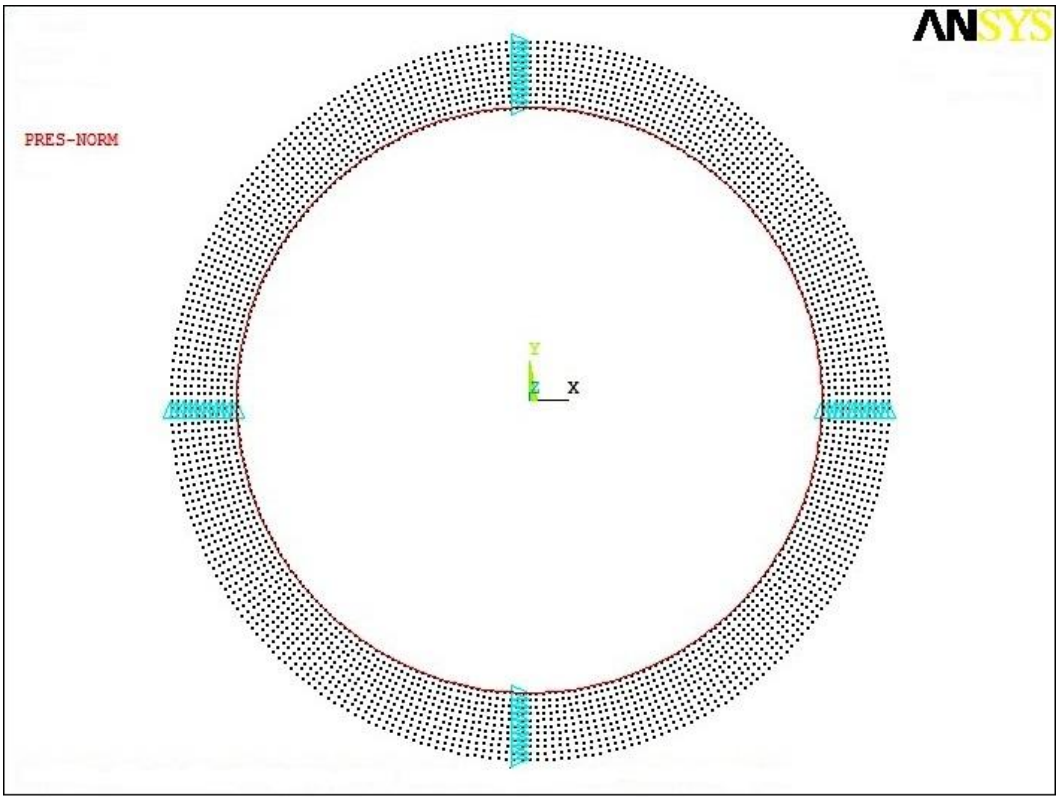

Figure 2.8 Nodal view of finite element model of healthy artery: the block dots are nodes; the blue triangles represent the constraints in circumferential direction, which are applied to some nodes in order to prevent rigid body motion and simulate more realistic expansion of artery; red line shows pressure imposed to nodes at lumen side in normal (radial) direction.

Governing equations that are derived with respect to large deformations and/or nonlinear strain-displacement relation (complete expression for strain components) are considered as geometrically nonlinear. In other words, presence of large strains, small strains but large displacements, loss of stability of structure, and rotations give rise to geometrical nonlinearity.

In this study the model is solved under steady-state assumptions (static analysis) when the pressure value is 16KPa (equivalent to 120 mmHg systolic physiological pressure) while the displacements assumed small, which implies that deformation is supposed linear. In continue, the solution control options are changed to large displacements, and the model is solved again with imposed geometric nonlinearity. Indeed, geometrically nonlinear finite element model is solved in seven different

pressure values (load-steps) starting from 10KPa (75 mmHg diastolic physiological pressure) and increased to 16KPa in six equal 1KPa increments. Solving nonlinear problems is based of Newton-Raphson method in ANSYS [71].

Finally, when the model is solved, results of the analysis can be demonstrated via general postprocessor module in ANSYS. The plotted and/or listed stresses, displacements, contours of model with respect to different variables and physical quantities, deformed shapes, and many other featured will be displayed and discussed in next chapter.

2.4 Finite Element Modelling of Aneurismal Artery

Once healthy artery was modelled, the last step is to model the arterial wall with sac-like aneurysm. Again common carotid artery, as part of intracranial vasculature, has been selected and all geometric data obtained according to that particular artery. Similar to healthy artery, the geometric domain is created and meshed with PLANE182 element type. The most distinct difference between healthy artery and diseased one is in generation of finite element model. Solution and post processing stages in FEA of diseased and healthy models are almost same. In order to simulate the artery that suffers from aneurysm in part of its wall, a segment of wall is assumed diseased and material properties of wall at that part are assumed deteriorated.

The geometric model of diseased artery is as same as healthy one with all same assumptions. Created domain is meshed with PLANE182 element type. Elements in each layer have their own mechanical properties according to Table 2.5. Remind from chapter 1 that aneurysm occurs because of deterioration of part of vessel's wall. Then, in order to simulate diseased part the new sets of material parameters are defined and material properties of elements in aneurismal section are determined according to new material properties. In other words, the Young's modulus of diseased elements is reduced in particular ratio in order to simulate the deteriorated wall.

Since there is no precise experimental data about the proportion at which material properties change in aneurismal arteries, reducing the material properties of each layer in specific different ratios as various cases could be examined, but it is not perspective of this study. Instead, decreasing the modulus of elasticity of different layers in constant ratio is evaluated in format of some cases. It means in each case one or more that one layer is assumed diseased and in another case different layer or distinct combination of layers are considered to be diseased. In all these cases, diseased arterial layer means 39 elements along wall in circumferential direction belong to that layer (2.34 mm long) have 20 times smaller Young' modulus (mechanical properties) than other healthy elements. Seven different cases are supposed as below:

1- Case I: all three layers (intima, media, and adventitia) are diseased and their Young's moduli reduced to 1/20 of healthy value.

2-Case II: only media layer is assumed to be diseased and its Young's modulus reduced to 1/20 of healthy value.

3-Case III: only adventitia layer is assumed to be diseased and its Young's modulus reduced to 1/20 of healthy value.

4-Case IV: only intima layer is assumed to be diseased and its Young's modulus reduced to 1/20 of healthy value.

5-Case V: intima and media layers are assumed to be diseased and their Young's moduli reduced to 1/20 of healthy value.

6-Case VI: media and adventitia layers are assumed to be diseased and their Young's moduli reduced to 1/20 of healthy value.

7-Case VII: intima and adventitia layers are to be diseased and their Young's moduli reduced to 1/20 of healthy value.

In Figure 2.9 finite element mesh of arterial wall with three diseased layers in its small fragment is depicted. Each colour represents different material properties.

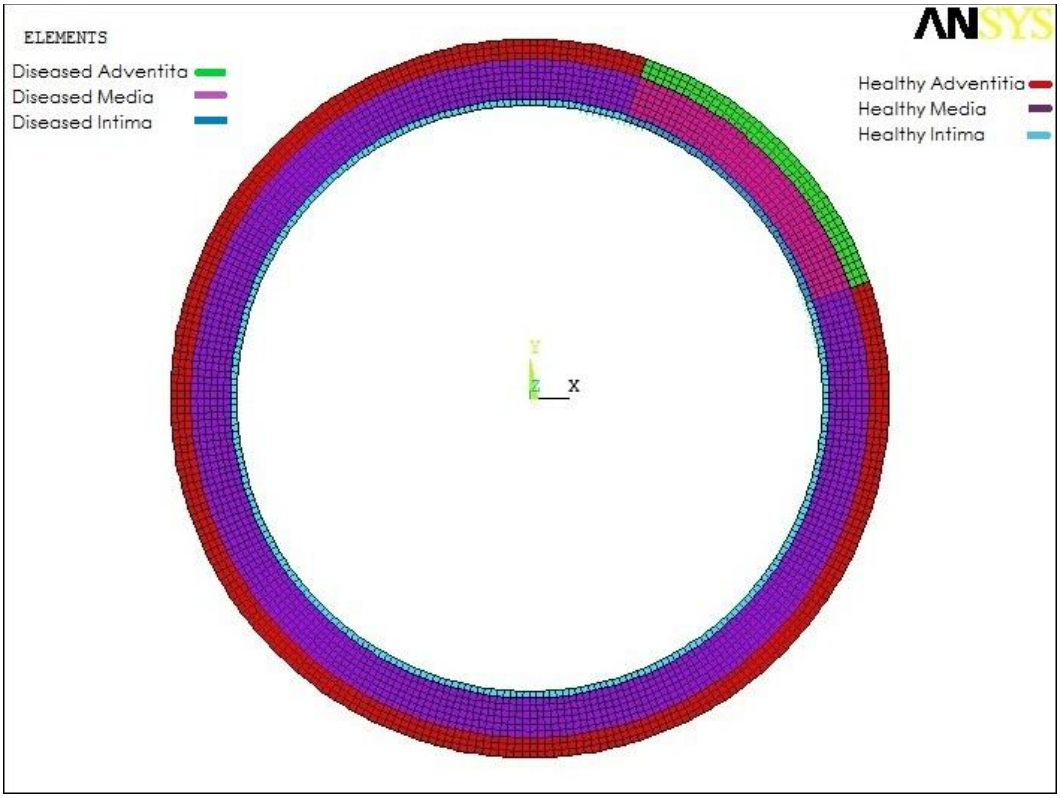

Figure 2.9 Elements of arterial wall with deteriorated wall in part: different colours represent materials with different Young's moduli. Pale blue, deep purple and red colours refer to healthy intima, media, and adventitia elements respectively; while deep blue, pale purple and green ones are diseased elements of intima, media, and adventitia sequentially. Note that diseased elements have 1/20 modulus of elasticity of healthy elements of that layer.

To complete finite element model the constraints and applied load should be added to model. The pressure-ranging from 5KPa (37.5mmHg) to 20KPa (150mmHg)-is applied to 33 elements (1.98mm long) in the most inner side of artery, adjacent to lumen, as simulation of blood flow pressure. Note that 10 elements from the last pressure applied element away in positive and negative circumferential directions have been supported by spring-type elements with stiffness 250000N/m in order to approach to more realistic simulation. COMBIN14 is the type of element that has

been used to model springs in ANSYS. The line elements in Figure 2.10 are those springs.

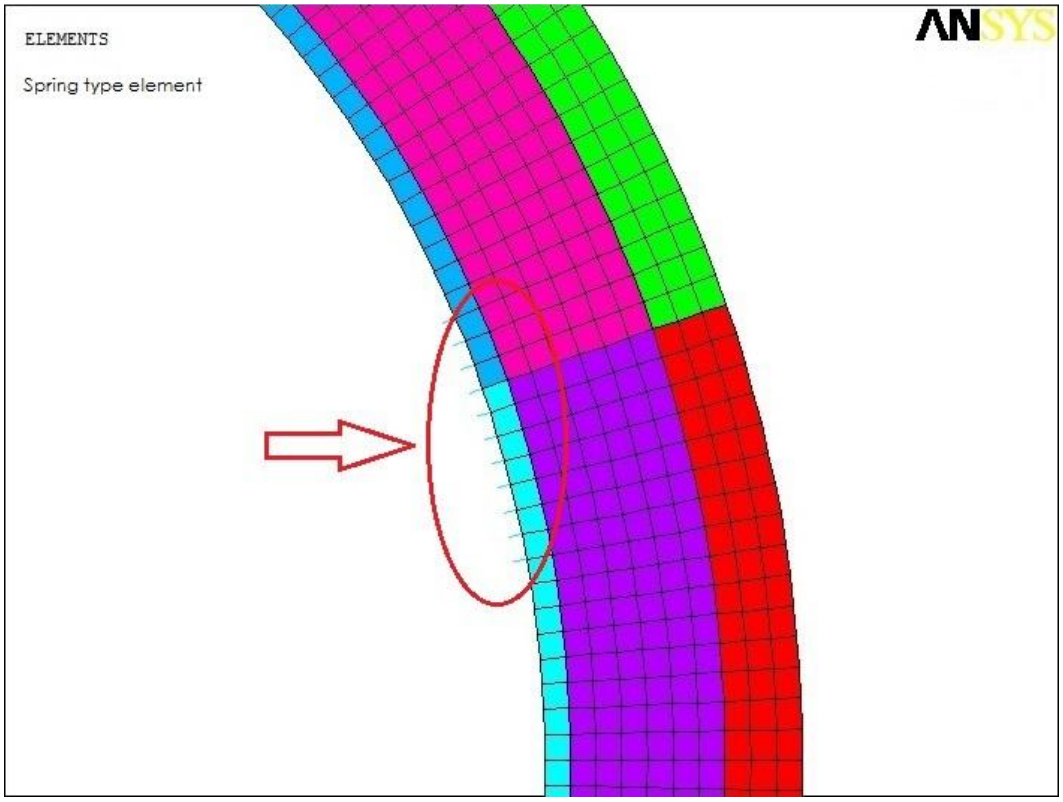

Figure 2.10 Different types of element used for mesh of geometric unhealthy arterial wall: the rectangle elements are solid type elements PLANE 182, and line elements, which demonstrated by red flash and circle are spring type elementCOMBIN14.

The last stage to accomplish finite element model is constrains. In addition to constraints of healthy artery, also all nodes adjacent to lumen are restrained from displacement in radial direction except pressure applied nodes. This constraint pattern lets the pressure to render sac-like bulge in arterial wall and simulates sac-like aneurysms. Figure 2.11 depicts nodes, applied pressure and constraints. Notice that in both models, healthy and diseased, the general element length is 0.06mm.

After creation of finite element model the solution and post processor stage are virtually as healthy model. The results and discussion about them will be presented in next chapter. Moreover, the finite element meshes of seven different cases are displayed in Figures 2.12 and 2.13.

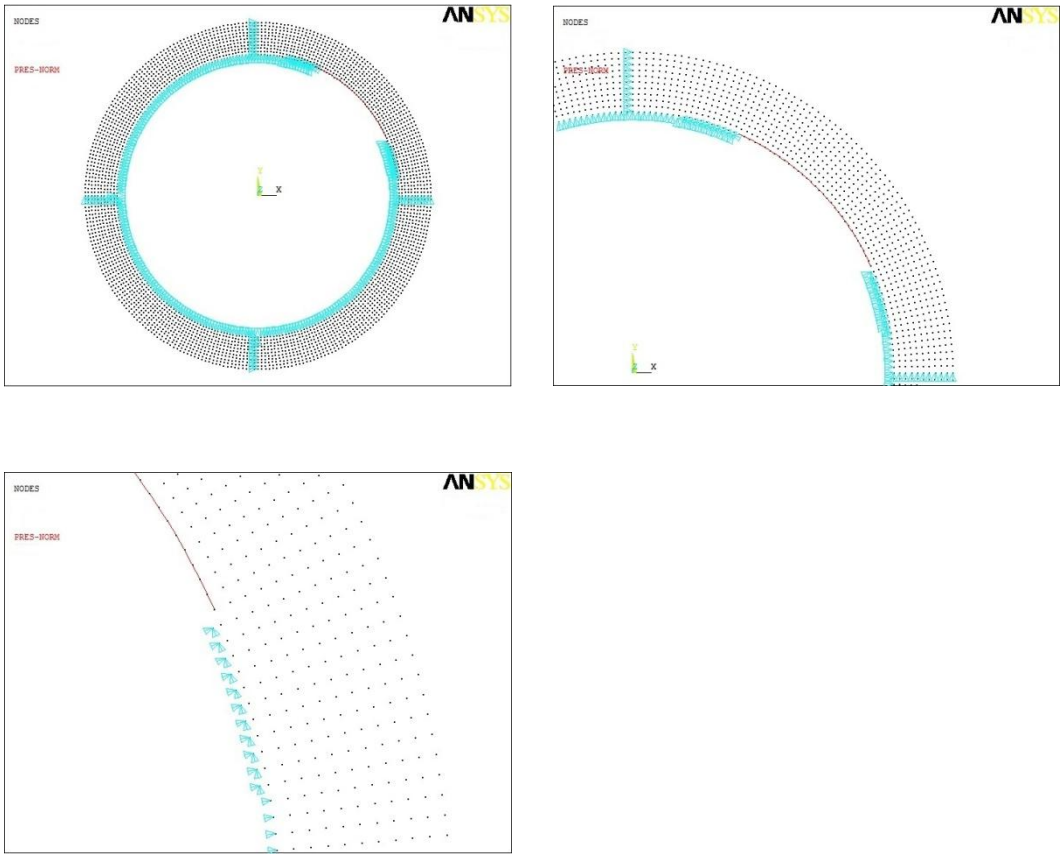

Figure 2.11 Nodes, constraints and pressure applied nodes: the constraints are depicted in blue triangles and restrain the nodes adjacent to lumen from radial displacement. Red line has drawn on nodes which are subjected to pressure. Also in lower picture there are some nodes which have been restricted in both radial and circumferential directions; they are the nodes dedicated to spring elements in one end and are assumed fixed.

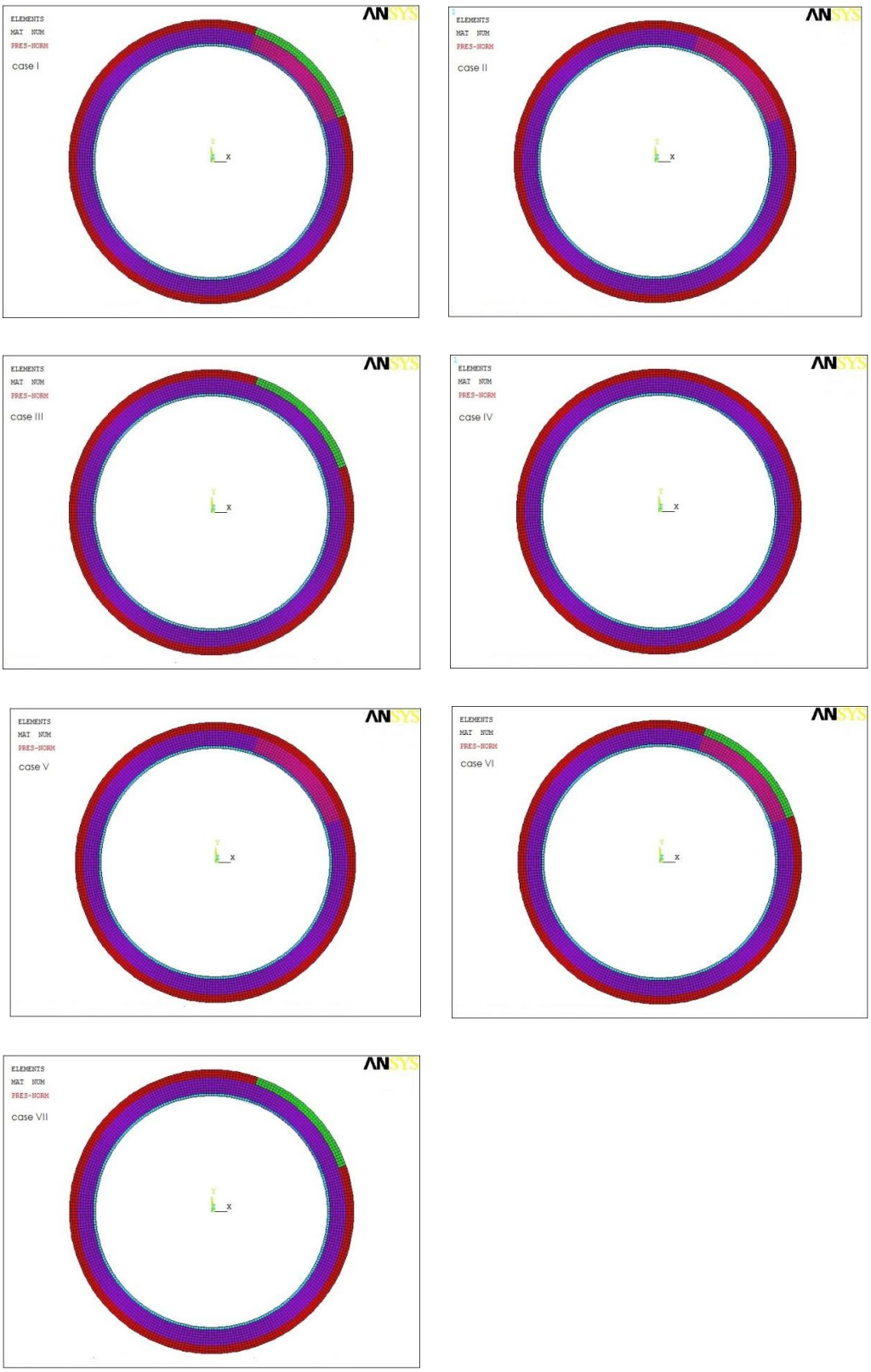

Figure 2.12 Finite element mesh of Different cases

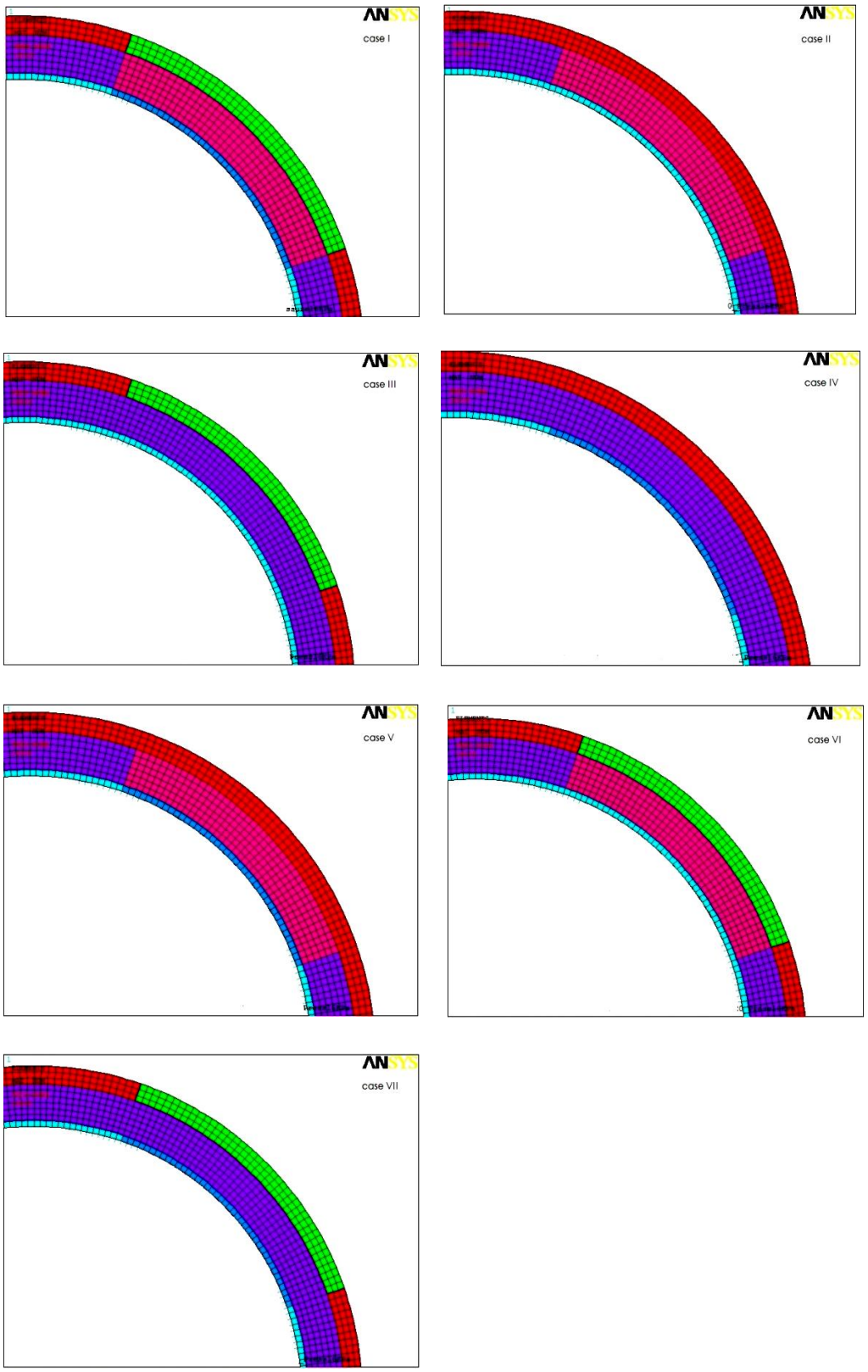

Figure 2.13 Finite element mesh of Different cases (enlarged image)

CHAPTER 3

RESULTS AND DISCUSSION

In the present study, the two dimensional common carotid arterial wall (plane-strain), including three layers with linear elastic, isotropic, homogeneous, and non-viscous material properties, under constant pressure in lumen was modelled and analyzed numerically with respect to finite element analysis (FEA) principles in two healthy and sac-like aneurismal conditions. The aneurysm was introduced as bulge in healthy wall through decreasing mechanical properties of wall in small segment and applying pressure to that part.

The present chapter contains the numerical results of healthy artery and its comparison with other studies done in literature. Next, the aneurismal model results would be demonstrated and discussed; and finally, there will be comparison between physical quantities of healthy and diseased arterial wall in seven different diseased cases.

3.1. Healthy Arterial Wall

Analyzing mechanics of healthy arterial wall, as starting point to examine aneurismal vessel, can address a new path that must be travelled to find answer to questions about aneurysm's natural history. For instance, it can introduce the physical quantities that should be evaluated in aneurysms to offer new standard for rupture potential. In addition, it obtains the basic gauge for comparing the values of interested quantities in healthy functional artery and diseased one. From perspective of mechanics the wall thickness and distribution of stresses are very significant, so

the focus in result section will be on displacements and stresses. In first section of healthy artery the results of linear geometrical model is presented and in the next section nonlinear geometry effects will be displayed.

3.1.1_Linear Healthy Artery

Recall from chapter two, once 2D finite element model was created, systolic 16KPa pressure was applied to lumen; consequently, it displaced and deformed. The displacements render stresses in different directions. The distribution and value of generated stresses in different directions as well as thickness change because of applied pressure are desired physical quantities in this study.

The deformation and change in wall thickness are the first physical quantities that seem significant in arteries under physiological pressure. Figure 3.1 represents the edges of undeformed artery and deformed shape under 16KPa pressure.

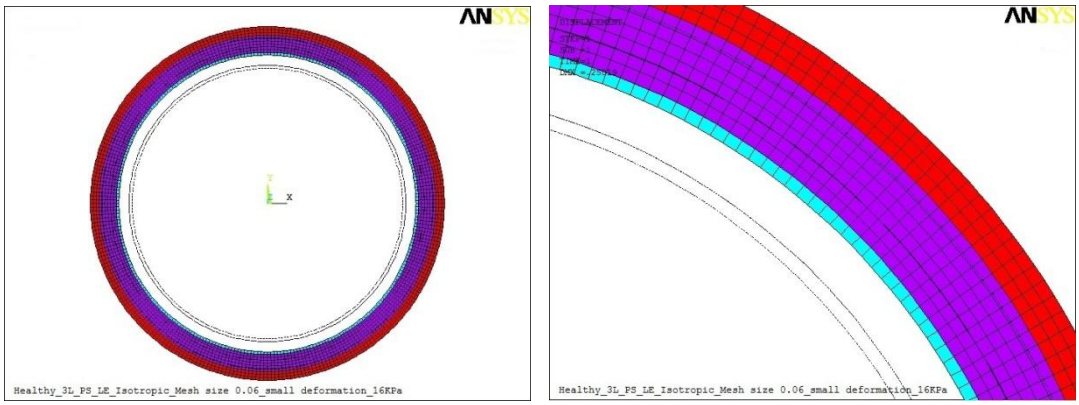

Figure 3.1 Deformed shape and edges of undeformed shape of artery under 16KPa pressure: the coloured elements belong to deformed shape while the edges of undeformed shape are shown in black dot lines. Like finite element model in chapter 2 blue, purple and red coloured elements represent intima, media, and adventitia layers respectively.

Recall the wall thickness of healthy model before imposing any pressure was 0.6 mm; whereas, wall thickness after applying pressure reduces to 0.55787mm. As expected the maximum radial displacement occurs in elements adjacent lumen and

the displacement's value is decreasing as travelling along wall thickness toward outer fibres in radial direction. In addition, the value of circumferential displacement is relatively very small throughout model. Note that continuity of displacements is consistent to mathematical model's assumptions in previous chapter.

Figure 3.2 represents the radial and circumferential displacements of healthy artery along path defined through wall thickness. The continuous radial displacement is maximum in the most inner layer and reducing as going away toward outer fibers. The minimum radial displacement occurs in the most outer nodes of adventitia layer.

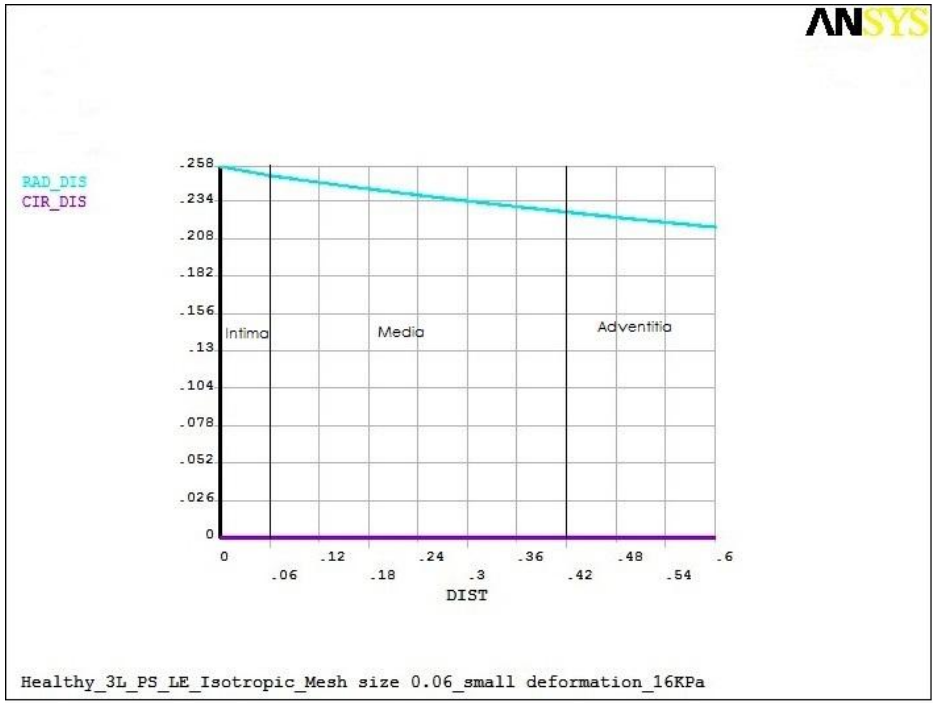

Figure 3.2 Radial and circumferential displacements along wall thickness in radial direction: blue line represents the radial displacement and purple line shows circumferential displacement.

Another desirable variable in this study is distribution of stresses as substantial biomechanical factor. Because the displacements have been defined in radial and circumferential direction the stresses in these directions as main membrane stresses are very important. The Figures 3.3 and 3.4 represent the radial and circumferential

stress distributions in deformed shape after applying 16KPa pressure. It is clear from Figure 3.3 that the maximum radial stress happens in intima elements adjacent lumen; whereas, the minimum radial stress occurs in the most outer nodes of adventitia layer. Note that the developed radial stress is compression in all regions. Circumferential stress distribution is presented in Figure 3.4 and it is noted that it is tensile stress throughout model. Moreover, the maximum circumferential stress occurs in media layer just after interface between media and intima.

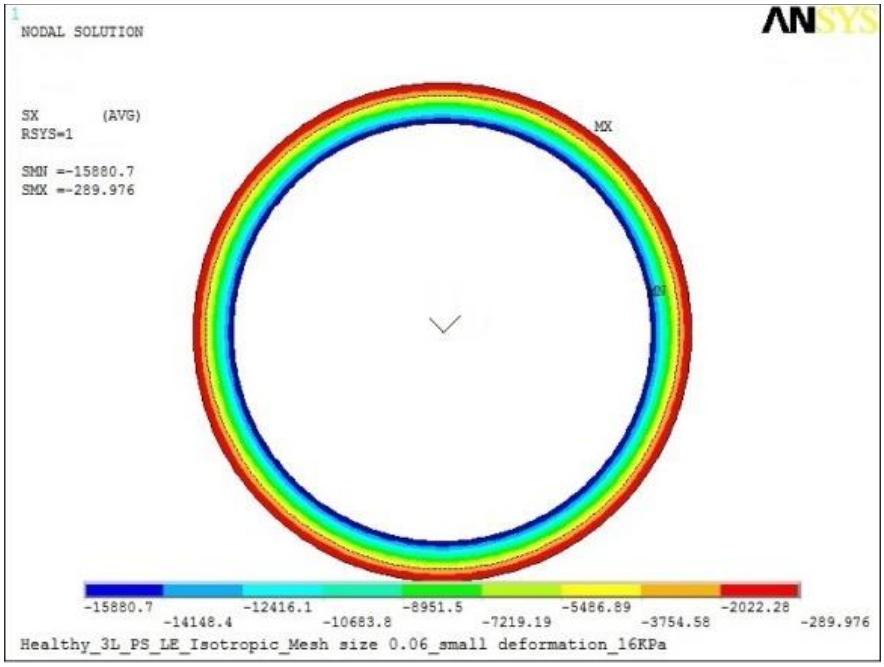

Figure 3.3 Radial stress distribution in deformed healthy artery after applying 16KPa pressure. Note that negative sign refers to adverse direction. The positive radial direction is from inside of lumen to outward. Also, the x-axis refers to radial and y-axis to circumferential directions.

Generally in all mechanical problems, which dealing with stresses, finding the maximum tensile or compressive stress and its direction is essential for failure discussion. So, principal stresses and their distribution contribute to better analysis of problem. Figure 3.5 illustrates the maximum principal stress distribution on deformed arterial wall. The results of maximum principal stress reveal that the circumferential stress is the principal stress. Thus, it is clear that the media layer is enduring the higher values of stress than other layers.

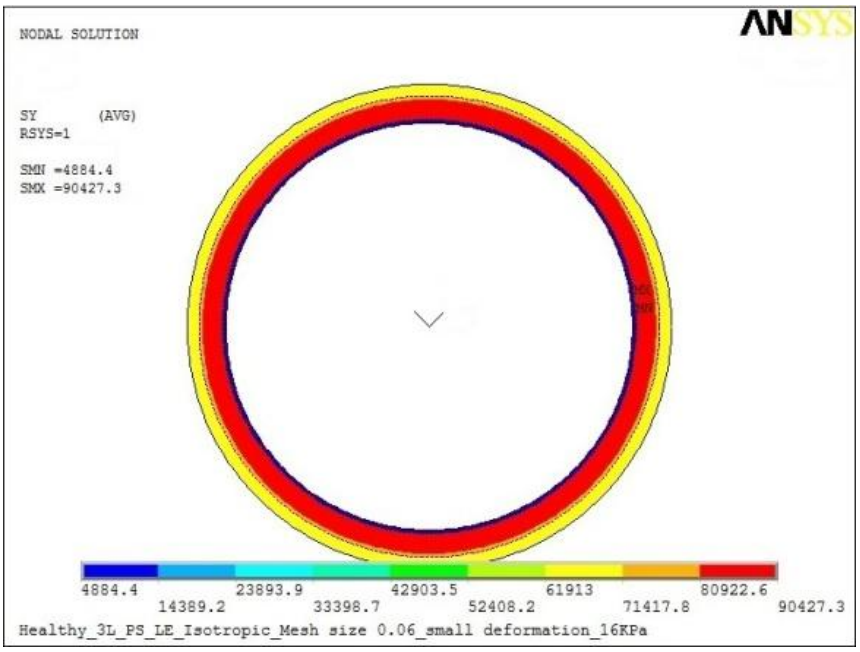

Figure 3.4 Circumferential stress distribution in deformed healthy artery after applying 16KPa pressure. Note that the positive circumferential direction is counter clockwise direction.

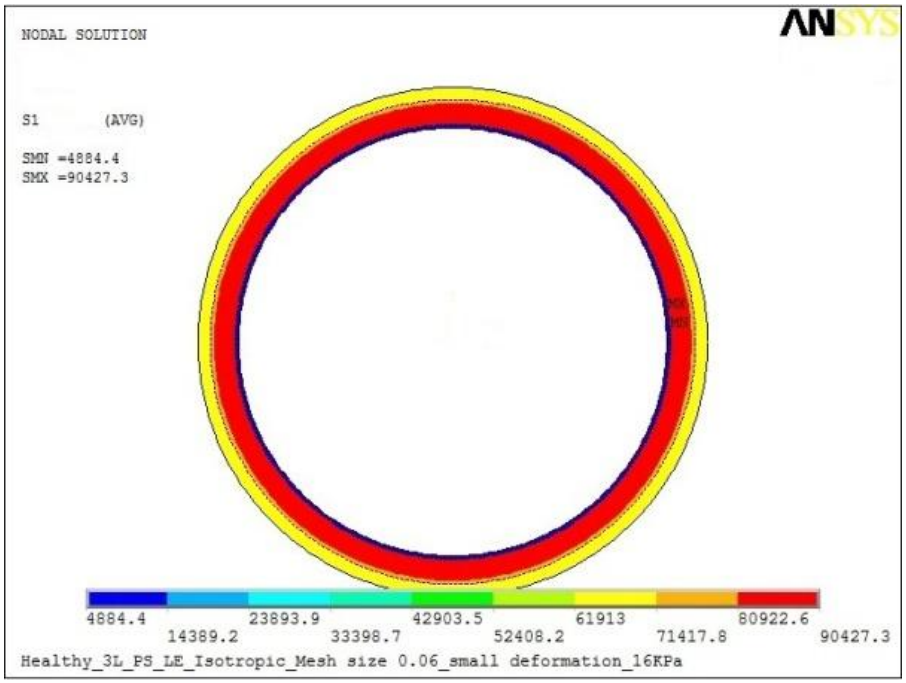

Figure 3.5 Maximum principal stress distribution in deformed healthy artery under 16KPa pressure

Von Mises stress is another criterion about yielding of materials. The interesting point about Von Mises stress distribution is that it almost follows the pattern of circumferential stress, and off course 1st principal stress, just with small deviations in values. Figure 3.6 depicts the distribution of Von Mises stress on deformed healthy artery, which is imposed to 16KPa pressure.

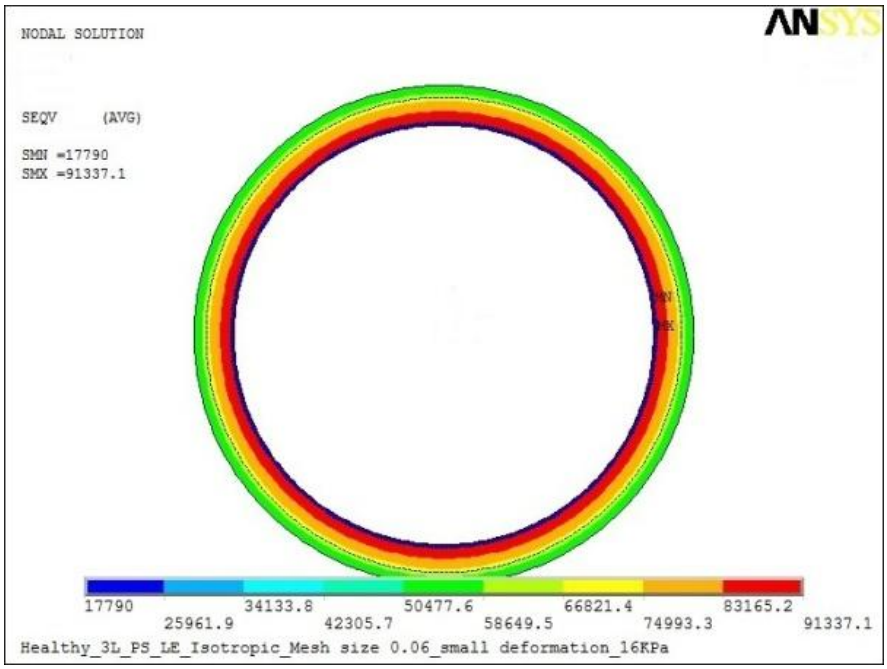

Figure 3.6 Von Mises stress distribution in deformed healthy artery under 16KPa pressure

The maximum values of different stress types as well as the locations that the maximum stress happen are collected in Table 3.1.

Table 3.1 Maximum value of different stresses and their location

Stress type	Maximum value	Location of maximum value
Radial	-15880.7	Intima adjacent lumen
Circumferential	88733.7	Media near intima
Max. principal	88733.7	Media near intima
Von Mises	88406.03	Media near intima
Shear	0	-

In order to examine stress variations more precisely the changes of radial, circumferential and shear stresses have been plotted in Figure 3.7 along the wall thickness.

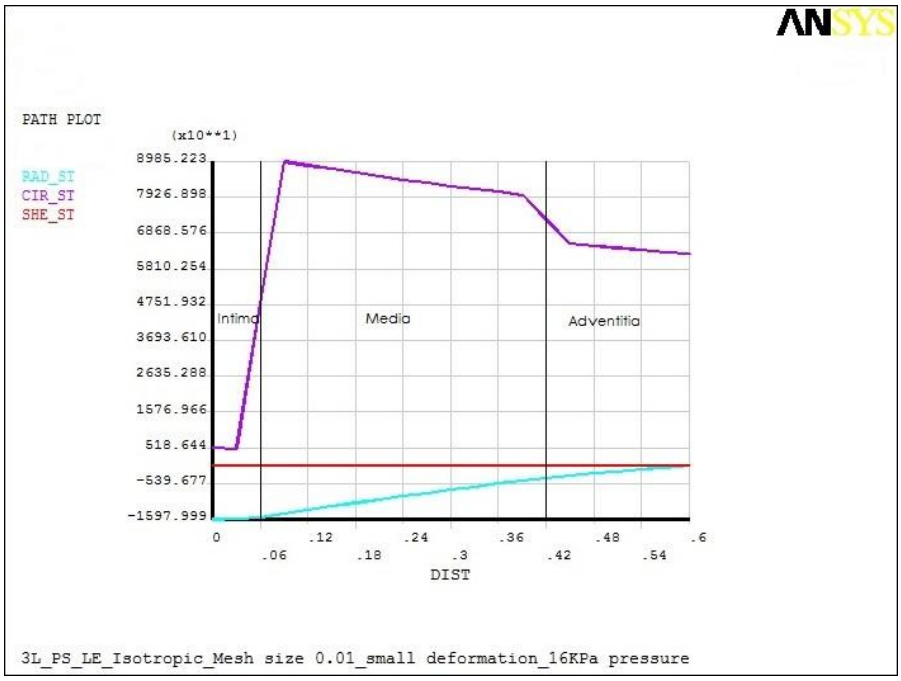

Figure 3.7 Radial, circumferential, and shear stresses along wall thickness of undeformed arterial wall: note that this graph is plotted with smaller mesh size (0.01mm), thus there exist a small differences in values of stresses compared to previous figures.

Stress distribution results make it clear that the most important stress, which has higher value in comparison to others, is circumferential stress. Therefore, focusing of variation of circumferential stress, which is principal stress (due to relatively very small shear stress) at the same time, seems logical. Change in this stress along wall thickness has been plotted in Figure 3.7. It is obvious that maximum circumferential stress occurs in media near intima layer. Also, there exists step-like stress transient in layers interface. Radial stress changes continuously along wall thickness and no discontinuity or step-like transient is being observed in interface of layers. However, the value of radial stress is about 5 times smaller than circumferential stress.

The acquired numerical results from healthy model should be verified via comparing to some proved results. Recall from chapter two that couple of boundary conditions, either natural or essential, were derived by using minimum total potential energy principle. Equations (B.4) to (B.9) offer useful information about boundary conditions of model. Equation (B.4) and (B.9) state that the radial stress at nodes adjacent lumen should be same as applied pressure just in opposite direction:

$$\sigma_r^I = -p \quad @\, r = R_0 \;\&\; 0 \le \theta \le 360$$

and it also have to be zero at the most outer nodes of adventitia layer:

$$\sigma_r^A = 0 \quad @\, r = R_3 \;\&\; 0 \le \theta \le 360$$

while the radial displacement is not zero at those locations. Simply by controlling the evoked numerical results it is emerged that radial stresses at intima nodes adjacent lumen is – 15979.99, which is very close to 16000Pa applied pressure, and tends to zero as going through wall thickness toward media and adventitia layers and becomes -290 in the most outer nodes of adventitia (Figure 3.7).Note that at both those locations the radial displacement is not zero (Figure 3.2). The small differences between assumed boundary conditions and numerical results stem from the fact that numerical method is giving rise to approximations; and if the mesh size gets smaller the results will approach to true values and it confirms a convergence of numerical solutions to assumed ones. For example, in Figure 3.3 and Table 3.1 the maximum radial stress has been derived with mesh size 0.06mm then its value is 15880.7; whereas, is Figure 3.7 the smaller mesh size (0.01mm) has been used and the value of circumferential stress is 15980Pa and very close to 16000Pa.

Likewise, according to the fact the circumferential displacement and shear stress are almost zero in whole model with respect to numerical results (Figures 3.2 & 3.6) all other boundary conditions in equations (B.3) to (B.9) are satisfied. Moreover, there is study documented in literature that also offers the finite element analysis results for circumferential Cauchy stress along the arterial wall [125]. In that study a normal left anterior descending coronary artery has been modelled and numerically

analyzed as a two layer, thick walled tube, where each layer treated as a fibre-matrix anisotropic material. The distribution of the circumferential Cauchy stress σ_θ through deformed wall thickness (just media and adventitia) from Holzapfel study [125] and present study with three layers is plotted in Figure 3.8.

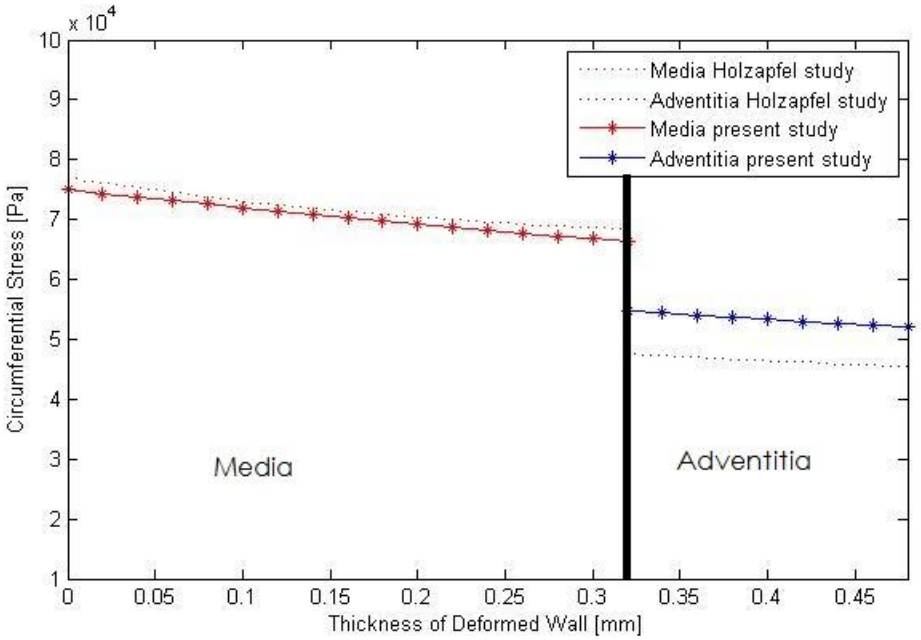

Figure 3.8 Finite element results of circumferential Cauchy stress through deformed wall thickness (media and adventitia) at the physiological mean blood pressure 13.3KPa. The solid lines show stress calculated in the present study, while the dotted lines represent results of Holzapfel study.

Hopzapfel has used more sophisticated material model as well as considered residual stresses of arteries. Despite the fact that the model used in this study has linear material model and the residual stresses have not been considered, the results of both studies are very close, especially in media, which is also the critical layer.

3.1.2. Geometrical Nonlinear Healthy Artery

Recall from previous chapter section 2.3 that geometrical nonlinearity was considered by using whole strain-displacement relation:

$$\varepsilon_r = \frac{\partial u}{\partial r} + \frac{1}{2}\left(\frac{\partial u}{\partial r}\right)^2$$
$$\varepsilon_\theta = \frac{1}{r}\frac{\partial v}{\partial \theta} + \frac{u}{r} + \frac{1}{2}\left(\frac{u}{r}\right)^2 + \frac{1}{2r^2}\left(\frac{\partial u}{\partial \theta}\right)^2 \qquad (3.1)$$
$$\varepsilon_{r\theta} = \frac{1}{r}\frac{\partial u}{\partial \theta} + \frac{\partial v}{\partial r} + \frac{\partial u}{\partial r}\frac{1}{r}\frac{\partial u}{\partial \theta}$$

The results of geometrical linear healthy artery revealed that the wall thickness and circumferential stress are most important features that should be considered in healthy artery analysis. Thus, in this part the differences of these features between linear and geometrical nonlinear model are going to be illustrated.

The wall thickness of healthy artery with geometric nonlinearity reduces from 0.6mm in unload state to 0.55211mm after applying 16 KPa pressure. It is obvious that geometric nonlinearity does have an effect on wall thickness change as the arterial wall deforms under pressure. For example, under systolic pressure (16KPa) the difference between linear and nonlinear deformed wall thickness is 0.00576mm:

$$\Delta t = t_L - t_{NL} = 0.55787 - 0.55211 = 0.00576$$

where t_L is wall thickness of deformed arterial wall with geometric linearity, and t_{NL} is wall thickness of deformed wall when there is geometric nonlinearity. The changed thickness ratio percentage was calculated about 1%:

$$\frac{t_L - t_{NL}}{t_L} = \frac{0.55787 - 0.55211}{0.55787} = 0.0103 = 1.03\%$$

and this number will be reduced for smaller pressure values; for instance, this ratio is 0.35% for diastolic pressure 10KPa. Table 3.2 confirms the effects of geometrical nonlinearity in wall thickness of artery. However, this effect increasing in higher

pressures. Figure 3.9 represents the arterial wall thickness with both linear and geometrical nonlinear assumptions. It is clear that in linear model the wall thickness decreases linearly as pressure increases, but with geometrical nonlinearity wall's thickness reduces nonlinear when pressure changes.

Table 3.2 Wall thickness values in linear and geometrical nonlinear models and their change ratios: first column shows different pressure levels, second and third columns are whole wall thickness of artery in nonlinear and linear model, and fourth column represents the change ratio of wall thickness in percentage.

Pressure [KPa]	$(t_{NL})_W$ [mm]	$(t_L)_W$ [mm]	$\left(\frac{\Delta t}{t_L}\right)_W \times 100$
10	0.5716	0.5737	0.35%
11	0.5686	0.5710	0.43%
12	0.5654	0.5684	0.53%
13	0.5622	0.5658	0.63%
14	0.5589	0.5631	0.75%
15	0.5555	0.5605	0.88%
16	0.5521	0.5579	1.03%

Figure 3.10 demonstrates the arterial wall thickness change ratio percentage between linear and geometrical nonlinear model, $\left(\Delta t / t_L\right)_W \times 100$, with respect to pressure in physiological range and reveal the nonlinearity effect more apparent.

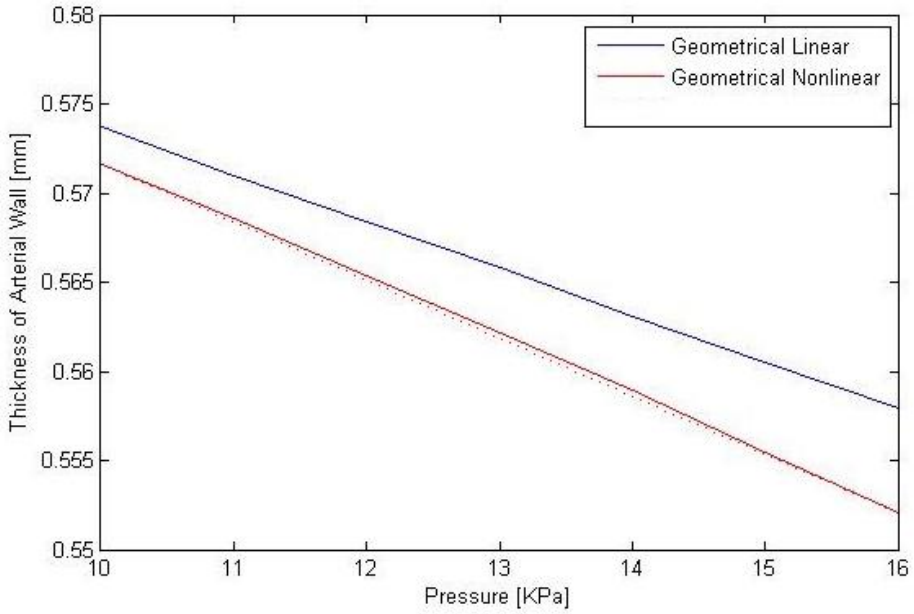

Figure 3.9 Wall thickness of healthy artery in linear and nonlinear model versus pressure. Note that dotted line is linear baseline to show deviation of nonlinear model from linearity.

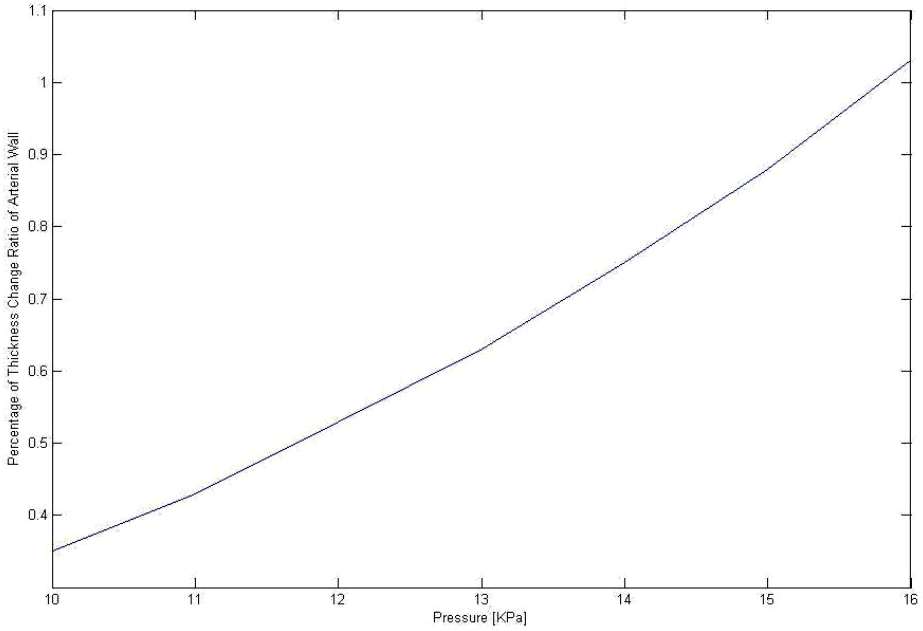

Figure 3.10 Percentage of thickness change ratio of linear and geometrical nonlinear model to linear value versus pressure

As mentioned the circumferential stress is the most important stress type in arterial wall mechanics due to linear healthy model. The differences of circumferential stress between linear and nonlinear model in middle of each layer, when pressure is changing from diastolic 10KPa to systolic 16KPa, is depicted in Figure 3.11.

Due to the fact that circumferential stress experiencing step-like transition in interface of layers, the stress versus different pressure values has been depicted in middle nodes of each layer. R_{01}, R_{12} , and R_{23} refer to middle nodes of intima, media and adventitia layers respectively. Note that the radial stress changes with respect to nonlinearity are negligible, so related graph has not been illustrated.

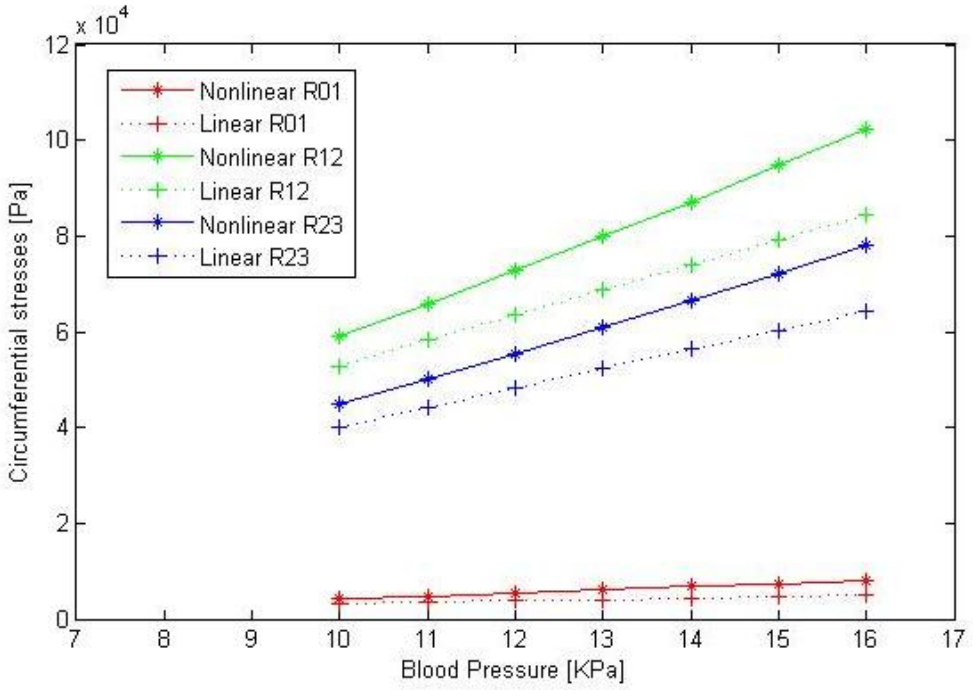

Figure 3.11 Circumferential stress of healthy artery with respect to pressure in middle of each layer in two states of geometrical linear and nonlinear assumptions. R01, R12, and R23 are nodes in middle of intima, media and adventitia layers respectively.

Figure 3.11 implies that the difference between linear and nonlinear circumferential stress will increase, if applied pressure increases. The increment is happing in all three layers. Interestingly, although the value of difference between linear and

nonlinear model (in specific pressure) is largest for media and smallest for intima, the ratio of this difference to initial value of stress (linear state) is higher in intima (Table 3.3).It means that the change rate of circumferential stress is higher in intima rather than other layers.

For example, consider the pressure 16KPa; the circumferential stress increases from 84.583KPa in linear state to 102.470KPa in nonlinear model at middle of media layer. The stress has been increased 17.887KPa and the ratio of this change with respect to linear value is about 21.15%. It means in nonlinear state the media layer actually has been subjected to 21.15% more stresses than linear state.

The circumferential stress value of node at middle of adventitia has been increased 21.62% in comparison to its linear state, whereas the increased value is just 13.908KPa. Finally a node at middle of intima layer has incurred to 63.7% change (3.185KPa increment) in its stress value when geometric nonlinearity is imposed. Table 3.3 demonstrates increments in amount of circumferential stress and its ratio for three layers at mid-points in different pressures.

Finally, according to Table 3.3 and Figure 3.11, two points can be elicited. First, the nonlinear geometry can affect the model more as the pressure value is rising up. Second, the elements that are enduring smaller values of circumferential stress can be affected more by geometrical nonlinearity. In three layered arterial wall the intima layer elements are subjected to lower values of circumferential stress so they affected more than media and adventitia layers elements, which are subjected to higher circumferential stresses.

Table 3.3 Table represents increment of circumferential stress when geometrical nonlinearity is imposed to linear model. First column shows pressure, second column is difference between values of circumferential stress in linear and nonlinear model for node at middle of intima layer, and third column represents the ratio of difference to linear value of circumferential stress at the same point Likewise, columns four and five are same quantities for node in middle of media layer; and sixth and seventh columns for a node at middle of adventitia layer.

Pressure [KPa]	Intima		Media		Adventitia	
	$\sigma_N - \sigma_L$ [Pa]	$\left(\frac{\Delta\sigma}{\sigma_L}\right)_I$	$\sigma_N - \sigma_L$ [Pa]	$\left(\frac{\Delta\sigma}{\sigma_L}\right)_M$	$\sigma_N - \sigma_L$ [Pa]	$\left(\frac{\Delta\sigma}{\sigma_L}\right)_{Ad}$
10	1112.3	35.6%	6243	11.81%	4846	12.05%
11	1369.9	39.85%	7687	13.22%	5969	13.50%
12	1659.6	44.26%	9314	14.68%	7234	14.99%
13	1983.7	48.83%	11134	16.20%	8651	16.55%
14	2344.3	53.59%	13161	17.78%	10228	18.17%
15	2743.9	58.54%	15407	19.43%	11976	19.86%
16	3184.8	63.70%	17887	21.15%	13908	21.62%

3.2. Aneurismal Artery

Arterial sac-like aneurysms have many features in common with familiar structural engineering problem. In fact, it analogizes the deformation and permanent bulging of a pipe under oscillatory internal pressure, which undergoes rupture due to fatigue failure. Although the natural history of aneurysm is complicated combination of mechanical and physiological processes that change the composition and strength of arterial wall, it is obvious that aneurismal rupture is stemmed from failure of the wall's structure to endure the wall's stresses resulting from the pressure applied by pulsatile blood flow.

Therefore, definition of new criteria for calculation of rupture risk based on stresses distribution in distended membrane and knowledge of the corresponding stress failures seem essential. This is place where solid mechanics can really contributes to deeper understanding of natural history and possible treatment of saccular intracranial aneurysms.

Remind in chapter 2, for simulating aneurismal wall the part of arterial wall was supposed deteriorated and the Young's modulus of each layer was reduced to specific ratio of its normal (healthy) value in seven different combinations of diseased layers; later the pressure was applied to that segment in order to create the bulge of sac-like aneurysm. From perspective of mechanics, the shape of deformed artery, wall thickness, and the most importantly stresses distribution are substantial features that should be analyzed and discussed. In the present section, after demonstration of deformed shapes and wall thickness results, the stresses will be depicted and examined.

Figures 3.12 and 3.13 represent the deformed shape of seven diseased cases, mentioned in previous chapter, when the deteriorated section is subjected to 16KPa pressure. Note that mentioned layers in each picture mean diseased layers in that specific case. It is being observed that the shape and size of bulge vary with respect to the fact that which layer or layers have been considered to be diseased.

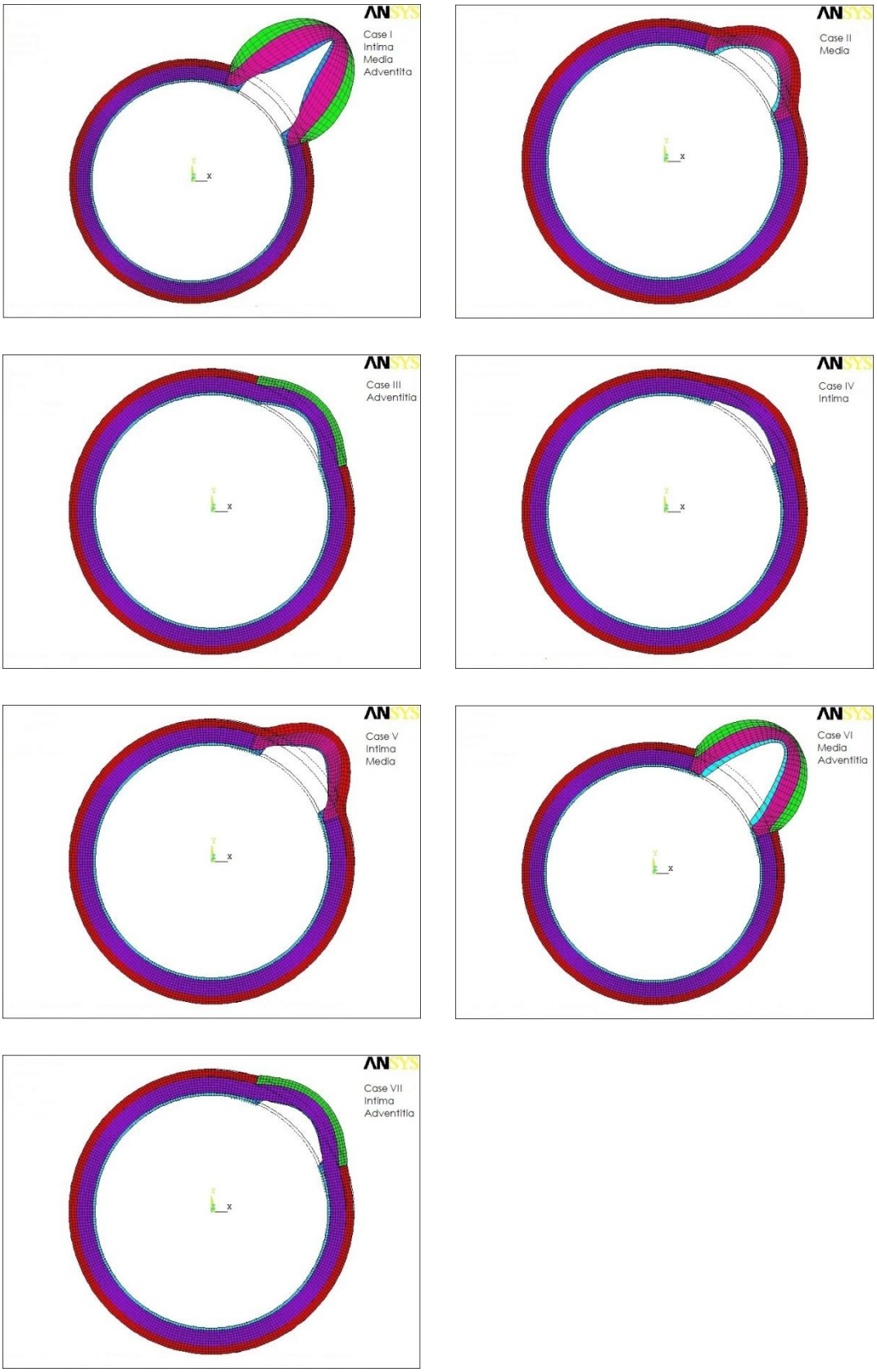

Figure 3.12 Deformed shapes and edges of undeformed models under 16KPa pressure for 7 cases

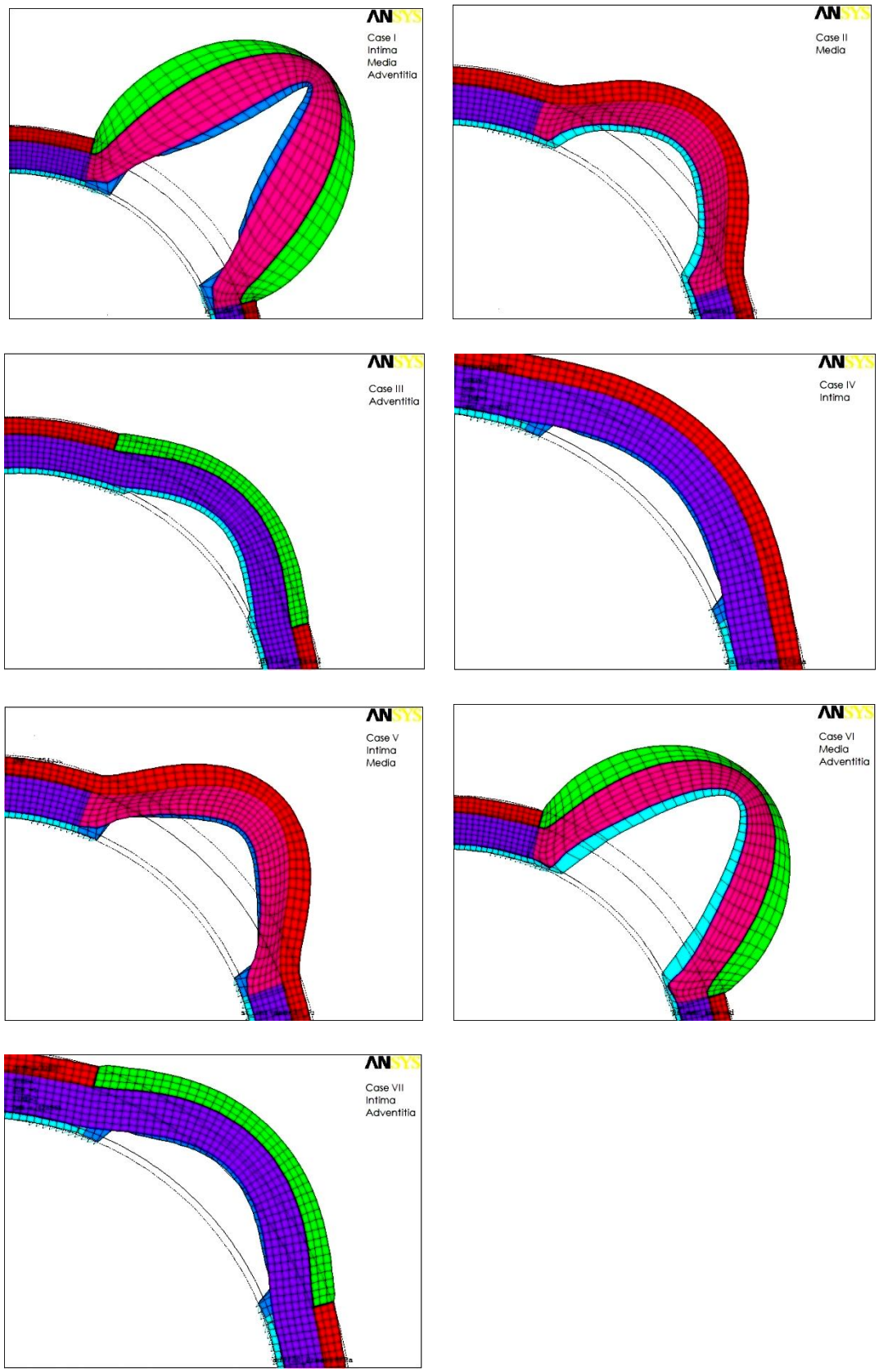

Figure 3.13 Deformed shapes and edges of undeformed models under 16KPa pressure for 7 cases

The size of bulge or the radial and circumferential displacements are the largest in case I where the all three layers are deteriorated. Cases VI (diseased media and adventitia), V (unhealthy media and intima), II (diseased media), VII (diseased adventitia and intima) , III (diseased adventitia) and IV (diseased intima) have the larger displacements and size in sequence. Figures 3.14 and 15 represent the radial and circumferential displacements of all cases with respect to pressure.

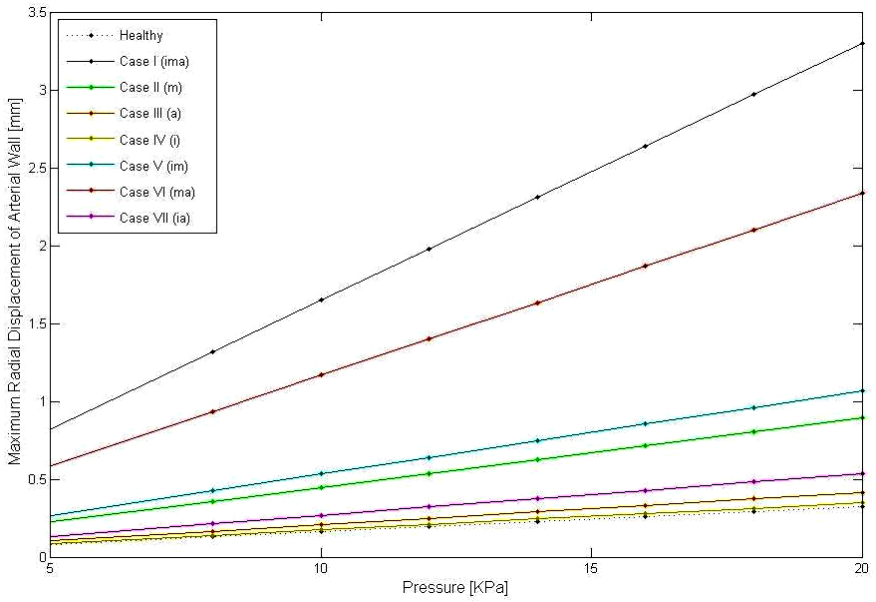

Figure 3.14 Maximum radial displacements in healthy and seven cases of aneurismal wall with respect to pressure. Note that abbreviations represent the first letter of diseased layers.

Through comparison of cases II, III, and IV in Figure 3.13, 3.14 and 3.15, where only media, adventitia or intima layer is diseased respectively, it could be deduced that deterioration of media causes larger deformation and bugle-formation than adventitia, and diseased adventitia leads to larger bulge than unhealthy intima. When more than one layer is diseased, the combination of diseased layers is also important. For example in case VII, although both adventitia and intima are supposed deteriorated, still the value of displacement is less than single diseased media layer. Consider two cases V and VI, where the media is diseased in both, just in case V intima is also assumed diseased but in case IV adventitia is unhealthy second layer.

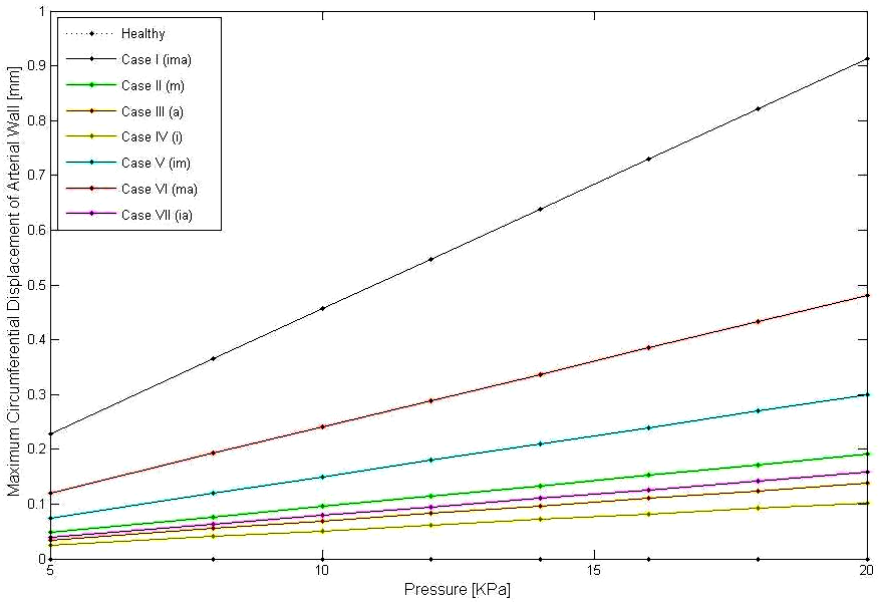

Figure 3.15 Maximum circumferential displacements in healthy and seven cases of aneurismal wall with respect to pressure

It is clear that diseased adventitia layer effects the deformation of aneurismal wall more than unhealthy intima layer and leads to larger bulge formation. Of course when whole wall is diseased the deformation will be larger than other cases. Therefore, the media layer is playing the most significant role in deformation of aneurismal wall. Later, the adventitia is considered as second important structural constituent, while the intima layer is least effective unit when the deformation is being regarded. The evaluation of deformed shape not only revealed that the media is the most important layer in artery's deformation, but also can contribute to find thickness changes of aneurismal arteries in comparison to healthy one, which in turn is more important factor than general size. The following paragraphs contain the wall thickness results.

The thickness of aneurismal wall depicted versus pressure change in Figure 3.16. As expected from displacements the thinnest wall belongs to case I, where all layers are damaged. After that the case VI, where both media and adventitia are diseased is thinnest aneurismal wall. Cases II is almost as thin as case V, but only case V,

where both media and intima are damaged, is a little bite thinner due to deteriorated intima layer.

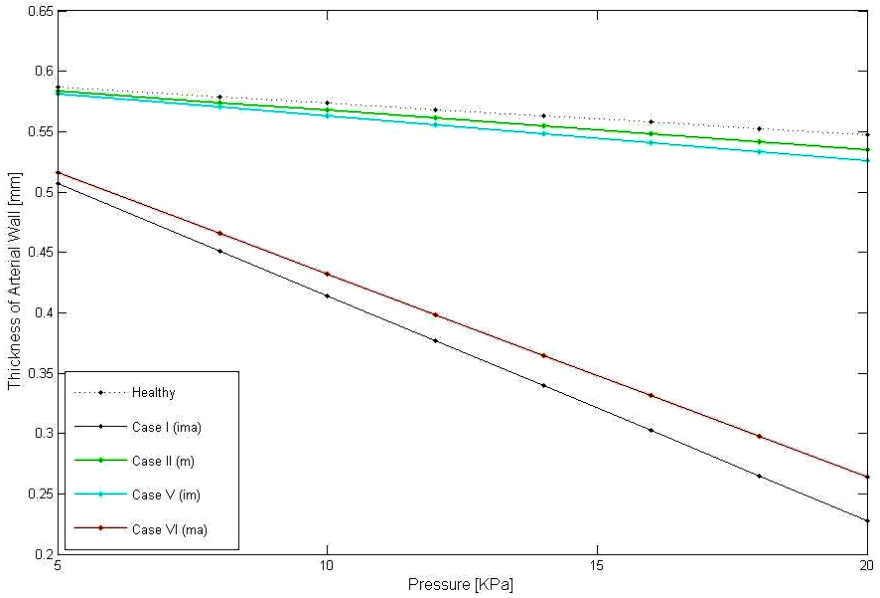

Figure 3.16 Thickness of healthy and aneurismal wall in different pressures

More detailed graphs about thicknesses of whole wall and three layers separately have been illustrated in Figure 3.17 to 19 for cases I, V, and VI, which have the larger bulge than other cases. In those figures vertical axis represents the wall thickness ratio of loaded aneurismal artery to unloaded healthy artery at the thinnest part (fundus) of lesion, while horizontal axis is ratio of maximum radial displacement (d_0) to lumen diameter of unloaded artery (D=5.3mm). Notice that greater d_0 / D means the larger bulge-size on arterial wall. The thickness ratio of whole wall and each layer is calculated by division of thickness of diseased artery wall or that specific layer after applying pressure to thickness of wall or that layer in healthy artery before imposing any pressure. In healthy state the thicknesses of intact wall, intima, media, and adventitia layers are 0.6, 0.06, 0.36, and 0.18mm respectively.

By comparison of wall thickness ratios of three layers in four cases, it is clear that damaged adventitia layer experiences higher thickness change rates than other

layers. For example in case I where all three layers are damaged, despite the fact that media is almost twice thicker than adventitia, its thickness change is less than adventitia (Figure 3.17); or also in case VI the rate of change in thickness of adventitia is higher that media (Figure 3.18).

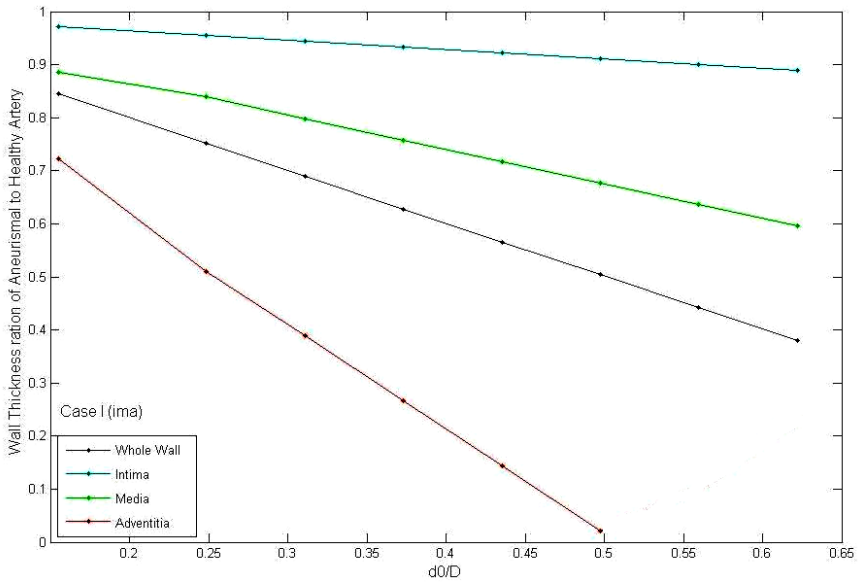

Figure 3.17 Thickness ratio of whole wall, intima, media, and adventitia in aneurismal case I (all three layers are diseased) to healthy values with respect to d0/D

Note that in case I (Figure 3.17) the adventitia graph ends at specific point; in fact the adventitia thickness approach to zero (just 3% its healthy thickness) at the point d0/D=0.5 and after this point its thickness change should not be considered anymore.

Although in case V the adventitia is healthy, its thickness change ratio is greater than damaged media (Figure 3.19). Therefore, the adventitia layer incurs to more severe thickness change rates than media and intima, especially when it is diseased.

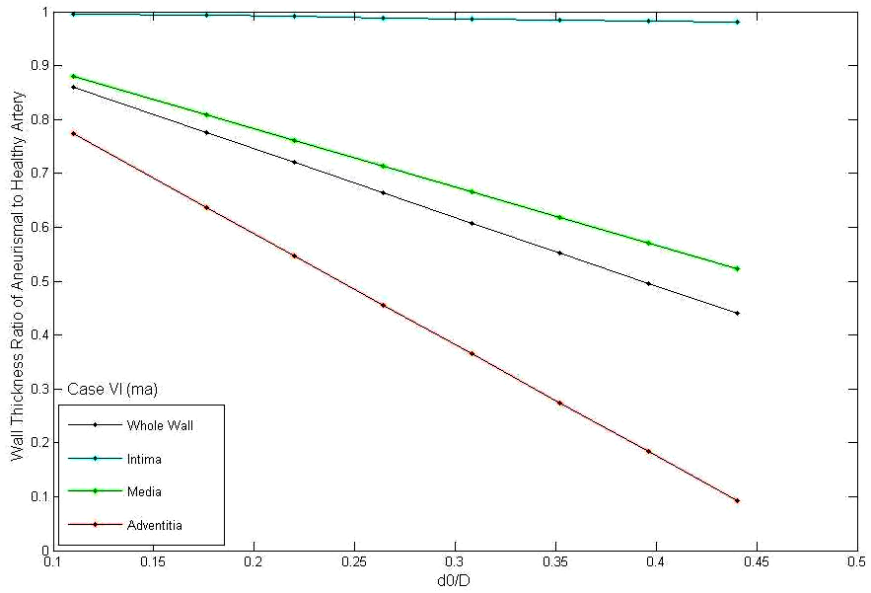

Figure 3.18 Thickness ratio of whole wall, intima, media, and adventitia in aneurismal case VI (media and adventitia layers are diseased) to healthy values with respect to d0/D

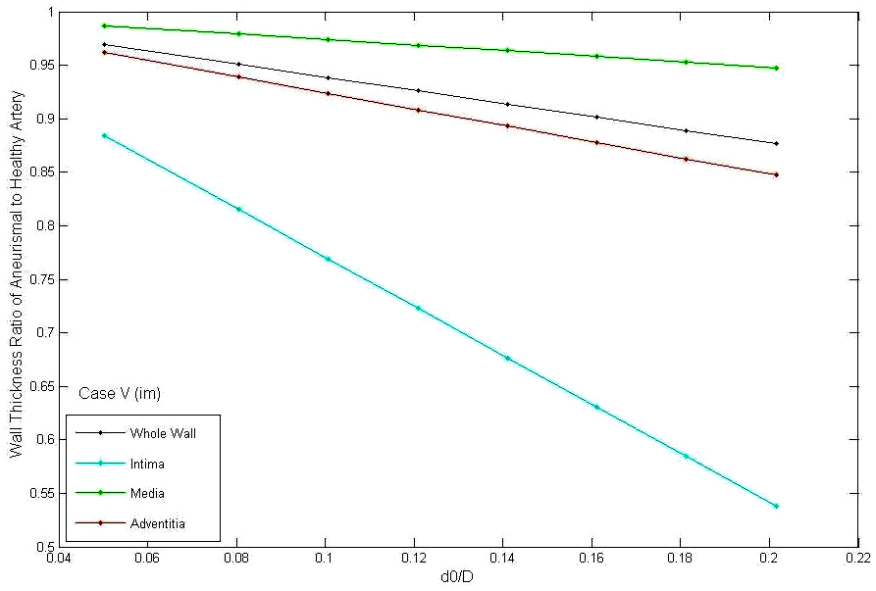

Figure 3.19 Thickness ratio of whole wall, intima, media, and adventitia in aneurismal case V (media and intima layers are diseased) to healthy values with respect to d0/D

As mentioned before the aneurismal wall ruptures because it cannot support the induced stresses from blood flow stream any longer. Calculating different types of stresses, their distributions and values reveal some hints to recognize weak spots as well as understanding role of layers in stress distribution of aneurismal wall.

Among the different stress types, healthy artery modelling decoded that circumferential stress has higher values compared to radial and shear stresses. Moreover, Von Mises stress as criteria for yielding of materials, and maximum principal stress have the same patterns as circumferential stress, and their values are very close to circumferential stress; thus the focus will be on circumferential stress. The circumferential stress distribution in seven different diseased cases is depicted in Figure 3.20. Note mentioned layers in each picture mean diseased layers in that specific case.

Some useful information is made known by comparison of stress distributions in Figure 3.20. Notice that the location, at which the maximum circumferential stress occurs, varies in different cases. Table 3.4 contains information about the location of maximum circumferential stress in healthy and diseased arterial wall. Deterioration of different single layer or distinct combination of diseased layers gives rise to different stress distribution patterns throughout aneurismal wall.

Overall, when one layer is diseased (has weaker material properties) the induced stress is tolerated by other stronger layers. Referring to Figure 3.20 it is clear that for example in cases II when media is diseased or in case V when both media and intima layers are diseased then induced stress is supported by adventitia; as well as when adventitia supposed to be diseased (case III) or intima and adventitia (case VII) both have lower material properties the stress would endured by media layer. For case IV, where the intima has deteriorated, the part of stress is supported by media at neck and part of it endured by adventitia at fundus. In case VI, where both media and adventitia have been weakened the intima supports stress, and finally in case I when all layers are diseased the stress is generally supported by media which has still higher material properties.

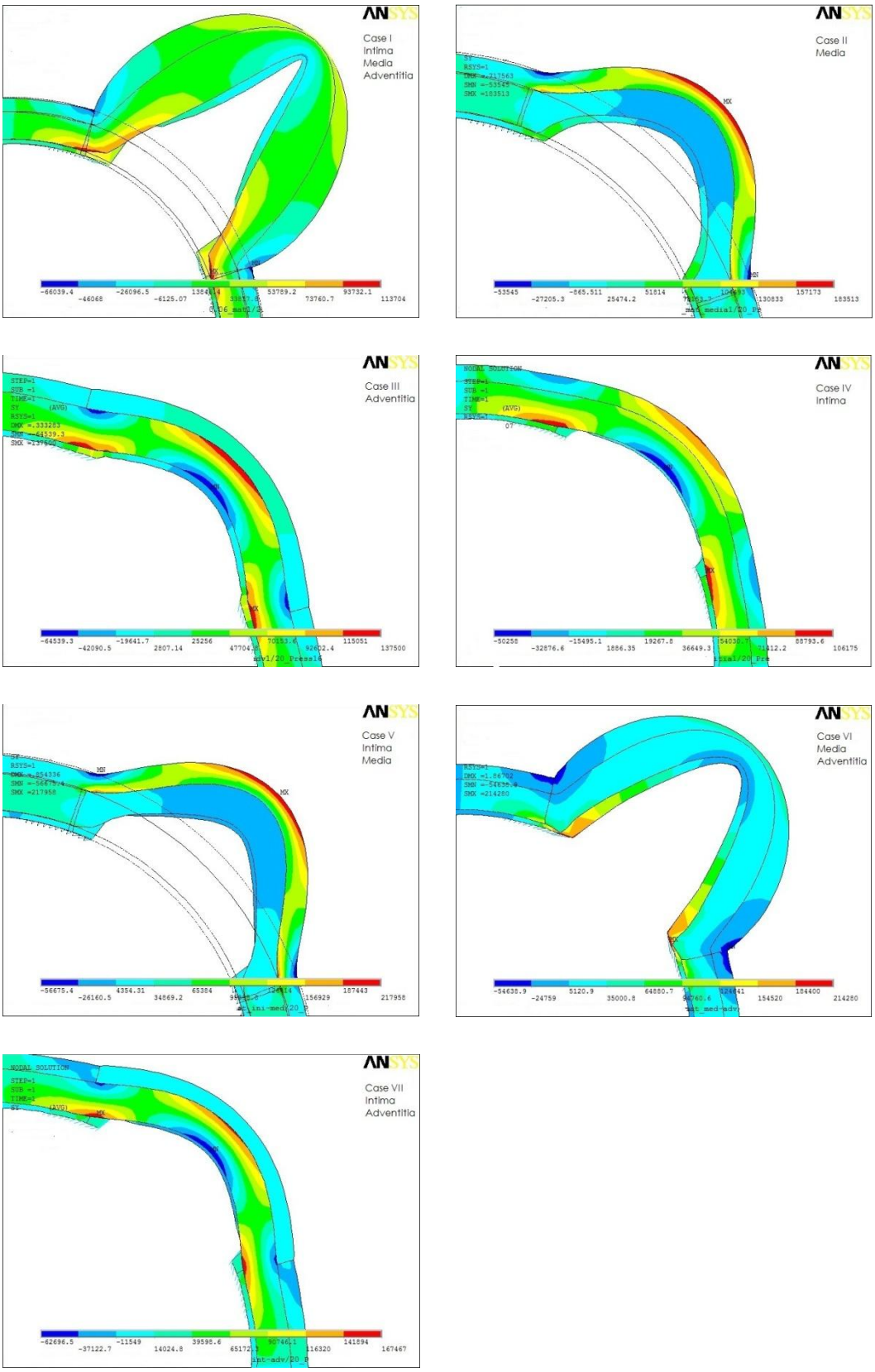

Figure 3.20 Circumferential stress distributions under 16KPa pressure for aneurismal wall in 7 cases

Table 3.4 Location of maximum circumferential stress in healthy and aneurismal artery

Artery type	Description	Max. Circumferential stress location
Healthy	all layers are intact in whole wall	throughout media layer adjacent to intima interface
Diseased_caseI	intima,media and adventitia are deteriorated in part of wall	media adjacent to intima interface at neck
Diseased_caseII	media is deteriorated in part of wall	adventitia away from media interface at top of fundus
Diseased_caseIII	adventitia is deteriorated in part of wall	media adjacent to adventitia interface at top of fundus and media adjacent to intima at neck
Diseased_caseIV	intima is deteriorated in part of wall	adventitia away from media interface at top of fundus and media adjacent to intima at neck
Diseased_caseV	Media and intima are deteriorated in part of wall	adventitia away from media interface at top of fundus
Diseased_caseVI	Media and adventitia are deteriorated in part of wall	intima adjacent to lumen at neck
Diseased_caseVII	adventitia and intima are deteriorated in part of wall	media adjacent to adventitia interface at top of fundus and media adjacent to intima at neck

Interestingly, any time that media is diseased and adventitia is healthy, neglecting intima status, the maximum stress occurs at fundus of lesion in adventitia layer. However when the adventitia is diseased and media is healthy the maximum stress is observed at both fundus and neck in media. Moreover, when both media and adventitia are considered unhealthy, the maximum stress is seen just at neck. Briefly, the media and adventitia are dominant layers in stress distribution pattern of arterial wall with aneurysm.

The value of circumferential stress is also determinant factor that its role should be considered in failure of arterial wall in aneurysms. Figure 3.21 represents the maximum value of circumferential stresses for different cases with respect to

pressure changes from 5KPa to 20KPa. Paying attention to cases that only single layer is assumed diseased- cases II, III, and IV- it is obvious that that the case II has been subjected to remarkable higher values of circumferential stress. Even when both adventitia and intima are diseased (case VII) the stress amount is less than single deteriorated media. The largest values of stress belong to case V and VI where the media plus intima and adventitia are diseased. The common feature of two cases is diseased media layer. Therefore, it can be concluded the media deterioration influences stress value more than other two layers.

Although when single layer is diseased the unhealthy adventitia affect stress value more than intima, in presence of diseased media the effect of adventitia and intima in stress values are almost same. It means that the media as most fundamental layer dominates value of circumferential stress in aneurismal wall like healthy artery.

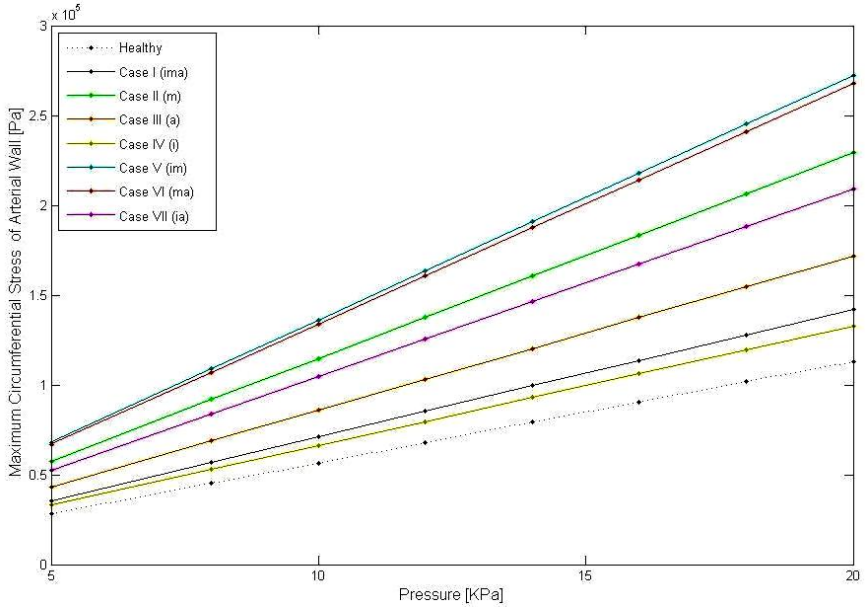

Figure 3.21 Maximum value of circumferential stress with respect to pressure in healthy and seven diseased cases for aneurismal wall

Maximum principal and Von Mises stress distributions and values are approximately as same as circumferential stress. The small deviation from circumferential stress stems from the fact that shear stress is not zero in aneurismal

wall; however its value is remarkably smaller than circumferential stress. Appendix A contains the maximum principal and Von Mises stresses distribution at 16KPa and their maximum values with respect to pressure in healthy and aneurismal artery.

Further processing of elicited data gives rise to diagrams that contribute to better interpretation of aneurysms. The graph with two vertical axes is demonstrated in Figure 3.22. The left vertical axis corresponds to wall thickness ratio of aneurismal artery to healthy one, whereas the right vertical axis corresponds to circumferential stress differences between the aneurismal and healthy wall. These two variables are depicted in various pressures, ranging from 5KPa to 20KPa. Note that the circumferential stress has been recorded from top of fundus in both healthy and diseased models.

Simply by comparison of wall thickness and increased (case I, II, and V) or even decreased (case VI) amount of circumferential stress it is possible to compare rupture potential of different lesions. For example, consider is case I (Figure 3.22)

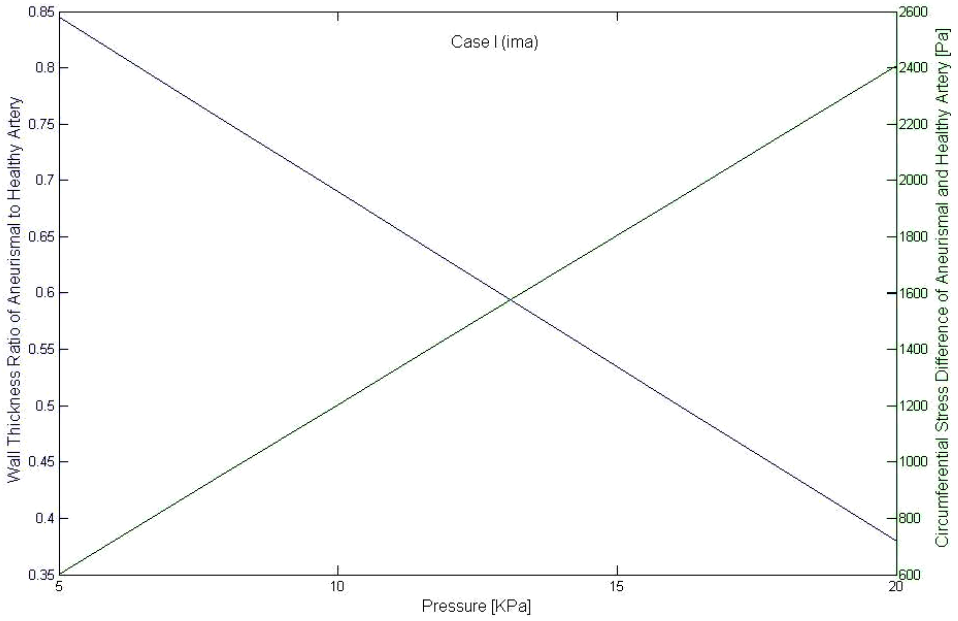

Figure 3.22 Wall thickness ratio of aneurismal artery to healthy (blue) and circumferential stress difference (green) of aneurismal and healthy wall with respect to pressure in case I when all layers are diseased

at pressure 18KPa the wall thickness of lesion is about 0.26mm (44% of its healthy value) at thinnest part of fundus of bulge and stress is just 2.167KPa larger than its healthy amount (about 3 %), whereas in case V (Figure 3.23), at same location, the wall thickness has been decreased to 0.53mm (88% of its healthy value) but it has been subjected to almost 175KPa larger stress than its normal value (about 350%). It means the 56 % reduced wall thickness in case I is subjected merely to 0.03 times higher circumferential stress, while 12 % decreased wall thickness in case V is incurred to 3.5 times increased stress compared to healthy artery. Therefore, although the aneurysm size is larger in case I and the lesion has thinner wall, the rupture of smaller bulge in case V with thicker wall seems more possible due to remarkably higher stress than normal state. In other words, it is possible to base rupture criterion on circumferential stress, which is principal tensile stress near fundus due to small shear stress (Figure A5) at the same time [81].

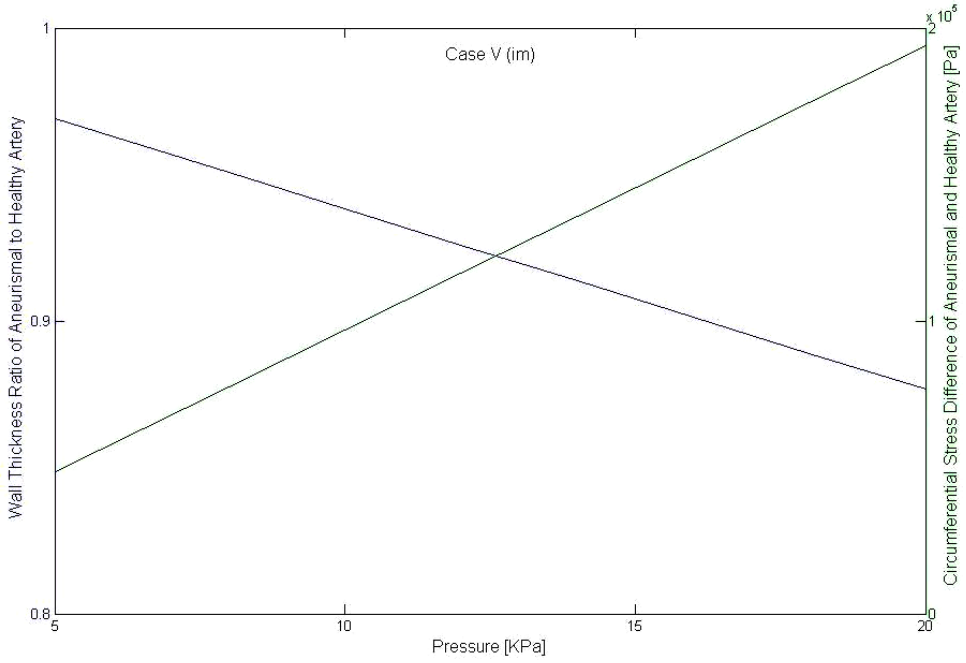

Figure 3.23 Wall thickness ratio of aneurismal artery to healthy (blue) and circumferential stress difference (green) of aneurismal and healthy wall with respect to pressure in case V when intima and media layers are diseased

These kinds of diagrams with two vertical axes can be more useful and practical if the dimensionless quantities are being used. For example, in diagraph depicted in Figure 3.24 the left vertical axis corresponds to wall thickness ratio of loaded aneurismal to unloaded healthy arterial wall, while the right vertical axis represents the circumferential stress difference between aneurismal and healthy artery with respect to d_0/D for case V. The d_0/D ratio is maximum radial displacement of aneurysm to lumen diameter of unload healthy artery and means how large the aneurysm bulge is. The figure helps to estimate the change in amount of circumferential stress as function of thickness change ratio.

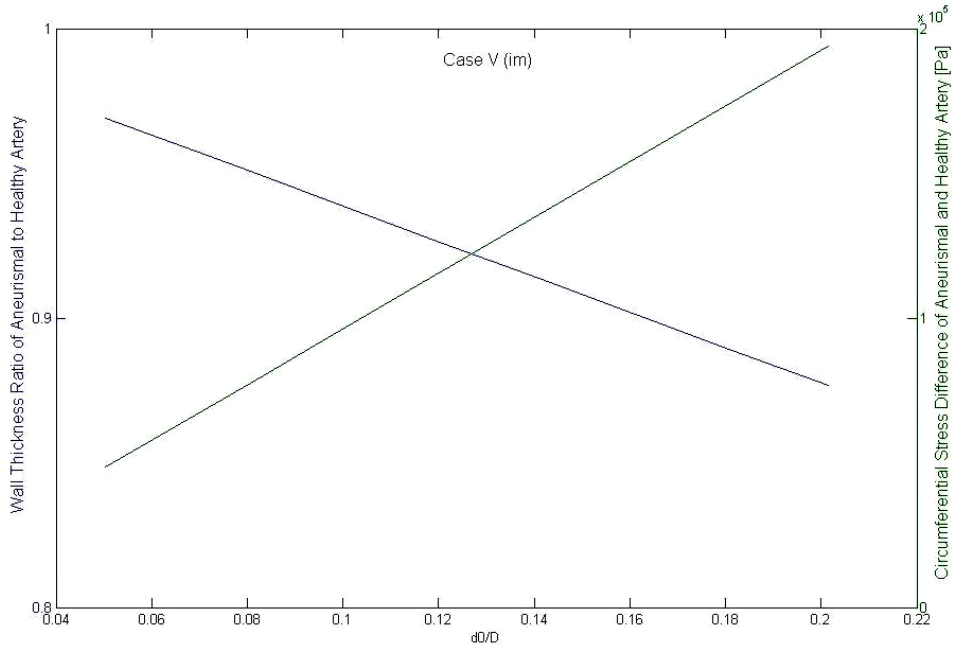

Figure 3.24 Wall thickness ratio of aneurismal artery to healthy (blue) and circumferential stress difference (green) of aneurismal and healthy wall with respect to d0/D ratio in case V, where media and intima layers are diseased

For example, if thickness decreases 10 %, the circumferential stress will rises 155KPa, and if thickness reduced 12%, the stress would increase 194KPa compared to healthy values in case V. Simultaneously one can derive data about bulge size through d_0/D ratio value at the same time. These types of information help physicians to estimate critical thickness of aneurysm according to failure stress

values documented in literature [151] and compare different lesions according to bulge size, wall thickness and stress distribution. Similar diagrams for other cases are available in appendix A.

CHAPTER 4

CONCLISION

Stress analysis of linear healthy artery under constant pressure reveals that circumferential stress has the highest value among the plane stresses. This stress is incurred to step transient in the interface of layers and the maximum value is observed in media layer right after interface of media-intima. However radial stress decreasing continuously along path throughout arterial wall, and its maximum value happens in intima layer adjacent lumen. Shear stress is very small compared to radial and circumferential stresses, so is considered negligible. Therefore, in absence of shear stress, the circumferential stress can be considered as first principal and most significant stress, which its value is 3 to 5 times of radial stress. Thus, the media layer is supporting the higher values of stress than other layers in healthy artery.

Adding geometrical nonlinearity to linear model of healthy artery influences wall thickness and stress distribution of vessel when it is imposed to pressure inside lumen. Geometrical nonlinearity in systolic pressure makes the wall thickness 1.03% thinner than linear model under same load. This small thickness change causes about 20% stress increase in media and adventitia layers and more than 60% increase in intima's circumferential stress. However, radial stress changes with respect to nonlinearity are negligible according to results. In other words, the Geometrical nonlinearity affects intima more than two other layers. Moreover, as applied pressure increases the effect of geometrical nonlinearity becomes more remarkable.

It is being observed that the deformation (shape), wall thickness and stress distribution of aneurysm vary with respect to the fact that which layer or layers have been considered to be diseased. The damaged media causes larger deformation and bugle-formation than adventitia, and in the same way diseased adventitia leads to larger bulge than unhealthy intima. The wall thickness change of aneurismal artery in comparison to healthy one is more important factor than bulge size from mechanical point of view. Although damaged media leads to thinner wall due to its healthy larger thickness, the adventitia layer incurs to more severe thickness change rates than media and intima, especially when it is diseased.

The media deterioration influences stress value more than other two layers in aneurismal artery. Although sole diseased adventitia case affects stress value more than a case in which sole intima is unhealthy, in presence of diseased media the effect of adventitia and intima in stress values are almost same. Overall, the media layer is most fundamental layer that dominates value of stresses, wall thickness and even size of sac and thus shape of aneurysm. However, the adventitia is also very effective in stress distribution pattern. Once one layer is diseased (has a weaker material property) the pressure-induced stress is tolerated by other stronger layers. Any time that media is diseased and adventitia is healthy, neglecting intima status, the maximum stress occurs at fundus of lesion in adventitia layer. Whenever the adventitia is diseased and media is healthy the maximum stress is observed at both fundus and neck. Moreover, when both media and adventitia are considered unhealthy, the maximum stress is seen just at neck. Therefore, the media and adventitia are dominant layers in stress distribution pattern of arterial wall with aneurysm.

Designing diagrams with two vertical axes contributed to better interpretation of data and better understanding of natural history of aneurysm consequently. In these diagrams, the left y-axis corresponds to wall thickness or ratio of aneurismal artery wall thickness to healthy thickness, whereas the right y-axis corresponds to circumferential stress or its differences between the aneurismal and healthy wall.

The horizontal axis corresponds to pressure or d_0/D, which represents the bulge size. Simply, comparison of wall thickness change ratio with increased or even decreased (e.g. case VI) amount of circumferential stress in specific pressure or d0/D, as well as knowing alteration in amount of circumferential stress as function of thickness change obtains new tool for physicians in order to estimate rupture potential of different lesions.

These diagrams demonstrated that the aneurismal lesion, which has thicker wall and smaller bulge (case V), might have more tendency to rupture than lesion with larger bulge and thinner wall just due to biaxial stresses such as circumferential stress. Therefore the circumferential stress as well as other biaxial stresses such as maximum principal stress or Von Mises stress distribution can be new criteria for rupture potential of sac-like intracranial aneurysms.

REFERENCES

[1] Gerard J. Tortora, Bryan Derrickson, *Principles of Anatomy and Physiology, 11th edition*, John Wiley & Sons, Inc., 2006.

[2] Kenneth S. Saladin, Donna Van Wynsberghe, *Anatomy and Physiology, the unity of form and function, 2nd edition*, McGraw Hill Companies, Inc., 2001.

[3] Martini F. H., *Anatomy and Physiology*, Pearson Education, Inc, 2005.

[4] David Shier, Jackie Butler, Ricki Lewis, *Hole's Human Anatomy and Physiology, 8th edition*, McGraw Hill Companies, Inc., 1999.

[5] Robertson A., Watton P. N., *Mechanobiology of the Arterial Wall*, In: Ed. Andrey Kuznetsov and Sid Becker (ed.) Modelling of Transport in Biological Media, Elsevier, pp. 275-347, 2013.

[6] Holzapfel G. A., Gasser T. C., Ogden R. W., *A New Constitutive Framework for Arterial Wall Mechanics and a Comparative Study of Material Models*, Journal of Elasticity, vol. 61, pp. 1–48, 2000.

[7] Wang JH-C, Thampatty B. P., *An Introductory Review of Cell Mechanobiology*, Biomech Model Mech, vol. 5, pp. 1–16, 2006.

[8] Tim McGloughlin, *Biomechanics and Mechanobiology of Aneuryms*, Springer-Verlag Berlin Heidelberg, 2011.

[9] Alisa Selimovic, Yiannis Ventikos, Paul N. Watton, *Modelling The Evolution of Cerebral Aneurysms: Biomechanics, Mechanobiology and Multiscale Modelling*, International Congress of Theoretical and Applied Mechanics, vol. 10, pp. 396-409, 2014.

[10] Cummins PM, von Offenberg Sweeney N, Killeen MT, Birney YA, Redmond EM, Cahill PA, *Cyclic Strain-Mediated Matrix Metalloproteinase Regulation Within the Vascular Endothelium: A Force to be Reckoned With*, American Journal of Physiology, Heart and Circulatory Physiology, pp. 292: H28-42, 2007.

[11] Juan C. Lasheras, *The Biomechanics of Arterial Aneurysms*, the Anuual Review of Fluid Mechanics, vol. 39, pp. 293-319, 2007.

[12] Rubin E, JL Farber, *Pathology*, Lippincott, Philadelphia, 1988.

[13] J. D. Humphrey, C. A. Taylor, *Intracranial and Abdominal Aortic Aneurysms: Similarities and Differences, and Need for a New Class of Computational Models*, Annu. Rev. Biomedical Engineering, vol. 10, pp. 221-46, 2008.

[14] H. Prasetya, T. L. R. Mengko, O. S. Santoso and H. Zakaria, *Detection Method of Cerebral Aneurysm Based on Curvature Analysis from 3D Medical Images*, International Conference on Instrumentation, Communication, Information Technology and Biomedical Engineering, 2011.

[15] J. D. Humphrey, *Cardiovascular Solid Mechanics: Cells, Tissues and Organs*, Springer-Verlag New York, Inc., 2002.

[16] Mayfield Clinic and Spine Institute

[17] Ferguson GG, *Intracranial Arterial Aneurysms: A Surgical Perspective*, In: Handbook of Clinical Neurology, (JF Toole, ed) Elsevier B.V., vol. 11(55), pp. 41-87, 1989.

[18] Hashimoto N, H Handa, *The Size of Cerebral Aneurysms in Relation to Repeated rupture,* Surg Neurol., vol. 19, pp. 107-lll, 1983.

[19] Kassel NF, JC Tomer, *Size of Intracranial Aneurysms,* Neurosurgery, vol.12, pp. 291-297, 1983.

[20] Wiebers DO, JP Whisnant, TM Sundt, WM O'Fallon, *The Significance of Unruptured Intracranial Aneurysms,* J. Neurosurg, vol. 66, pp.23-29, 1987.

[21] Pokrovskii AV, Dan VN, Zlatovchen AM, Il'in SA, *The Impact of Cardiac Status and Arterial Hypertension on the Results of Surgical Treatment of Patients Over 70 Years with Abdominal Aortic Aneurysms,* Angiol. Sosud. Khir., vol. 9, pp. 71–76, 2003.

[22] Szilagyi DE, *Clinical Diagnosis of Intact and Ruptured Abdominal Aortic Aneurysms in Aneurysms, Diagnosis and Treatment*, ed. JJ Bergan, JS Yao, New York: Grune & Stratton, pp. 205–16, 1982.

[23] Peters DG, Kassam AB, Feingold E, Heidrich-O'Hare E, Yonas H, Ferrell RE, *Molecular Anatomy of an Intracranial Aneurysm: Coordinated Expression of Genes Involved in Wound Healing and Tissue Remodelling,* Stroke ; vol. 32, pp. 1036-1042, 2001.

[24] Cant´on G, Levy DI, Lasheras JC., *Changes in the Intra-aneurysmal Pressure Due to Hydrocoil Embolic System*", Am. J. Neuroradiol. Vol. 26, pp. 904–7, 2005.

[25] Cant´on G, Levy DI, Lasheras JC., *Hemodynamical Changes in Bifurcating Intracranial Aneurysms Due to Stent Placement,* J. Neurosurg. Vol. 103, pp. 146–55, 2005.

[26] Cant´on G, Levy DI, Nelson PK, Lasheras JC., *Flow Changes Caused by the Sequential Placement of Stents Across the Neck of Sidewall Cerebral Aneurysms*, J. Neurosurg. Vol. 103, pp. 891–902, 2005.

[27] de la Monte SM, GW Moore, MA Monk, GM Hutchins, *Risk Factors for Development and Rupture of Intracranial Berry Aneurysms,* Am. J. Med. Vol. 78, pp. 957-964, 1985.

[28] Brisman JL, Song JK, Newell DW, *Cerebral Aneurysms*, The New England journal of medicine, vol. 355, pp. 928-939, 2006.

[29] Steiger HJ, *Pathophysiology of Development and Rupture of Cerebral Aneurysms*, Acta Neurochir Supp., vol. l48, pp. 1-57, 1990.

[30] Stehbens WE, *Pathology and Pathogenesis of Intracranial Berry Aneurysms*, Neural. Res., vol. 12, pp.29-34, 1990.

[31] Hassler, The *Windows of the Internal Elastic Lamella of the Cerebral Arteries*, Virchows Arch [A], vol. 335, pp. 127-132, 1962.

[32] Finlay HM, P Whittaker, PB Canham, *Collagen Organization in the Branching Region of Human Brain Arteries*, Stroke vol. 29, pp. 1595-1601, 1998.

[33] Ferguson GG, *Direct Measurement of Mean and Pulsatile Blood Pressure at Operation in Human Intracranial Saccular Aneurysms*, J. Neurosurg., vol. 36, pp. 560-563, 1972.

[34] Ferguson GG, *Physical Factors in the Initiation, Growth, and Rupture of Human Intracranial Aneurysms,* J. Neurosurg., Vol. 37, pp. 666-677, 1972.

[35] Sekhar LN, RC Heros, *Origin, Growth and Rupture of Saccular Aneurysms: A Review,* Neurosurgery, vol. 8, pp. 248-260, 1981.

[36] Hegedus K, *Some Observations on Reticular Fibers in the Media of the Major Cerebral Arteries*, Surg. Neurol. Vol. 22, pp. 301-307, 1984.

[37] Ostergaard JR, E Reske-Nielsen, H Oxlund, *Histological and Morphometric Observations on the Reticular Fibers in the Arterial Beds of Patients With Ruptured Intracranial Saccular Aneurysms*, Neurosurgery, vol.20, pp.554-558, 1987.

[38] Kilic T, Sohrabifar M, Kurtkaya O, Yildirim O, Elmaci I, *Expression of Structural Proteins and Angiogenic Factors in Normal Arterial and Unruptured and Ruptured Aneurysm Walls*, Neurosurgery, vol. 57, pp. 997–1007, 2005.

[39] Wilmink ABM, Quick CRG, Hubbard CSF, Day NE, *The Association Between Connective Tissue Laxity and the Risk of an Abdominal Aortic Aneurysm*, Eur. J. Endovasc. Surg., vol.20, pp. 290–95, 2000.

[40] Kayembe KNT, Sasahara M, Hazama F., *Cerebral Aneurysms and Variations in the Circle of Willis*, Stroke, vol. 15(5), pp.846–50, 1984.

[41] van den Berg JS, Limburg M, Pals G, Arwert F, Westerveld A., *Type III Collagen Deficiency in a Family With Intracranial Saccular Aneurysms*, *Cerebrovasc. Dis.*, vol. 11, pp. 92–94, 2003.

[42]. Krex D, Rohl H, Konig IR, Ziegler A, Schackert HK, Schackert G., *Tissue Inhibitor of Metalloproteinases-1, -2, and -3 Polymorphisms in a White Population With Intracranial Saccular Aneurysms*, Stroke, vol. 34, pp. 2817–21, 2003.

[43] Yoneyama T, Kasuya H, Onda H, Akagawa H, Jinnai N., *Association of Positional and Functional Candidate Genes FGF1, FBN2, and LOX on 5q31 With Intracranial Aneurysms*, J. Hum. Genet., vol. 48, pp.309–14, 2003.

[44] Hofer A, Ozkan S, Hermans MJ, Kubassek N, Sitzer M., *Mutations in the lysyl oxidase Gene Not Associated With Intracranial Aneurysm in Central European Families*, Cerebrovasc. Dis., vol. 18, pp. 189–93, 2004.

[45] Kassam AB, Horowitz M, Chang Y-F, Peters D., *Altered arterial Homeostasis and Cerebral Aneurysms: A Molecular Epidemiology Study*, Neurosurgery, vol. 54, pp. 1450–62, 2004.

[46] Akagawa H, Kasuya H, Onda H, Yoneyama T, Sasahara A., *Influence of Endothelial Nitric Oxide Synthase T-786C Single Nucleotide Polymorphism on Aneurysm size*, J. Neurosurg., vol. 102, pp. 68–71, 2005.

[47] Juvela S, Poussa K, Porras M., *Factors Affecting Formation and Growth of Intracranial Aneurysms: A Long-term Follow-up Study*, Stroke, vol. 32(2), pp. 485–91, 2001.

[48] Krex D, Schackert HK, Schackert G., *Genesis of Cerebral Aneurysms: An Update*, Acta Neurochir., vol. 143, pp. 429–49, 2001.

[49] Wanhainen A, Bergqvist B, Boman K, Nilsson TK, Rutegard J., Risk Factors Associated With Abdominal Aortic Aneurysm: *A Population-based Study With Historical and Current Data*, J. Vasc. Surg., vol. 41, pp. 390–96, 2005.

[50] Lee AJ, Fowkes FG, CarsonMN,Leng GC, Allan PL., *Smoking, Atherosclerosis and Risk of Abdominal Aortic Aneurysm*, Eur. Heart J., vol. 18, pp. 545–46, 1997.

[51] MacSweeney ST, Ellis M,Worrell PC, Greenhalgh RM, Powell JT., *Smoking and Growth Rate of Small Abdominal Aortic aneurysms*, Lancet 344, pp. 651–52, 1994.

[52] Simkins TE., Stehbens WE., *Vibrational Behavior of Arterial Aneurysms*, Lett. Appl. Eng. Sci., vol. 1, pp.85–100, 1973.

[53]. Hung EJN, Botwin MR., *Mechanics of Rupture of Cerebral Saccular Aneurysms*, J. Biomech., vol. 8, pp. 385–392, 1975.

[54] Austin GM, Schievink W,Williams R., *Controlled Pressure-Volume Factors in the Enlargement of Intracranial Saccular Aneurysms*, Neurosurgery, vol.24, pp. 722–30, 1989.

[55] Akkas N., *Aneurysms as a Biomechanical Instability Problem In Biomechanical Transport Processes*, ed. F Mosora, New York: Plenum Press, pp. 303–11, 1990.

[56] Kyriacou SK, Humphrey JD., *Influence of Size, Shape and Properties on the Mechanics of Axisymmetric Saccular Aneurysms*, J. Biomech., vol. 29, pp. 1015–22, 1997.

[57] David G, Humphrey JD., *Further Evidence For the Dynamic Stability of Intracranial Saccular Aneurysms*, J. Biomech., vol. 36, pp. 1143–50, 2003.

[58] 34. Allcock JM, Canham PB., *Angiographic Study of the Growth of Intracranial Aneurysms*, J. Neurosurg., vol. 45, pp. 617–12, 1976.

[59] Mitchell P, Jakubowski J., *Estimate of the Maximum Time Interval Between Formation of Cerebral Aneurysm and Rupture*, J. Neurol. Neurosurg. Psychiatry, vol. 69, pp. 760–67, 2000.

[60] Cant´on G., *Hemodynamics of Intracranial Aneurysms*, PhD thesis, Univ. Calif. San Diego, 2004.

[61] Steinman DA, Vorp DA, Ethier CR., *Computational Modeling of Arterial Biomechanics: Insights into Pathogenesis and Treatment of Vascular Disease*, J.Vasc. Surg., vol. 37, pp. 1118–28, 2003.

[62] Foutrakis GN, Yonas H, Sclabassi RJ., *Finite Element Methods in The Simulation and Analysis of Intracranial Blood Flow*, Neurol. Res., vol. 19, pp. 174–86, 1997.

[63] Ryan JM, Humphrey JD., *Finite Element Based Predictions of Preferred Material Symmetries in Saccular Aneurysms*, Ann. Biomed. Eng., vol. 27, pp. 641–647, 1999.

[64] Chyatte D, I Lewis, *Gelatinase Activity and the Occurrence of Cerebral Aneurysms*, Stroke, vl.28, pp. 799-804, 1997.

[65] Connolly ES, AJ Fiore, CJ Winfree, CJ Prestigiacomo, JE Goldman, RA Solomon, *Elastin Degradation in the Superficial Temporal Arteries of Patients With Intracranial Aneurysms Reflects Changes in Plasma Elastase*, Neurosurgery, vol. 40, pp. 903-909, 1997.

[66] Gaetani P, F Tartara, F Tancioni, *Deficiency of Total Collagen Content and of Deoxypyridinoline in Intracranial Aneurysm Walls*, FEBS Lett 404, pp.303-306, 1997.

[67] Bruno G, R Todor, I Lewis, D Chyatte, *Vascular Extracellular Matrix Remodelling in Cerebral Aneurysms*, J. Neurosurg., vol. 89, pp. 431-440, 1998.

[68] Hegedus K., *Some Observations on Reticular Fibers in the Media of the Major Cerebral Arteries*, Surg. Neuro. Vol.l22, pp. 301-307, 1984.

[69] Jianping Geng, Weiqi Yan, Wei Xu, *Application of Finite Element Method in Implant Dentistry*, Zhejiang University Press and Springer-Verlag, 2008.

[70] Canham PB, HM Finlay, JA Kiernan, GG Ferguson, *Layered Structure of Saccular Aneurysms Assessed by Collagen Birefringence*, Neurol. Res., vol. 21, pp. 618-626, 1999.

[71] Erdogan Madenci, Ibrahim Guven, *The Finite Element Methods and Applications in Engineering Using Ansys*, Springer, 2006.

[72] Canham PB, HM Finlay, JG Dixon, S Ferguson, *Layered Collagen Fabric of Cerebral Aneurysms Quantitatively Assessed by the Universal Stage and Polarized Light Microscope*, Anat, Rec., vol. 231, pp. 579-592, 1991.

[73] Canham PB, P Whittaker, SE Barwick, ME Schwab, *Effect on Circumferential Order of Adventitial Collagen in Human Brain Arteries*, Can. J. Physiol. Pharmacal, vol. 70, pp. 296-305, 1991.

[74] Canham PB, HM Finlay, SY Tong, *Stereological Analysis of the Layered Structure of Human Intracranial Aneurysms*. J Microsc 183:170-180, 1996.

[75] MacDonald *D1*, HM Finlay, PB Canham, *Directional Wall Strength in Saccular Brain Aneurysms from Polarized Light Microscopy*, Annis. Biomed. Eng., vol. 28, pp. 533-542, 2000.

[76] Juvela S., *Treatment Options of Unruptured Intracranial Aneurysms*, Stroke, Vol. 35, pp. 372-374, 2004.

[77] Juvela S., *Natural History of Unruptured Intracranial Aneurysms: Risks for Aneurysm Formation, Growth, and Rupture*, Acta Neurochir. Suppl., vol. 82, pp. 27–30, 2002.

[78] Juvela S., M. Porras, O. Heiskanen, *Natural History of Unruptured Intracranial Aneurysms: A Long-term Follow-up Study*, J. Neurosurg. Vol. 79, pp. 174-182, 1993.

[79] Crompton MR., *Mechanism of Growth and Rupture in Cerebral Berry Aneurysms,* Br. Med. J., vol. 1, pp. 1138-1142, 1966.

[80] Jain KK, *Mechanism of rupture of intracranial saccular aneurysms,* Surgery, vol. 54, pp. 347-350, 1963.

[81] Ma B, Harbaugh RE, Raghavan ML, *Three Dimensional Geometrical Characterization of Cerebral Aneurysms*, J.Biomech., vol.32, pp. 264-73, 2004.

[82] Asari S, T Ohmoto, *Growth and Rupture of Unruptured Cerebral Aneurysms Based on the Intraoperative Appearance*, Acta Med Okayama, vol. 48, pp. 257-262, 1994.

[83] Hademenos GJ, TF Massoud, F Turjman, JW Sayre, *Anatomical and Morphological Factors Correlating with Rupture of Intracranial aneurysms in Patients Referred for Endovascular Treatment*, Neuroradiology, vol. 40, pp. 755-760, 1998.

[84] Ruiz DSM, Yilmaz H, Dehdashti AR, Alimenti A, de Tribolet N, Rufenacht DA., *The Perianeurysmal Environment: Influence on Saccular Aneurysm shape and Rupture*, Am. J. Neuroradiol., vol. 27, pp. 504–12, 2006.

[85] Seshaiyer P, Humphrey JD., *On the Potentially Protective Role of Contact Constraints on Saccular Aneurysms*, J. Biomech., vol. 34, pp. 607–612, 2001.

[86] Hassan T, Timofeev EV, Satto T, Shimizu H, Ezura M, *A Proposed Parent Vessel Geometrybased Categorization of Saccular Intracranial Aneurysms: Computational Flow Dynamics Analysis of the Risk Factors for Lesion Rupture*, J. Neurosurg., vol. 103, pp. 662–80, 2005.

[87] Rodriguez-Feo JA, Sluijter JPG, de Kleijn DPV, Pasterkamp G., *Modulation of Collagen Turnover in Cardiovascular Disease*, Curr. Pharmacol. Des., vol. 11, pp. 2501–14, 2005.

[88] Ujjie H, K Sato, H Onda, *Clinical Analysis of Incidentally Discovered Unruptured Aneurysms*, Stroke, vol. 24, pp. 1850-1856, 1993.

[89] Wiebers DO, Whisnant JP, Huston J 3rd, Meissner I, Brown RD Jr., *Unruptured Intracranial Aneurysms: Natural History, Clinical Outcome, and Risks of Surgical and Endovascular Treatment*, Lancet, vol. 362, pp. 103–10, 2003.

[90] Crompton MR., *The Pathology of Ruptured Middle-Cerebral Aneurysms With Special Reference to Differences Between the Sexes*, Lancet, vol. 2, pp. 421-425, 1962.

[91] Suzuki J, H Ohara, *Clinicopathological Study of Cerebral Aneurysms*, J. Neurosurg., vol.48, p. 505-514, 1978.

[92] Humphrey JD., *Computer Methods in Membrane Biomechanics*, Comp. Methods Biomech. BiomedEng., vol. 1, pp. 171–210, 1998.

[93] Brown PM, Zelt DT, Sobolev B., *The Risk of Rupture in Untreated Aneurysms: The Impact of Size, Gender, and Expansion Rate*, J. Vasc. Surg., vol. 37, pp. 280–284, 2003.

[94] Nichols WW, O'Rourke MF., *McDonald's Blood Flow in Arteries: Theoretic, Experimental and Clinical Principles*, London: Edward Arnold, 1990.

[95] Wang DH, Makaroun M, Webster MW, Vorp DA., *Mechanical Properties and Microstructure of Intraluminal Thrombus from Abdominal Aortic Aneurysm*, ASME J. Biomech. Eng., vol. 123, pp. 536–39, 2001.

[96] Thubrikar MJ, Labrosse M, Robicsek F, Al-Soudi J, Fowler B., *Mechanical Properties of Abdominal Aortic Aneurysm wall*, J. Med. Eng. Technol., vol. 25, pp. 133– 142, 2001.

[97] MacSweeney ST,Young G, Greenhalgh RM, Powell JT., *Mechanical Properties of the Abdominal Aorta*, Br. J. Surg. Vol. 79, pp. 1281–84, 1992.

[98] Lopez-Candales A, Holmes D, Liao S, Scott M,Wickline SA, Thompson RW., *Decrease Vascular Smooth Muscle Cell Density in Median Degeneration of Human Abdominal Aortic Aneurysms*, Am. J. Pathol., vol. 150(3), pp. 993–1007, 1997.

[99] Thompson RW, Liao S, Curci JA., *Vascular Smooth Muscle Cell Apoptosis in Abdominal Aortic Aneurysms*, Coron. Artery Dis., vol. 8, pp. 623–31, 1997.

[100] Austin G., *Biomathematical Model of Aneurysm of the Circle of Willis: The Duffing Equation and Some Approximate Solutions*, Math. Biosci., vol. 11, pp. 163-172, 1971.

[101] Cronin J., *Biomathematical Model of Aneurysm of the Circle of Willis: A Qualitative Analysis of the Differential Equation of Austin*, Math. Biosci., vol. 16, pp. 209-225, 1973.

[102] Hademenos GJ, T Massoud, DJ Valentino, G Duckwiler, F Vinuela, *A Nonlinear Mathematical Model for the Development and Rupture of Intracranial Saccular Aneurysms*, Neurol. Res., vol. 16, pp. 376-384, 1994.

[103] Canham PB, GG Ferguson, *A Mathematical Model for the Mechanics of Saccular Aneurysms*, Neurosurgery, vol. 17, pp. 291-295, 1985.

[104] Humphrey JD, SK Kyriacou, *The Use of Laplace's Equation in Aneurysm Mechanics*, Neurol. Res., vol. 18, pp. 204-208, 1996.

[105] Meng H, Feng Y,Woodward SH, Bendok BR, Hanel RA, *Mathematical Model of the Rupture Mechanism of Intracranial Saccular Aneurysms Through Daughter Aneurysm Formation and Growth*, Neurol. Res., vol. 27, pp. 459–65, 2005.

[106] Scott S, Ferguson GG, Roach MR., *Comparison of the Elastic Properties of Human Intracranial Arteries and Aneurysms*, Can. J. Physiol. Pharmacol., vol. 50, pp. 328–32, 1972.

[107] Steiger HJ, Aaslid R, Keller S, Reulen HJ., Strength, Elasticity and Viscoelastic Properties of Cerebral Aneurysms, Heart Vessels, vol. 5, pp. 41–46, 1986.

[108] Toth M, Nadasy GL, Nyary I, Kerenyi T, Orosz M, *Sterically Inhomogeneous Viscoelastic Behavior of Human Saccular Cerebral Aneurysms*, J. Vasc. Res., vol. 35, pp. 345–55, 1998.

[109] Hsu FPK, Liu AMC, Downs J, Rigamonti D, Humphrey JD., *A Triplane Video-Based Experimental System for Studying Axisymmetrically Inflated Biomembranes*, IEEE Trans. Biomed. Eng., vol. 42, pp. 442–50, 1995.

[110] Shah AD, JD Humphrey, *Finite Strain Elastodynamics of Saccular Aneurysms*, J. Biomech., vol. 32, pp. 593-599, 1999.

[111] Kyriacou SK, C Schwab, JD Humphrey, *Finite Element Analysis of Nonlinear Orthotropic Hyperelastic Membranes*, Comp. Mech., vol.18, pp. 269-278, 1996.

[112] Kyriacou SK, A Shah, JD Humphrey, *Inverse Finite Element Characterization of Nonlinear Hyperelastic Membranes*, J. Appl. Mech., vol. 64, pp. 257-262, 1997.

[113] Shah AD, Harris JL, Kyriacou SK, Humphrey JD., *Further roles of Geometry and Properties in Saccular Aneurysm Mechanics*, Comp. Methods Biomech. Biomed. Eng., vol. 1, pp. 109–21, 1997.

[114] Haslach HW, Humphrey JD., *Dynamics of Biological Soft Tissue or Rubber: Internally Pressurized Spherical Membranes Surrounded by a Fluid*, Int. J. Nonlin. Mech., vol. 39, pp. 399–420, 2003.

[115] Seshaiyer P, Shah AD, Kyriacou SK, Humphrey JD., Multiaxial *Mechanical Behavior of Human Saccular Aneurysms*, Comp. Methods Biomech. Biomed. Eng., vol. 4, pp. 281–89, 2001.

[116] Hsu FPK, Schwab C, Rigamonti D, Humphrey JD., *Identification of Response Functions For Nonlinear Membranes Via Axisymmetric Inflation Tests: Implications for Biomechanics*, Int. J. Sol. Struct., vol.31, pp. 3375–86, 1994.

[117] Ma B, Lu J, Harbaugh RE, Raghavan ML., *Nonlinear Anisotropic Stress Analysis of Anatomically Realistic Cerebral Aneurysms*, J. Biomech. Eng., vol. 129, pp. 88–96, 2007.

[118] Lee MC, RC Haut, *Strain Rate Effects on Tensile Failure Properties of the Common Carotid Artery and Jugular Veins of Ferrets*, J. Biomech., vol. 25, pp. 925-927, 1992.

[119] Mohan M, JW Melvin, *Failure Properties of Passive Human Aortic Tissue. II. Biaxial Tension Tests*, J. Biomech., vol.16, pp. 31-44, 1983.

[120] Sforza DM, Putman CM, Cebral JR., *Computational Fluid Dynamics in Brain Aneurysms, International Journal for Numerical Methods in Biomedical Engineering*, vol. 28, pp. 801–808, 2011.

[121] J. N. Reddy, *Energy and Variational Methods in Applied Mechanics*, John Wiley and Sons Inc., Newyork, 1984.

[122] Peter Joot, *Introduction to Strain Tensor*, 2012.

[123] Henry L. Langharr, *Energy Methods in Applied Mechanics*, John Wiley and Sons Inc.,Newyork, 1962.

[124] Francis B. Hildebrand, *Methods of Applied Mechanics*, 2nd edition, Prentice-Hall Inc., 1965.

[125] G. A. Holzapfel, Thomas C. Gasser, *Computational Stress-deformation Analysis of Arterial Walls Including High-pressure Response*", international journal of Cardiology, vol. 116, pp. 78-85, 2006.

[126] L.H. Peterson, R.E. Jensen, J. Parnell, *Mechanical Properties of Arteries in Vivo*, Circ. Res., vol. 8, pp. 622-639, 1960.

[127] K. Cheng, *Arterial Elastic Properties and Cardiovascular Risk/Event*, European Journal of Vascular and Endovascular Surgery, vol. 24, pp. 383-397, 2002.

[128] P. Boutouyrie, *Determinants of Pulse Wave Velocity in Healthy People and in the Presence of Cardiovascular Risk Factors: Establishing Normal and Reference Values. The Reference Values for Arterial Stiffness Collaboration*, European Heart Journal, vol. 31, pp. 2338–2350, 2010.

[129] A. Paini, P. Boutouyrie, D. Calvet, A.I. Tropeano, B. Laloux, S. Laurent, *Carotid and Aortic Stiffness Determinants of Discrepancies*, Hypertension, vol. 47, pp. 371–376, 2006.

[130] C. Bussy, P. Boutouyrie, P. Lacolley, P. Challande, S. Laurent, *Intrinsic Stiffness of the Carotid Arterial Wall Material in Essential Hypertensives*, Hypertension, vol. 35, pp. 1049–1054, 2000.

[131] J.J. Oliver, D.J. Webb, *Noninvasive Assessment of Arterial Stiffness and Risk of Atherosclerotic Events*, Arteriosclerosis, Thrombosis, and Vascular Biology, vol. 23, pp. 554–566, 2003.

[132] C. Kleinstreuer, Z. Li, and M. a Farber, *Fluid-Structure Interaction Analyses of Stented Abdominal Aortic Aneurysms*, Annual review of biomedical engineering, vol. 9, pp. 169-204, 2007.

[133] T. Hirai, S. Sasayama, T. Kawazaki, S. Yagi, *Stiffness of Systemic Arteries in Patients with Myocardial Infarction: A Noninvasive Method to Predict Severity of Coronary Atherosclerosis*, Circulation, vol. 80, pp. 78–86, 1989.

[134] W.W. Nichols, M.F. O'Rourke, *McDonald's Blood Flow in Arteries: Theoretical, Experimental, and Clinical Principles*, 5th ed., A Hodder Arnold Publication, London, pp. 67–76, 2005.

[135] T. Kawazaki, S. Sasayama, S. Yagi, T. Asakawa, T. Hirai, *Non-invasive Assessment of the Age Related Changes in Stiffness of Major Branches of the Human Arteries*, Cardiovascular Research, vol. 21, pp. 678–687, 1987.

[136] L.H. Peterson, R.E. Jensen, J. Parnell, *Mechanical Properties of Arteries in Vivo*, Circulation Research, vol. 8, pp. 622–639, 1960.

[137] S.J. Vermeersch, E.R. Rietzschelb, M.L.D. Buyzereb, D.D. Bacquerc, G.D. Backerc, L.M.V. Borteld, T.C. Gillebertb, P.R. Verdoncka, P. Segers, *Age and Gender Related Patterns in Carotid–Femoral PWV and Carotid and Femoral Stiffness in a Large Healthy, Middle-Aged Population*, Journal of Hypertension, vol. 26 (7) , pp. 1411– 1419, 2008.

[138] Y. Nagai, J.L. Fleg, M.K. Kemper, T.M. Rywik, C.J. Earley, E.J. Metter, *Carotid Arterial Stiffness as a Surrogate for Aortic Stiffness: Relationship Between Carotid Artery Pressure–Strain Elastic Modulus and Aortic Pulse Wave Velocity*, Ultrasound in Medicine and Biology, vol. 25 (2), pp. 181–188, 1999.

[139] F. Hansen, D. Bergqvist, P. Mangell, A. Ryden, B. Sonesson, T. Lanne, *Noninvasive Measurement of Pulsatile Vessel Diameter Change and Elastic Properties in Human Arteries: A Methodological Study*, Clinical Physiology, vol. 13, pp. 631–643, 1993.

[140] A.R. Ahlgren, F. Hansen, B. Sonesson, T. Lanne, *Stiffness and Diameter of the Common Carotid Artery and Abdominal Aorta in Women*, Ultrasound in Medicine and Biology, vol. 23 (7), pp. 983–988, 1997.

[141] W.A. Riley, R.W. Barnes, H.M. Schey, *An Approach to the Noninvastve Periodic Assessment of Arterial Elasticity in the Young*, Preventive Medicine, vol. 13, pp. 169–184, 1984.

[142] C.M. Buntin, F.H. Silver, *Noninvasive Assessment of Mechanical Properties of Peripheral Arteries*, Annals of Biomedical Engineering, vol. 18, pp. 549–566, 1990.

[143] M.J.F. Kool, T. van Merode, R.S. Reneman, A.P.G. Hoeks, H.A.J. Struyker Boudier, L.M.A.B. van Bortel, *Evaluation of Reproducibility of a Vessel Wall Movement Detector System for Assessment of Large Artery Properties*, Cardiovascular Research, vol. 28, pp. 610–614, 1994.

[144] P.C.G. Simon, A. Algra, M.L. Bots, D.E. Grobbee, Y. van der Graaf, *Common Varotid Intima-Media Thickness and Arterial Stiffness: Indicators of Cardiovascular Risk in High-Risk Patients the SMART Study (Second Manifestations of Arterial Disease)*, Circulation, vol. 100, pp. 951–957, 1999.

[145] K.S. Cheng, A. Tiwari, C.R. Baker, R. Morris, G. Hamilton, A.M. Seifalian, *Impaired Carotid and Femoral Viscoelastic Properties and Elevated Intima-Media Thickness in Peripheral Vascular Disease*, Atherosclerosis, vol. 164, pp. 113–120, 2002.

[146] M. F. O'Rourke, J. A. Staessen, C. Vlachopoulos, D. Duprez, and G. E. Plante, *Clinical Applications of Arterial Stiffness; Definitions and Reference Values*, Am. J. Hypertens., vol. 15 (5), pp. 426-444, 2002.

[147] S. Laurent, J. Cockcroft, L. Van Bortel, P. Boutouyrie, C. Giannattasio, D. Hayoz, B. Pannier, C. Vlachopoulos, I. Wilkinson, and H. Struijker-Boudier, *Expert Consensus Document on Arterial Stiffness: Methodological Issues and Clinical Applications*, European heart journal, vol. 27, pp. 2588-605, 2006.

[148] T. Willum-Hansen, J. a Staessen, C. Torp-Pedersen, S. Rasmussen, L. Thijs, H. Ibsen, and J. Jeppesen, *Prognostic Value of Aortic Pulse Wave Velocity as Index of Arterial Stiffness in the General Population*, Circulation, vol. 113, pp. 664-70, 2006.

[149] J.I. Davies and A.D. Struthers, *Pulse Wave Analysis and Pulse Wave Velocity: A Critical Review of Their Strengths and Weaknesses*, Journal of hypertension, vol. 21, pp. 463-72, 2003.

[150] G. Mancia, G. De Backer, A. Dominiczak, R. Cifkova, R. Fagard, G. Germano, G. Grassi, A. M. Heagerty, S. E. Kjeldsen, S. Laurent, K. Narkiewicz, L. Ruilope, A. Rynkiewicz, R. E. Schmieder, H. Boudier, A. Zanchetti, and A. Task Force Management, *Guidelines for the Management of Arterial Hypertension*, J. Hypertens., vol. 25 (6), pp. 1105-1187, 2007.

[151] K.Y. Volokh, *Comparison of Biomechanical Failure Criteria for Abdominal Aortic Aneurysm*, Journal of Biomechanics, vol.43, pp. 2032–2034, 2010.

[152] Ronny x.Li, Tipapon khamdaeng, Elisa E. Konifagou, *Pulse Wave Imaging and Arterial Stiffness Measurement of the Human Carotid Artery: An In-Vivo Feasibility Study*, ultrasound system, 2011.

[153] K. Fujikura, J. Luo, V. Gamarnik, M. Pernot, R. Fukumoto, M. D. Tilson III, and E. E. Konofagou, *A Novel, Non-Invasive Technique for Pulse-Wave Imaging and Characterization of Clinically Significant Vascular Mechanical Properties In Vivo*, Ultrason. Imaging, vol. 29, pp. 137-154, 2007.

[154] J. Luo, K. Fujikura, L. S. Tyrie, M. D. Tilson, and E. E. Konofagou, Pulse *Wave Imaging of Normal and Aneurysmal Abdominal Aortas In-Vivo*, IEEE Trans. Med. Imaging, vol. 28 (4), pp. 477-486, 2009.

[155] J. Vappou, J. Luo, and E. E. Konofagou, *Pulse Wave Imaging for Noninvasive and Quantitative Measurement of Arterial Stiffness In-Vivo*, Am. J. Hypertens, vol. 23 (4), pp. 393-398, 2010.

[156] Ronny X. Li, Jianwen Luo, Snadhya K. Balaram, Farooq A. Chaudhry, John C. Lantis, Danial Shahmirzadi, and Elisa E. Konogahou, *In-Vivo Pulse Wave Imaging for Arterial Stiffness Measurement Under Normal and Pathological Conditions*, 33rd Annual international conference of the IEEE EMBS, 2011.

[157] A. Danpinid, J. Luo, J. Vappou, P. Terdtoon, E.E. Konofagou, *In Vivo characterization of the aortic wall stress–strain relationship*, Ultrasonics, vol. 50, pp. 654–665, 2010.

[158] M.W. Claridge, G.R. Bate, P.R. Hoskins, D.J. Adam, A.W. Bradbury, A.B. Wilmink, *Measurement of Arterial Stiffness in Subjects With Vascular Disease: Are Vessel wall Changes More Sensitive Than Increase in intima–media thickness?*, Atherosclerosis, vol. 205, pp. 477–480, 2009.

[159] R.H. Selzer, W.J. Mack, P.L. Lee, H. Kwong-Fu, H.N. Hodis, Improved *Common Carotid Elasticity and Intima-Media Thickness Measurements From Computer Analysis of Aequential Ultrasound Frames,* Atherosclerosis, vol. 154, pp. 185–193, 2001.

[160] D.K. Arnett, G.W. Evans, W.A. Riley, *Arterial Stiffness: A New Cardiovascular Risk Factor,* American Journal of Epidemiology, vol. 140 (4), pp. 669–682, 1994.

[161] D.K. Arnett, L.E. Chambless, H. Kim, G.W. Evans, W. Riley, *Variability In Ultrasonic Measurements of Arterial Stiffness In The Atherosclerosis Risk In Communities Study,* Ultrasound in Medicine and Biology, vol. 25 (2), pp. 175–180, 1999.

[162] F. Nogata, Y. Yokota, Y. Kawamura, W.R. Walsh, *System For Estimating Sclerosis of In Vivo Arteries Based On Ultrasound B-mode Image Analysis*, 10th ICARCV, pp. 1779–1782, 2008.

[163] T. Khamdaeng, J. Luo, J. Vappou, P. Terdtoon, E.E. Konofagou, *Arterial Stiffness Identification of The Human Carotid Artery Using The Stress–Strain Relationship in Vivo*, Ultrasonics ,vol. 52, pp. 402-411, 2012.

[164] Piotr Kalita, Robert Schaefer, *Mechanical Models of Artery Walls*, Arch. Comput. Methods Eng., vol. 15, pp. 1–36, 2008.

[165] Jaroslaw Krejza, Michal Arkuszewski, Scott E. Kasner, John Weigele, Andrzej Ustymowicz, Robert W. Hurst, Brett L. Cucchiara and Steven R. Messe, *Carotid Artery Diameter in Men and Women and the Relation to Body and Neck Size*, Stroke, vol. 37, pp. 1103-1105, 2006.

[166] Mathieu Couade, Christina Flanagan, Wei-Ning Lee, Emmanuel Messas, Amthias Fink, Mathieu Pernot, Mickael Tanter, *Evaluation of Local Arterial*

Stiffness Using Ultrafast Imaging: A Comparative Study Using Local Arterial Pulse Wave Velocity, Estimation and Shear Wave Imaging, International Ultrasonic Symposium, 2010.

[167] chulze-Bauer CA, Morth C, Holzapfel GA, *Passive Biaxial Mechanical Response of Aged Human Iliac Arteries***,** J. Biomech. Eng., vol. 125, pp. 395-406, 2003.

[168] Driessen NJB, Wilson W, Bouten CVC, Baaijens FPT, *A Computational Model for Collagen Fibre Remodeling in the Arterial Wall***,** J. Theor. Biol., vol. 226, pp.53-64, 2004.

[169] Feng Gao, Masahiro Watanabe and Teruo Matsuzawa, *Stress Analysis in a Layered Aortic Arch Model Under Pulsatile Blood Flow*, BioMedical Engineering OnLine, 5:25, 2006.

[170] N. Santhiyakumari, M. Madheswaran, *Non-invasive Evaluation of Carotid Artery Wall Thickness Using Improved Dynamic Programming Technique*, Signal, Image and Video Processing, vol. 2(2), pp. 183–193, 2008.

[171] David Maltete, Jeremy Bellien, Lucie Cabrejo, Michele Iacob, Francois Proust , Bruno Mihout , Christian Thuillez, Evelyne Guegan-Massardier, Robinson Joannides, *Hypertrophic Remodeling and Increased Arterial Stiffness in Patients With Intracranial Aneurysms,* Atherosclerosis, vol. 211, pp. 486-491, 2010.

[172] Kenneth H. Huebner, Donald L. Dewhirst, Douglas E. Smith, Ted G. Byrom, *The Finite Element Method for Engineers*, 4th edition, John Wiley & Sons Inc., 2001.

APPENDIX A

FIGURES

Maximum principal, Von Mises, Shear stresses distributions and maximum values, plus diagrams with two vertical axes for cases II and VI have been depicted in present section.

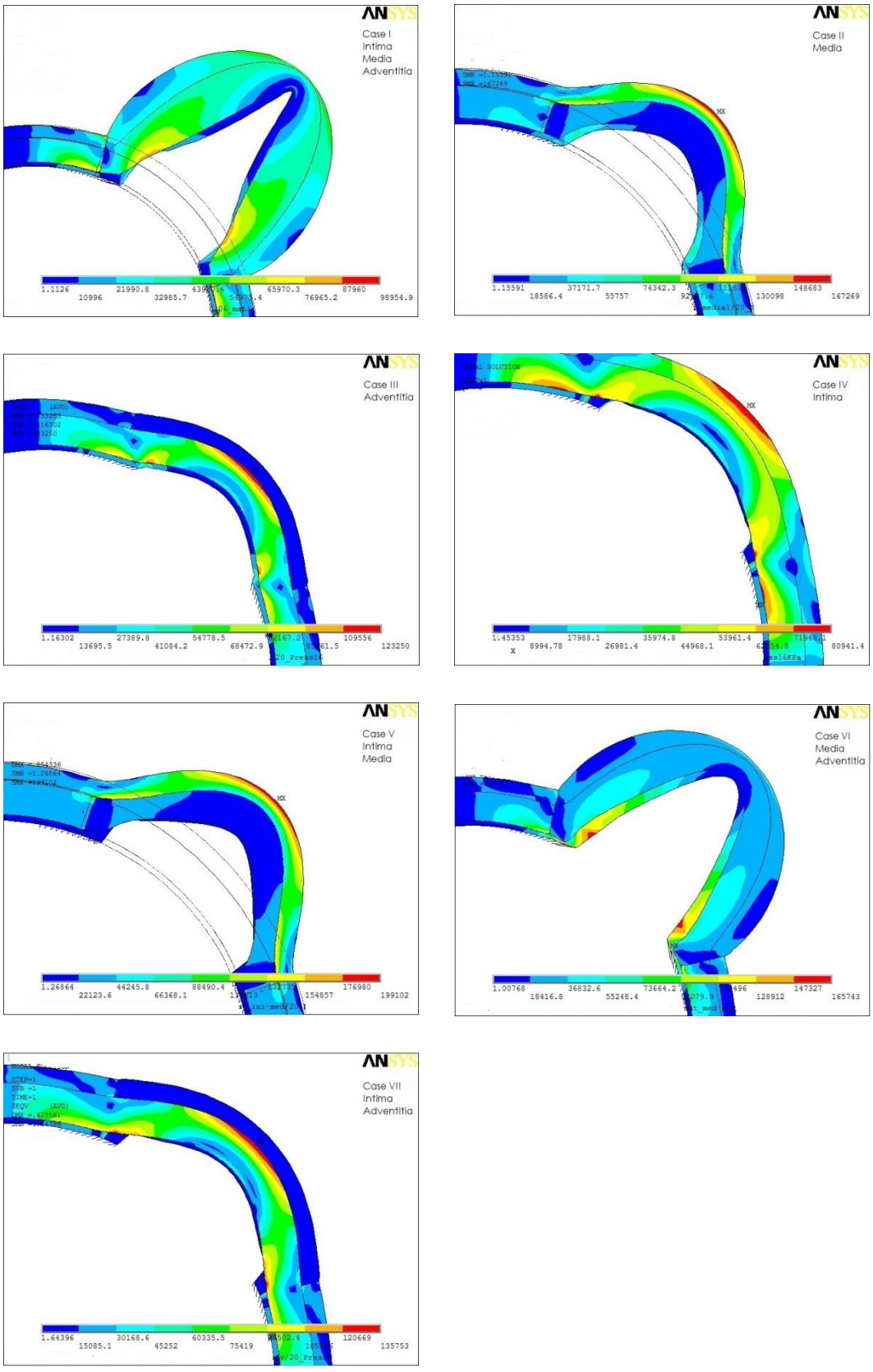

Figure A.1 Von Mises stress distributions under 16KPa pressure for aneurismal wall in 7 cases

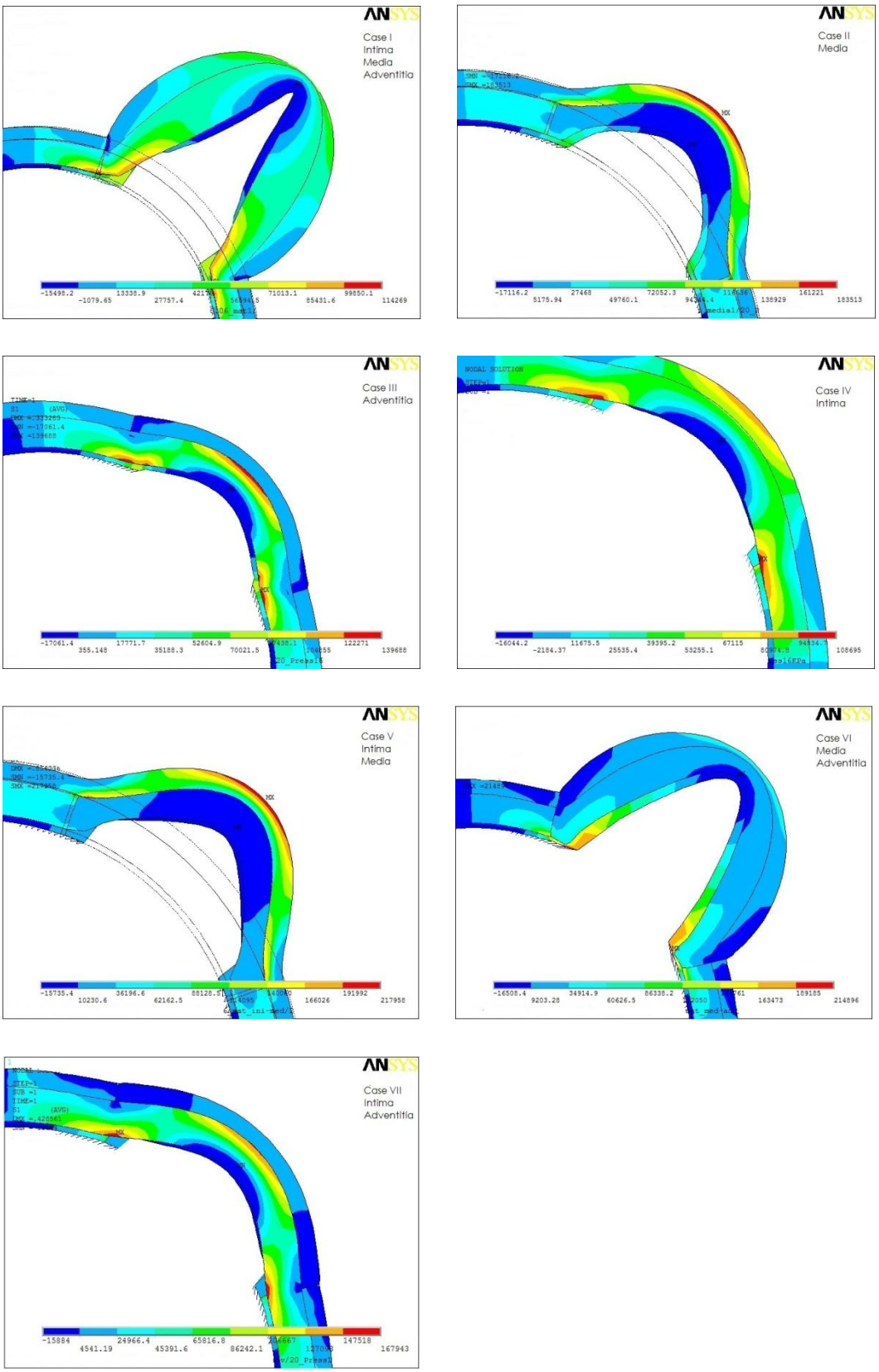

Figure A.2 Max. principal stress distributions under 16KPa pressure for aneurismal wall in 7 cases

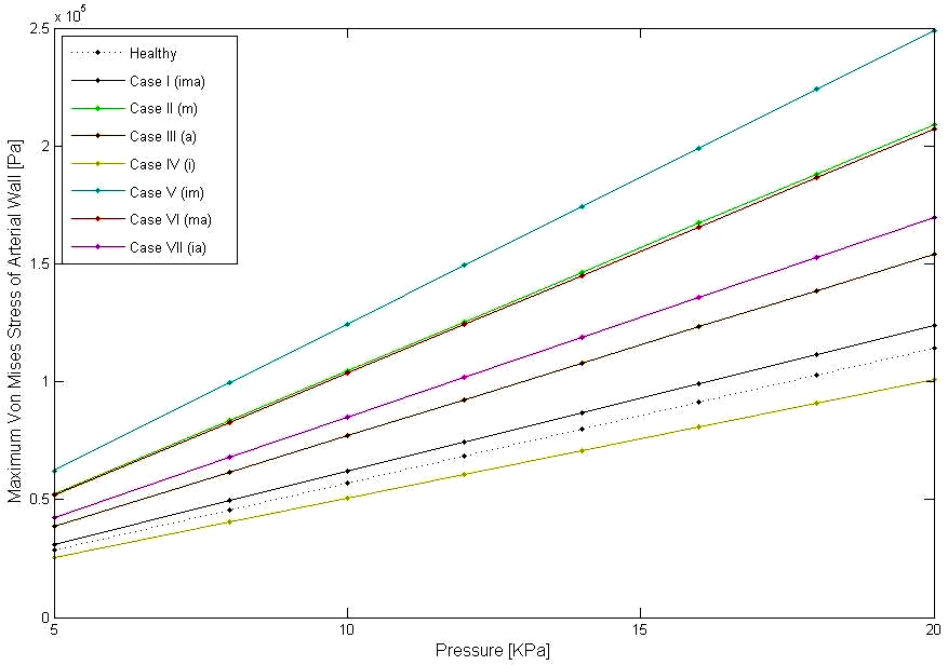

Figure A.3 Maximum values of Von Mises stress with respect to pressure in healthy and seven diseased cases for aneurismal wall

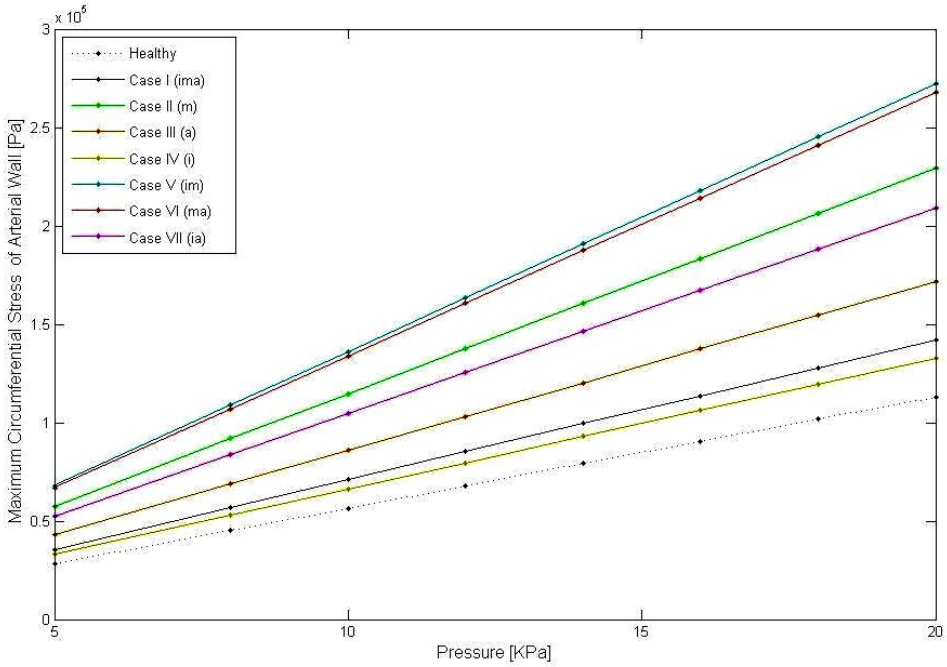

Figure A.4 Maximum values of maximum principal stress with respect to pressure in healthy and seven diseased cases for aneurismal wall

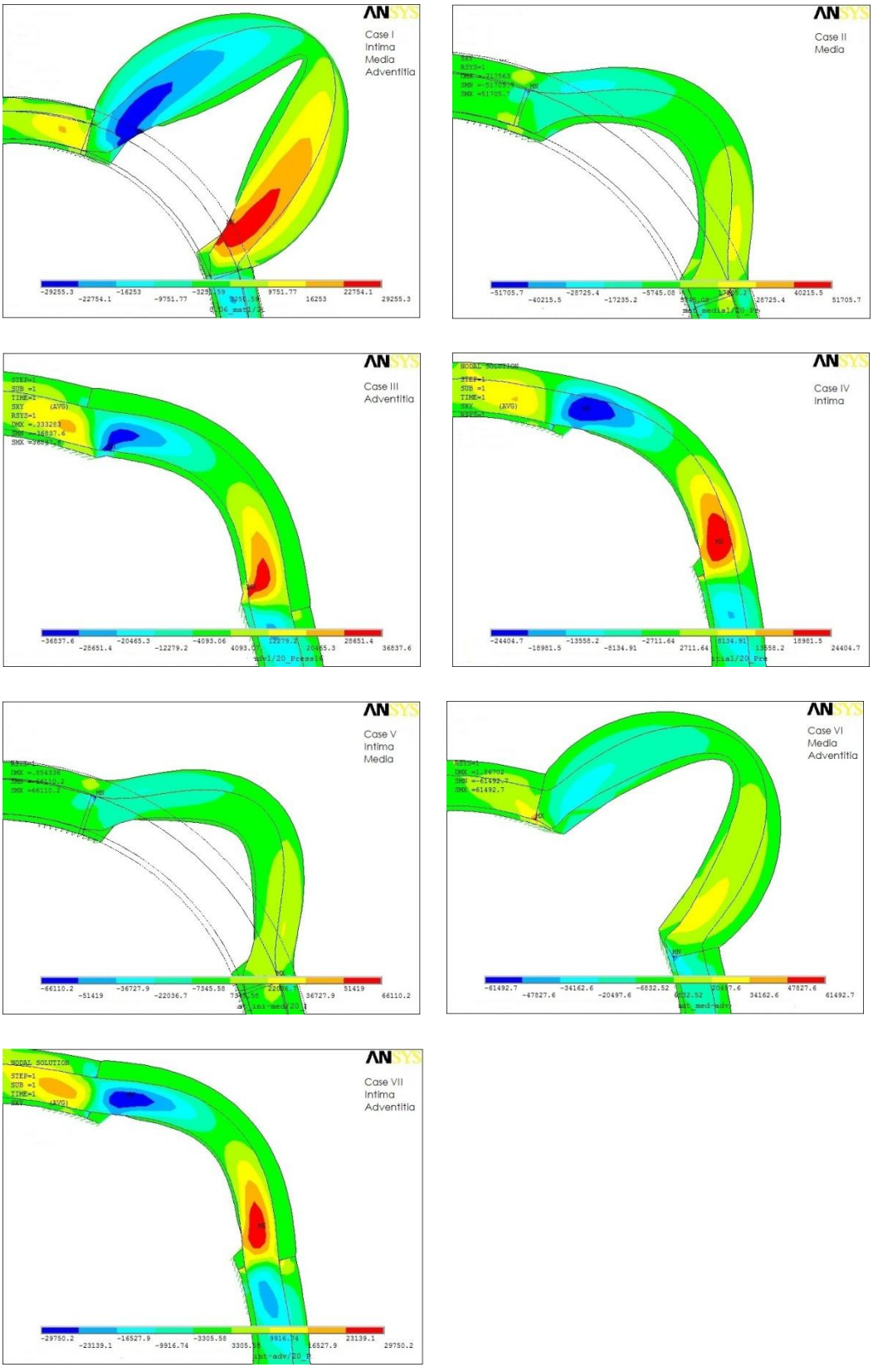

Figure A.5 Shear stress distributions under 16KPa pressure for aneurismal wall in 7 cases

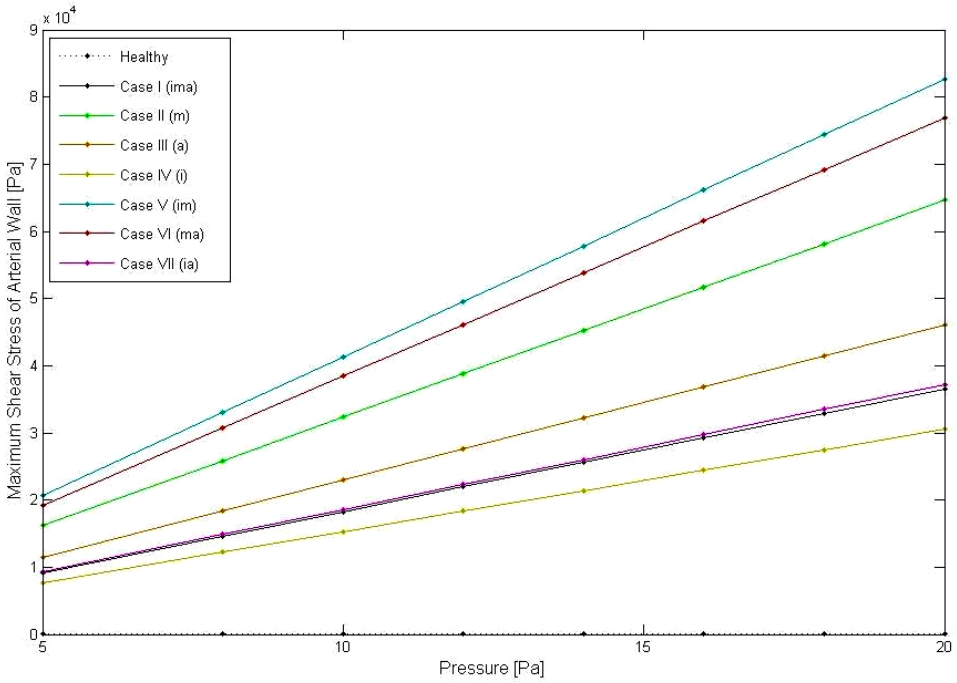

Figure A.6 Maximum values of shear stress with respect to pressure in healthy and seven diseased cases for aneurismal wall

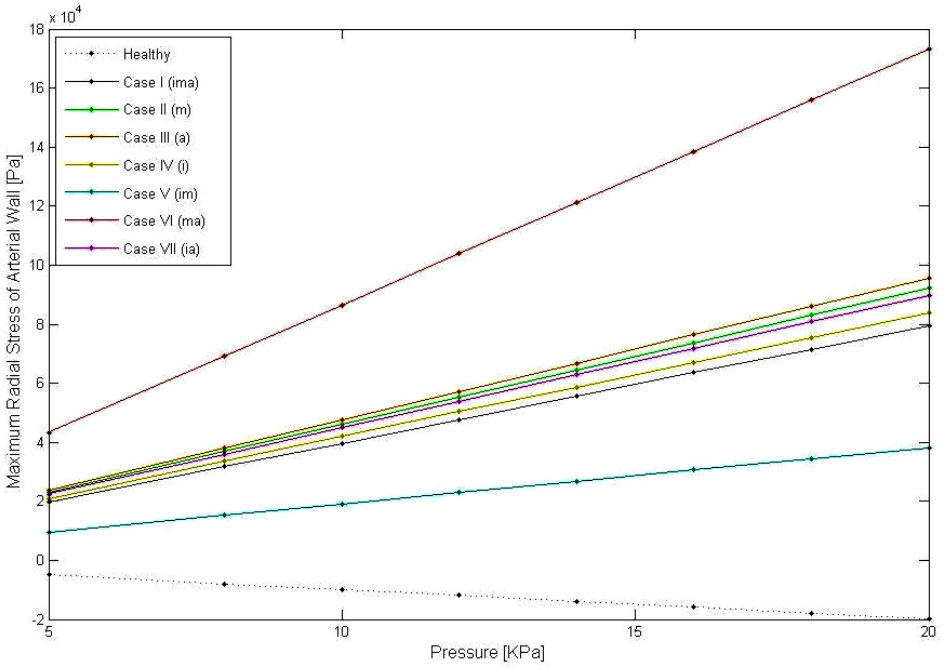

Figure A.7 Maximum values of radial stress with respect to pressure in healthy and seven diseased cases for aneurismal wall

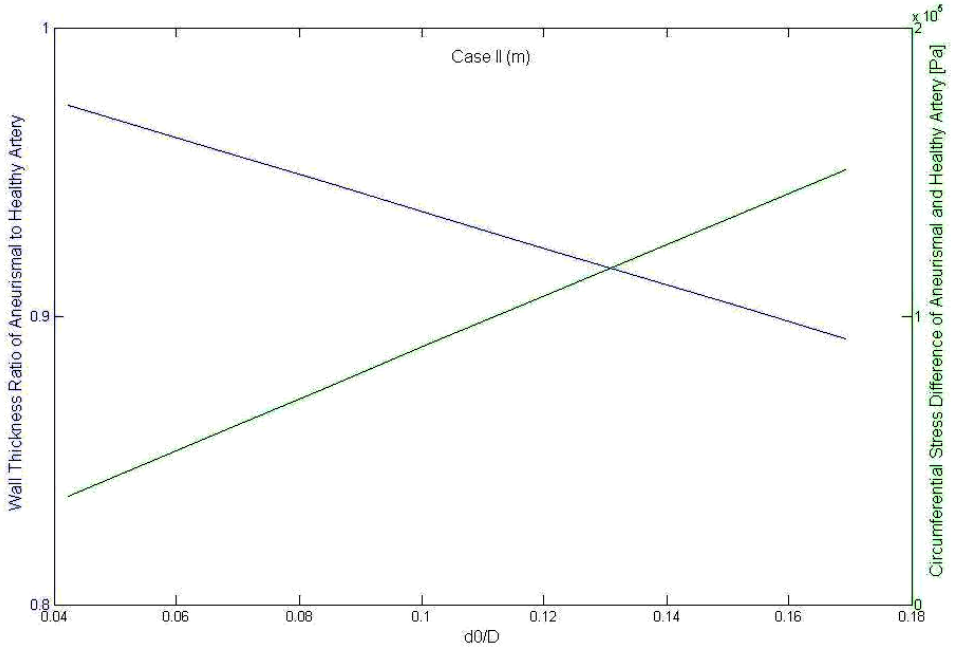

Figure A.8 Wall thickness ratio of aneurismal artery to healthy (blue) and circumferential stress difference (green) of aneurismal and healthy wall with respect to d0/D ratio in case II, where media is diseased layer.

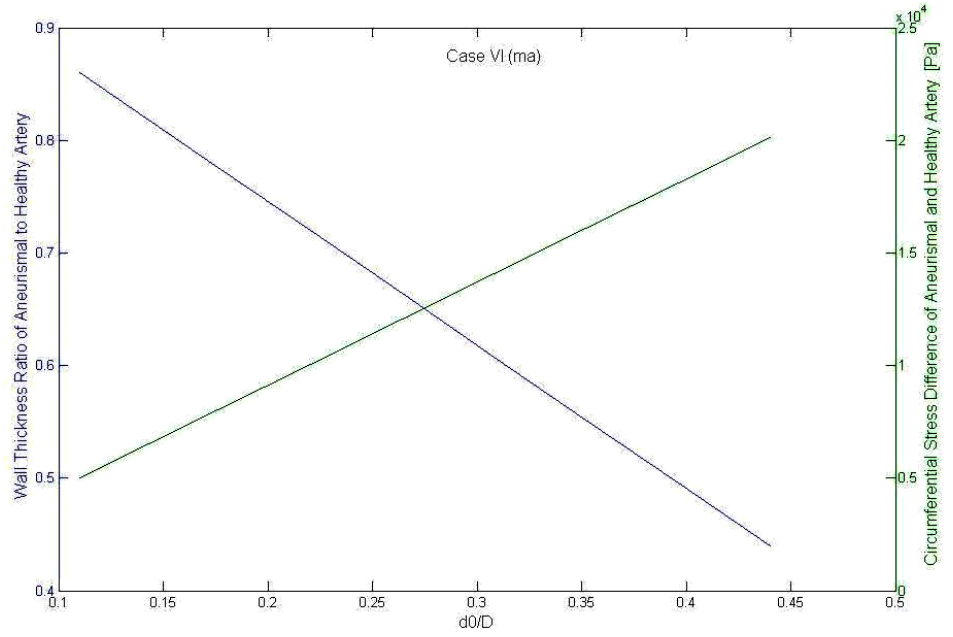

Figure A.9 Wall thickness ratio of aneurismal artery to healthy (blue) and circumferential stress difference (green) of aneurismal and healthy wall with respect to d0/D ratio in case VI, where media and adventitia are diseased layers.